Nuevos derivados basados en clústeres de boro: desarrollo, aproximaciones fotofísicas y funcionalización de plataformas

Justo Cabrera González

TESIS DOCTORAL

Programa de Doctorado en Química

Director: Dra. Mª Rosario Núñez Aguilera

Tutor: Dra. Rosa Mª Sebastián Pérez

Departament de Química
Facultat de Ciències
2016

8. MATERIALES NANOHIBRIDOS BASADOS EN CLÚSTERES DE BORO Y ÓXIDO DE GRAFENO

8.1. Sinopsis

La preparación de nuevos materiales basados en grafeno ha tenido un gran crecimiento en los últimos años debido a sus extraordinarias y particulares propiedades físico-químicas.[1,2] Por esta razón, encontramos de gran interés el desarrollo de nanohíbridos en los que se combinan el óxido de grafeno (**GO**) con clústeres de boro, para estudiar las propiedades de estos nuevos materiales. En el presente capítulo se describe la funcionalización de **GO** con derivados de 2 clústeres de boro aniónicos, el *closo*-dodecaborato o $[B_{12}H_{12}]^{2-}$ **[48]$^{2-}$**, y el cobaltabisdicarballuro o cosane, [3,3'-$Co(C_2B_9H_{11})_2]^-$ **[40]$^-$**. La funcionalización se ha relizado mediante la formación de enlaces convalentes entre el **GO** y los derivados de los clústeres de boro. Los materiales híbridos han sido caracterizados mediante Espectroscopía Fotoelectrónica de Rayos X (XPS), Infrarrojo (IR-ATR), Difracción de Electrones de Área Seleccionada (SAED), Microscopia Electrónica de Transmisión de Barrido-Espectroscopía de Energía Dispersiva (STEM-EDX), así como Análisis Termogravimétrico (ATG). Cabe señalar que además, por primera vez, la presencia de clústeres aniónicos de boro se ha podido confirmar por Espectroscopía de Electrones de Perdida de Energia (EELS) mapeando imagenes de TEM con filtrado energético (EFTEM). Finalmente, se ha estudiado la dispersabilidad de los nuevos compuestos en agua y medios orgánicos, empleando espectroscopía ultravioleta-visible (UV-vis).

8.2. Óxido de grafeno

El óxido de grafeno (**GO**) consiste en una única lámina de óxido de grafito producida generalmente por oxidación de grafito seguida de un proceso de dispersión y exfoliación, generando una estructura bidimensional de carbono funcionalizada con grupos epóxido e hidroxilo en la superficie de la lámina y grupos carboxílicos, carbonilos, fenoles, lactonas y quinonas en los bordes de la misma.[3] La preparación del **GO**, por un método modificado de Hummer,[4] es un trabajo realizado en colaboración con el Dr. Gerard Tobias y la Dra. Laura Cabana del Departamento de Química del Estado Sólido del Instituto de Ciencia de Materiales de Barcelona (ICMAB-CSIC).

Los grupos funcionales presentes en el **GO** le confieren una gran versatilidad para su funcionalización con diferentes moléculas, ya sea mediante enlaces covalentes o no covalentes, que posibilitan obtener una amplia variedad de derivados de grafeno.[5] Entre las diferentes reacciones para la funcionalización covalente de **GO** destacan las reacciones de acoplamiento sobre los grupos carboxílicos, como la amidación[6-8] y la esterificación,[9] así como las reacciones de apertura de ciclo sobre los grupos epoxi[10] y las reacciones de entrecruzamiento.[11] La preparación de híbridos basados en **GO** ha abierto amplias posibilidades en la ciencia de materiales, para aplicaciones por ejemplo en dispositivos electrónicos[12] o en biomedicina.[13]

8.3. Derivados de los clústeres de *closo*-dodecaborato y cobaltabisdicarballuro

Para la funcionalización de **GO** nos hemos propuesto llevar a cabo reacciones de amidación entre los grupos carboxílico del **GO**, –COOH, y una función amina, $–NH_2$, presente en derivados de los clústeres. Por ello se han seleccionado los compuestos **[50]**$^{2-}$ y **[51]**$^{-}$, que han sido preparados mediante una reacción de apertura del ciclo oxonio de los compuestos **[49]**$^{-}$ y **42** empleado NH_3 como nucleófilo (**Figura 8.1**).[14,15]

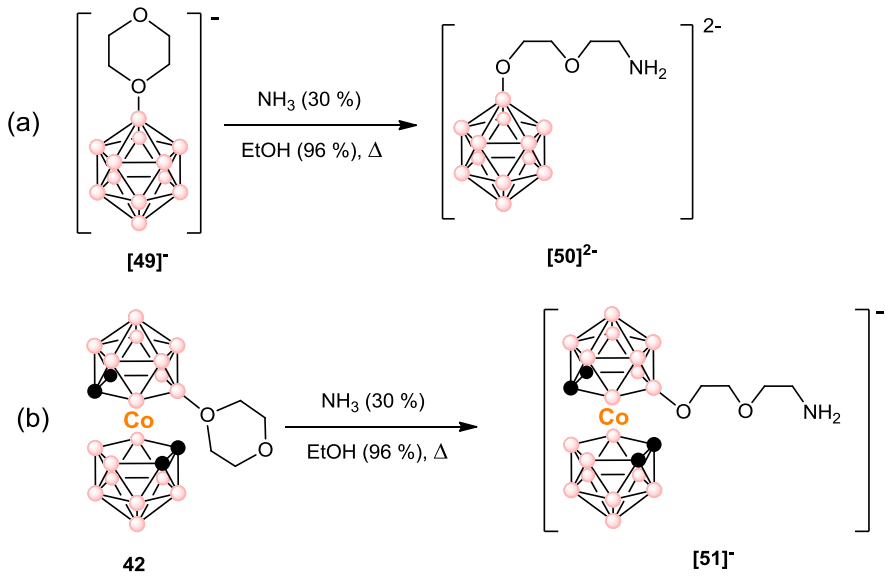

Figura 8.1. Preparación de los amino-derivados del cluster de (a) closo-dodecaborato y (b) cobaltabisdicarballuro.

Los compuestos se aislaron como $[Bu_4N][H]$**[50]** y [H]**[51]** y la presencia del grupo -NH_2 terminal les permite llevar a cabo las reacciones típicas de aminas primarias.

Sorprendentemente, para el compuesto **[50]**$^{2-}$ no se han encontrado reacciones en las que se haya utilizado como reactivo y, para el compuesto **[51]**$^{-}$ se han encontrado tan solo 3 trabajos, en funcionalización de superficies[15,16] y aplicaciones biomédicas.[17]

8.4. Funcionalización del GO con clústeres de boro

Para la funcionalización del **GO** mediante reacciones de amidación, ha sido necesario utilizar la N,N'-diciclohexilcarbodiimida (DCC) para activar los grupos –COOH y, el 1-hidroxibenzotriazol (HBOt) como aditivo para aumentar la eficacia en la formación de enlaces tipo amida.[18,19] Para ello, el **GO** se suspendió en DMF y se agregaron la DCC y el HBOt, agitando durante 30 min para asegurar la activación de los grupos –COOH y, seguidamente se agregaron los respectivos derivados de los clústeres de boro, [Bu_4N][H]**[50]** y [H]**[51]**, que tras agitar durante 72h a 40°C da lugar a la formación de los nanohíbridos **B_{12}-GO** y **Cosane-GO**, respectivamente (**Figura 8.2**).

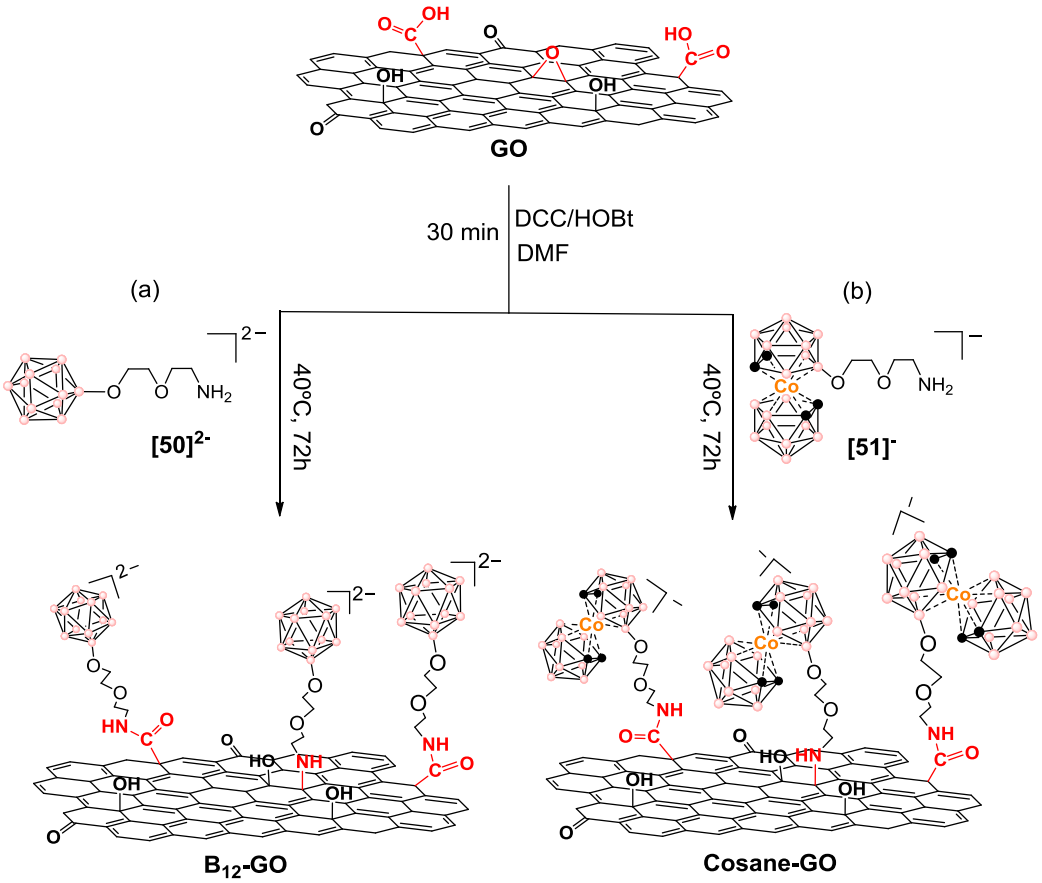

Figura 8.2. Reacciones de funcionalización de **GO** para obtener (a) **B_{12}-GO** y (b) **Cosane-GO**.

Tras las 72 h de reacción se eliminó el disolvente y el sólido obtenido se lavó con EtOH, se filtró por una membrana de policarbonato y volvió a lavarse con CH_3OH, asegurando que se elimina el posible exceso de las sales de **[50]**$^{2-}$ y **[51]**$^{-}$, que pudiera encontrarse adsorbido sobre el **GO**.

Durante la caracterización de los nuevos materiales, **B_{12}-GO** y **Cosane-GO**, se ha determinado que no solo han tenido lugar formación de enlaces amida con los grupos carboxílicos del **GO**, sino que además se han producido reacciones de apertura de ciclo de los grupos epóxido, C-O-C, presentes en la superficie del **GO**. (**Figura 8.2** y sección 8.5)

8.5. Caracterización de los materiales nanohíbridos B_{12}-GO y Cosane-GO

La caracterización de los nanohíbridos de **B_{12}-GO** y **Cosane-GO** se ha realizado mediante IR-ATR, ATG, XPS, SAED y STEM-EDX, además de establecer la presencia de los clústeres por EELS y mapear su distribución mediante EFTEM.

Los espectros de **IR-ATR** del **GO** de partida y de los materiales finales **B_{12}-GO** y **Cosane-GO** se muestran en la **Figura 8.3**. Al analizar el espectro del **GO**, pueden identificarse las bandas características a 1730 cm^{-1} (C=O), 1580 cm^{-1} (C=C de los grupos -COOH) y 1226 cm^{-1} (C-O de grupos C-O-C y C-OH).[20] Lo primero que cabe destacar es que, tras la formación de **B_{12}-GO** y **Cosane-GO**, surgen unas bandas a 2487 y 2541 cm^{-1}, respectivamente, correspondientes a la vibración del enlace B-H, ν(B-H), y que confirman la presencia de los clústeres de boro tras la funcionalización. Al comparar los 3 espectros, se evidencia que para el **B_{12}-GO** y **Cosane-GO** disminuye la intensidad de la señal a 1730 cm^{-1} como consecuencia de la reacción de los grupos –COOH. Además,

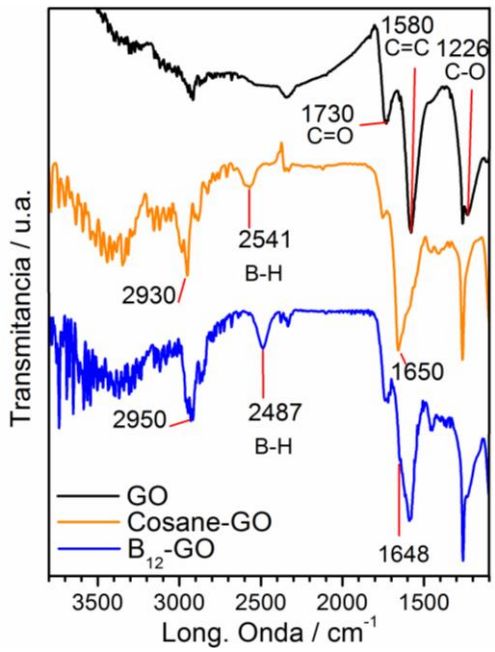

Figura 8.3. Espectros de IR-ATR del GO y de los nanohíbridos finales.

aparece una nueva señal ancha alrededor de 1650 cm^{-1}, que se asigna a la vibración C=O de las nuevas funciones amida, ν(NC=O).[6] En cuanto a la banda a 1226 cm^{-1}, se observa una clara disminución de intensidad tras la funcionalización, lo que se atribuye a la unión de **[50]$^{2-}$** y **[51]$^{-}$** mediante reacciones de apertura de ciclos epóxidos, formando nuevos enlaces tipo aminas secundarias, C-NH-C (**Figura 8.2**). También, en los espectros de **IR-ATR** de **B_{12}-GO** y **Cosane-GO**, se observan señales en el rango 2920-2960 cm^{-1}, que corresponden a las señales ν(C-H) de las cadenas etoxiladas que unen los clústeres de boro al **GO**. Los resultados derivados del análisis de los espectros de **IR** revelan que se ha producido una funcionalización covalente del **GO** a través de la formación de enlaces amida y amina.

El estudio de los **ATG** permite observar los cambios producidos en la estabilidad térmica del **GO** tras su funcionalización con los clústeres de boro. A continuación se representan los ATG de los clústeres de partida **[50]$^{2-}$** y **[51]$^{-}$** (**Figura 8.4a**) y de **GO**, **B_{12}-GO** y **Cosane-GO** (**Figura 8.4b**), realizados bajo una atmósfera de aire y representados a partir de 120 ˚C, tras realizar una etapa isotérmica a esta temperatura para eliminar posibles disolventes.

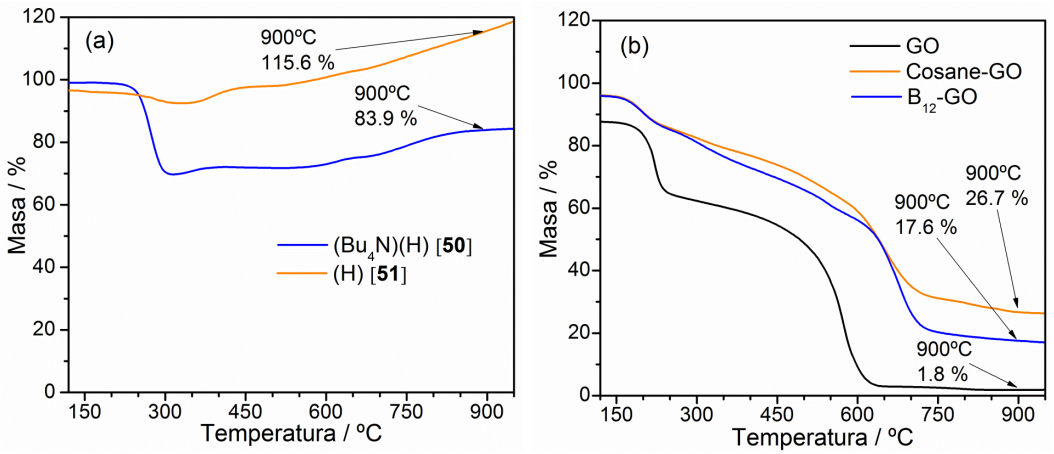

Figura 8.4. ATG bajo atmósfera de aire de (a) $(Bu_4N)(H)$**[50]** y (H)**[51]** y (b) **GO**, **B_{12}-GO** y **Cosane-GO**.

Para el **GO** de partida, el **ATG** muestra una importante disminución de masa a 220 ˚C debida a la pérdida de los grupos funcionales propios del **GO** y, sobre 600 ˚C ya se produce su combustión completa. Sin embargo, para el **B_{12}-GO** y **Cosane-GO** la

combustión total de las muestras se presenta a temperaturas entre 650-750 ˚C, lo que supone un incremento de aproximadamente 100 ˚C en la estabilidad térmica debido a la presencia de los clústeres de boro. Además, analizando los residuos de **ATG** tras calentar hasta 900 ˚C, puede estimarse el grado de funcionalización del **GO** con los clústeres, ya que al llegar a esta temperatura se habrá perdido todo el carbono perteneciente al **GO** y la parte orgánica de las cadenas eteradas que une el **GO** con los clústeres. Para el **GO** de partida, el residuo del **ATG** obtenido supone tan solo un 1.8 % m/m, y proviene de residuos inorgánicos empleados en su preparación. Sin embargo, para el **B_{12}-GO** y **Cosane-GO** se obtienen residuos del 17.6 y 26.7 % m/m, respectivamente, como consecuencia de la formación de óxidos de boro durante el calentamiento (**Figura 8.4b**). Teniendo en cuenta que los compuestos de partida, $[Bu_4N][H]$**[50]** y [H]**[51]**, generan unos residuos de **ATG** de 83.9 y 115.6 % m/m respectivamente (**Figura 8.4a**), puede establecerse que los híbridos **B_{12}-GO** y **Cosane-GO** contienen alrededor de un 18.3 y 20.8 % m/m de clústeres de boro. Considerando los pesos moleculares de $(Bu_4N)(H)$**[50]** y (H)**[51]** (488 y 429 g/mol, respectivamente), se determina que el grado de funcionalización es de 484 μmol/g para el **Cosane-GO** y 375 μmol/g para el **B_{12}-GO.**

La caracterización mediante **XPS** permite detectar la presencia de átomos de B y determinar en qué forma se encuentran dichos átomos. En la **Figura 8.5** se muestran las energías de enlace (eV) para el B 1s del **B_{12}-GO** y **Cosane-GO**, indicando energías ligeramente diferentes de 187.35 y 188.45 eV atribuidas los *B*-H,[21] confirmando que el *closo*-dodecaborato y el cosane se encuentran sobre el **GO** tras la reacción.

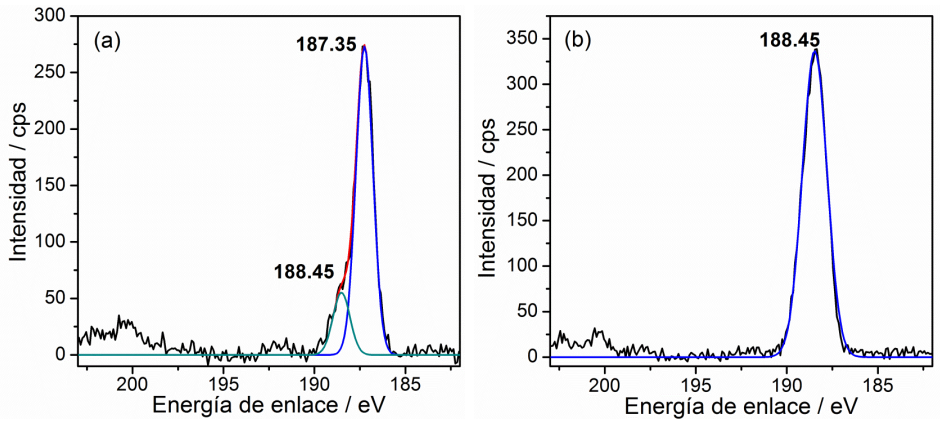

Figura 8.5. XPS de alta resolución en la región del B 1s de (a) **B_{12}-GO** y (b) **Cosane-GO**.

La deconvolución en curvas gaussianas del **XPS** de alta resolución en la región del C 1s, revela que en el **GO** de partida (**Figura 8.6a**) se produce una modificación química del patrón de C al formarse el **B_{12}-GO** (**Figura 8.6b**) y el **Cosane-GO** (**Figura 8.6c**). Como puede observarse, en los **XPS** de C de los nuevos materiales híbridos se produce una drástica reducción de las energías correspondientes a los grupos C-O/C-O-C, que tras la funcionalización se encuentra a valores de 285.8 y 285.5 eV, lo que se atribuye a las reacciones de apertura de ciclos epóxido en la superficie del **GO**. También destaca la disminución de intensidad relativa de la señal a 288.6 eV de los grupos O-C=O del **GO** de partida, como consecuencia de la amidación de los grupos –COOH. Finalmente, hay que señalar que aparece una nueva curva de deconvolución entre 286.0-286.4 eV, asignada a los nuevos enlaces C-N formados tras la apertura de ciclos epóxido.[22] Estos resultados del **XPS** de alta resolución del 1s de C confirman la funcionalización del **GO** con **[50]$^{2-}$** y **[51]$^{-}$** mediante enlaces covalentes tipo amida y amina.

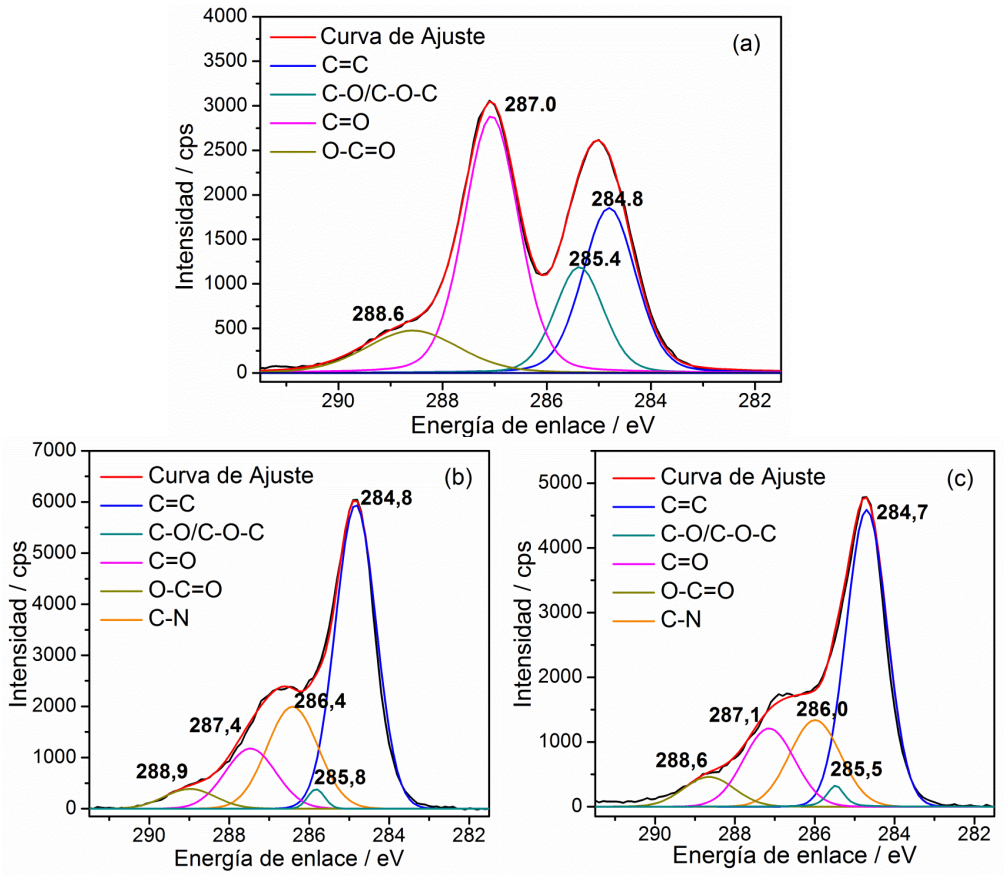

Figura 8.6. XPS de alta resolución en la región 1s del C de (a) **GO**, (b) **B_{12}-GO** y (c) **Cosane-GO**.

Mediante el análisis de **SAED** pueden compararse los patrones de difracción de electrones de los híbridos obtenidos, **B_{12}-GO** y **Cosane-GO**, con los clústeres de partida, **$[50]^{2-}$** y **$[51]^{-}$**, para establecer así cambios de estructura de los clústeres de partida tras la funcionalización del **GO**. Para ello se dispersaron las muestras en agua, se depositaron sobre una rejilla de cobre con film de carbono y se analizaron los patrones de difracción. Para los clústeres de partida, tan solo el compuesto **$[50]^{2-}$** produce una clara difracción de electrones (**Figura 8.7b**), mientras que el compuesto **$[51]^{-}$** no produce difracción alguna, lo que impediría comprarlo con el patrón del **Cosane-GO**.

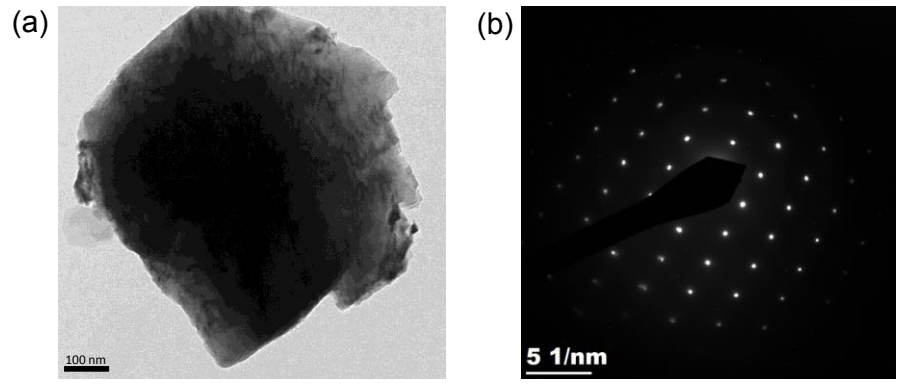

Figura 8.7. (a) Imagen TEM del compuesto **$[50]^{2-}$** y (b) su patrón de SAED.

Los materiales **B_{12}-GO** y **Cosane-GO** presentan el patrón de difracción correspondiente a la estructura cristalina de grafeno. Al analizar el patrón de **SAED** del **B_{12}-GO** (**Figura 8.8b**) es fácil observar que no hay rastro de difracción del compuesto **$[50]^{2-}$** (**Figura 8.7b**), lo que confirma que **$[50]^{2-}$** se enlaza al **GO** como unidades independientes, sin trazas adsorbidas del clúster de partida sobre las láminas de **GO**.

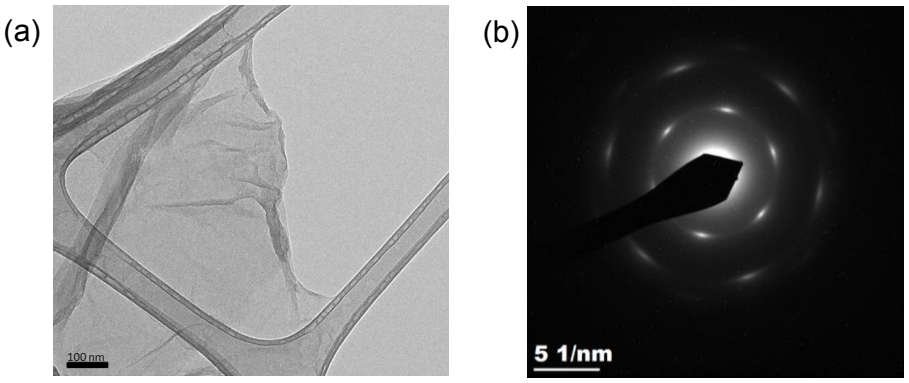

Figura 8.8. (a) Imagen TEM del nanohíbrido **B_{12}-GO** y (b) su patrón de SAED.

La técnica de **STEM-EDX** ha sido útil para determinar la presencia de **[51]**$^{-}$ en el híbrido **Cosane-GO** debido a que contiene un átomo de Co. Mediante esta técnica puede realizarse un análisis de los elementos presentes en la muestra y, como se observa en la **Figura 8.9** se puede identificar señales a 6.924 y 0.776 KeV que pertenecen a la energía dispersiva del Co, lo que confirma la presencia de clúster de cosane sobre el **GO**. En el caso del **B_{12}-GO** no ha sido posible emplear el **STEM-EDX** para confirmar la funcionalización del **GO** con **[50]**$^{2-}$, puesto que los nuevos átomos que en este caso se incorporan sobre el **GO** (como en B, O, N) son demasiado ligeros para detectarlos mediante esta técnica.

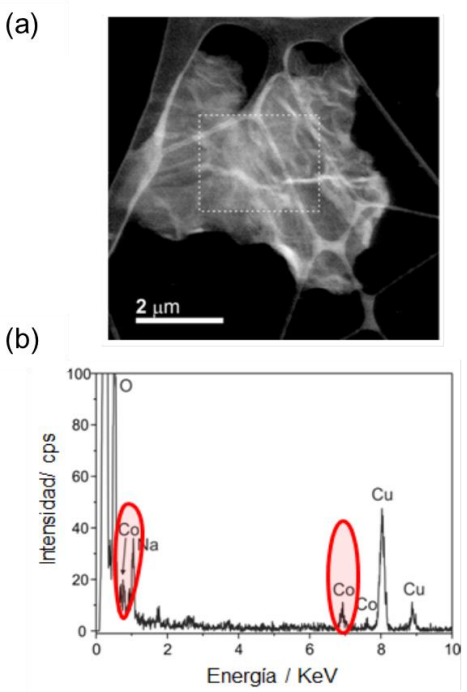

Figura 8.9. (a) Imagen STEM del **Cosane-GO** y (b) Espectro EDX en la región recuadrada.

Sin embargo, para el **B_{12}-GO** si ha sido posible utilizar la técnica de **EELS** para detectar C y B, creando un mapeado de la muestra mediante **EFTEM**. La **Figura 8.10** muestra 2 ejemplos del mapeado obtenido para el **B_{12}-GO** donde se ha representado en rojo la presencia de C y en verde el B.

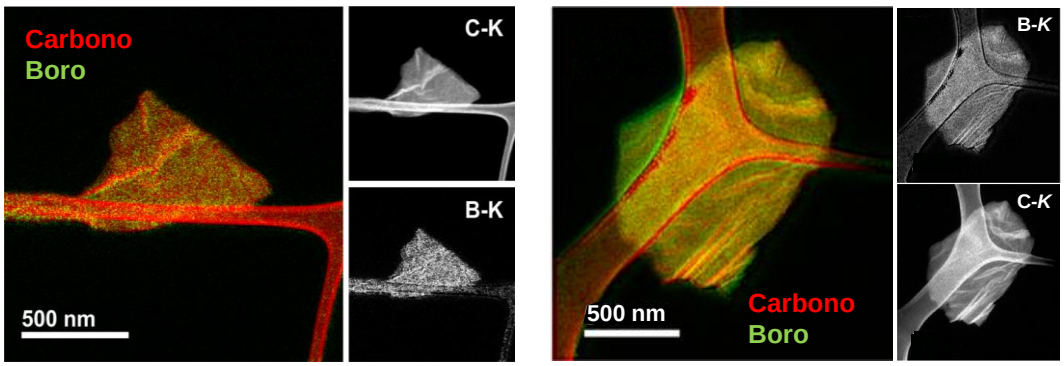

Figura 8.10. Mapa de distribución elemental EFTEM para C y B muestras de **B_{12}-GO.**

El C se encuentra presente tanto en la lámina de grafeno como en el soporte de film de carbono, mientras que el B solo está presente sobre el grafeno. Puede observarse además, que la distribución del clúster de *closo*-dodecaborato sobre la lámina de **GO** es muy homogénea, lo que confirma una funcionalización química y no la formación de agregados que pudieran encontrarse adsorbidos sobre el **GO**.

8.6. Estudios de dispersabilidad

Una vez confirmada la funcionalización covalente del **GO** con los clústeres de *closo*-dodecaborato y cosane, nos proponemos estudiar el grado de dispersabilidad en diferentes medios. Para ello se han preparado dispersiones con 1 mg/mL de cada nanohíbrido en agua, THF y acetona, se sonica durante 30 min y se dejan reposar durante 1 h. Luego se recoge el sobrenadante de las dispersiones y se analiza mediante UV-Vis. El patrón de absorbancia registrado para cada nanohíbrido se compara con el UV-Vis del **GO** de partida.

Es conocido que el **GO** presenta un grado alto de dispersabilidad en agua.[3] A continuación se muestran los UV-Vis del **GO**, **Cosane-GO** y **B_{12}-GO** en agua, al analizar el sobrenadante tras 1 h (**Figura 8.11a**) y después de 1 mes (**Figura 8.11b**). El **GO** muestra su máximo de absorción característico sobre λ = 240 nm debido a la transición π-π* de los enlaces C-C aromáticos.[23,24] Sin embargo, en los nuevos nanohíbridos, este máximo de absorción se encuentra desplazado al rojo 15-30 nm, hecho que ya fue observado en modificaciones químicas de **GO**.[23,25]

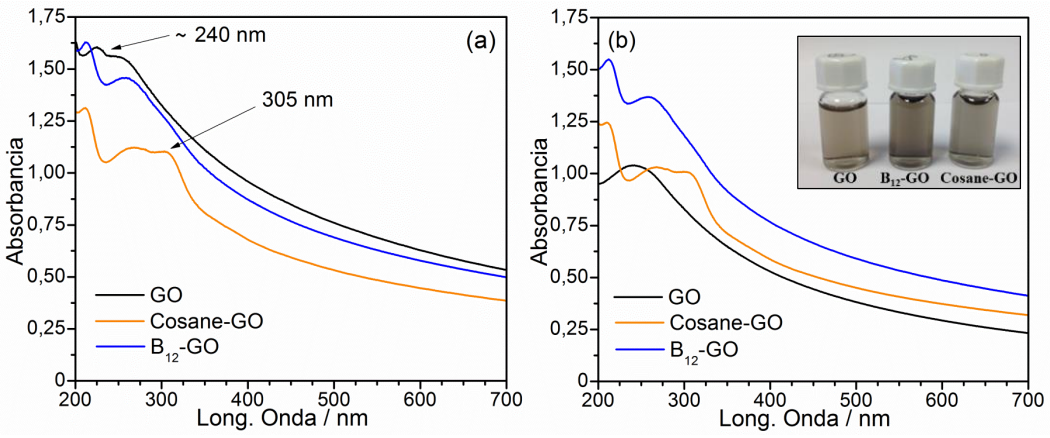

Figura 8.11. Espectros de UV-Vis de las dispersiones en agua de **GO**, **Cosane-GO** y **B_{12}-GO** (a) tras 1h y (b) después de 1 mes.

En las dispersiones de **Cosane-GO** también se aprecia una banda sobre λ_{abs} = 305 nm, que es característica del cobaltabisdicarballuro.[26] Para comparar el grado de dispersabilidad, se toma como referencia el valor de absorbancia del **GO** a 240 nm como un 100% de dispersabilidad. Al analizar los valores de absorbancia del sobrenadante pasada 1 h de la preparación de la dispersión (**Figura 8.11a**), se observa que el **GO** y el **B_{12}-GO** tienen un grado de dispersabilidad similar mientras que, al comparar con el **Cosane-GO** se observa que este nanohíbrido es un 28 % menos dispersable. Sin embargo, después de 1 mes (**Figura 8.11b**) hay una clara caída en el valor de **GO** dispersado en agua, que supone una disminución del 33 %, mientras que las especies funcionalizadas con los clústeres de boro mantienen su grado de dispersión prácticamente inalterable. El **B_{12}-GO** tras 1 mes se encuentra un 32 % más disperso que el **GO** y, el **Cosane-GO** es ahora ligeramente más dispersable que el **GO**. Estos resultados indican que la funcionalización del **GO** con estos clústeres de boro supone una mejora de la estabilidad de su dispersión en agua.

Parece evidente que la modificación química del **GO** con *closo*-dodecaborato y cosane produce un cambio en las características físico-químicas del **GO** y por ello, hemos querido observar su comportamiento en algunos disolventes orgánicos. Se seleccionaron THF y acetona para comprobar el grado de dispersabilidad de los nuevos nanohíbridos, analizando los sobrenadantes tras dejar reposar 1 h las dispersiones. En el caso del THF se pudo emplear UV-Vis para estudiarlo (**Figura 8.12**) y, el máximo de absorción del **GO** se encuentra alrededor de 290 nm, mientras que para el **B_{12}-GO** y **Cosane-GO** se encuentra a 285 y 295 nm, respectivamente. Al comparar las dispersiones en THF queda patente que el **Cosane-GO** presenta un mayor grado de dispersabilidad que el **GO**, por tanto, la funcionalización con el derivado de cosane **[51]**$^-$ mejora considerablemente esta propiedad en THF.

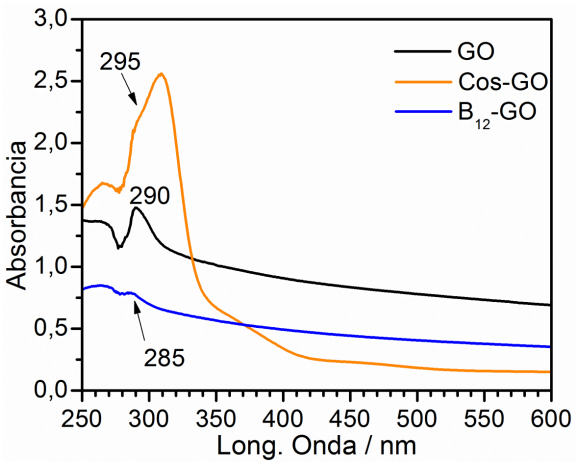

Figura 8.12. UV-Vis de las dispersiones en THF de GO, **Cosane-GO** y **B_{12}-GO** tras 1h.

En el caso de las dispersiones en acetona no es posible estudiarlas mediante UV-Vis debido a la absorbancia de este disolvente para valores de $\lambda < 340$ nm, por tanto, se inspeccionaron visualmente para apreciar las diferencias. Es conocido que el **GO** no se dispersa bien en acetona,[23] y por ello analizamos si la funcionalización con los clústeres de boro cambia este comportamiento. La **Figura 8.13** muestra los sobrenadantes de las dispersiones de **GO**, **B_{12}-GO** y **Cosane-GO**, donde se evidencia la poca o nula dispersabilidad del **GO** en acetona, mientras que el **B_{12}-GO** y **Cosane-GO** presentan una notable intensidad de color, especialmente marcado en el **B_{12}-GO**.

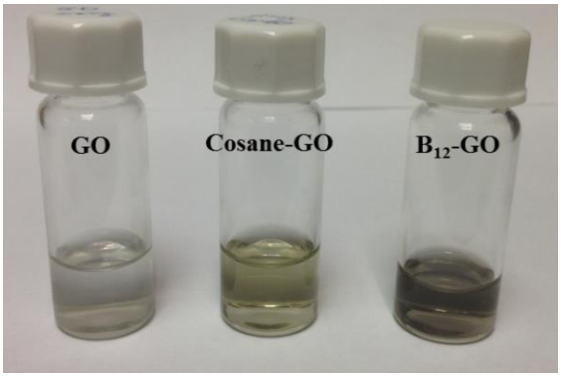

Figura 8.13. Aspecto de los sobrenadantes de las dispersiones de GO, **Cosane-GO** y **B_{12}-GO** en acetona tras 1h.

Los resultados obtenidos del estudio de dispersabilidad determinan que la presencia de los clústeres de boro, *closo*-dodecaborato y cosane, juegan un papel importante en la dispersabilidad del grafeno, mejorando considerablemente la estabilidad de las dispersiones en agua con el tiempo y, el grado de dispersabilidad en disolventes orgánicos como el caso del **Cosane-GO** en THF y de ambos nanohíbridos en acetona.

8.7. Resumen de resultados

Se han preparado materiales híbridos basados en **GO** funcionalizado con derivados de los clústeres de *closo*-dodecaborato **$[50]^{2-}$** y cobaltabisdicarballuro **$[51]^{-}$** que contienen una función -NH_2 terminal. La funcionalización covalente del **GO** con **$[50]^{2-}$** y **$[51]^{-}$** ha sido corroborada mediante IR-ATR y XPS. Además mediante las técnicas de SAED, STEM-EDX y por primera vez mediante EFTEM, ha sido posible confirmar la presencia de clústeres aniónicos, así como su distribución homogénea sobre el grafeno. Mediante ATG se ha estimado que los híbridos **B_{12}-GO** y **Cosane-GO** contienen un 18.3 y 20.8 % m/m de clústeres de boro, respectivamente. Es destacable que la presencia de los clústeres ha mejorado la estabilidad de la dispersión en agua del **GO** y, dependiendo del clúster también ha mejorado el grado de dispersabilidad en THF y acetona. La

mejora de la dispersabilidad se considera de gran importancia, ya que facilitaría la procesabilidad del GO para futuras aplicaciones. Además, hay que destacar la ventaja que supone la mejor dispersión en agua al realizar estudios biológicos para la posible aplicación de estos compuestos en BNCT.

REFERENCIAS

(1) Geim, A. K.; Novoselov, K. S. *Nat .Mater.* **2007**, *6*, 183.

(2) Geim, A. K. *Science* **2009**, *324*, 1530.

(3) Chen, D.; Feng, H.; Li, J. *Chem. Rev.* **2012**, *112*, 6027.

(4) Sandoval, S.; Kumar, N.; Sundaresan, A.; Rao, C. N. R.; Fuertes, A.; Tobias, G. *Chem. Eur. J.* **2014**, *20*, 11999.

(5) Dreyer, D. R.; Park, S.; Bielawski, C. W.; Ruoff, R. S. *Chem. Soc. Rev.* **2010**, *39*, 228.

(6) Niyogi, S.; Bekyarova, E.; Itkis, M. E.; McWilliams, J. L.; Hamon, M. A.; Haddon, R. C. *J. Am. Chem. Soc.* **2006**, *128*, 7720.

(7) Zhang, X.; Huang, Y.; Wang, Y.; Ma, Y.; Liu, Z.; Chen, Y. *Carbon* **2009**, *47*, 334.

(8) Liu, Z.; Robinson, J. T.; Sun, X.; Dai, H. *J. Am. Chem. Soc.* **2008**, *130*, 10876.

(9) Lo, C.-W.; Zhu, D.; Jiang, H. *Soft Matter* **2011**, *7*, 5604.

(10) Wang, S.; Chia, P.-J.; Chua, L.-L.; Zhao, L.-H.; Png, R.-Q.; Sivaramakrishnan, S.; Zhou, M.; Goh, R. G. S.; Friend, R. H.; Wee, A. T. S.; Ho, P. K. H. *Adv. Mater.* **2008**, *20*, 3440.

(11) Park, S.; Dikin, D. A.; Nguyen, S. T.; Ruoff, R. S. *J. Phys. Chem. C* **2009**, *113*, 15801.

(12) Kim, S. J.; Choi, K.; Lee, B.; Kim, Y.; Hong, B. H. *Annu. Rev. Mater. Res* **2015**, *45*, 63.

(13) Chung, C.; Kim, Y.-K.; Shin, D.; Ryoo, S.-R.; Hong, B. H.; Min, D.-H. *Acc. Chem. Res.* **2013**, *46*, 2211.

(14) Semioshkin, A.; Nizhnik, E.; Godovikov, I.; Starikova, Z.; Bregadze, V. *J. Organomet. Chem.* **2007**, *692*, 4020.

(15) Juárez-Pérez, E. J.; Granier, M.; Viñas, C.; Mutin, P. H.; Núñez, R. *Chem. - Asian J.* **2012**, *7*, 277.

(16) Cabana, L.; González-Campo, A.; Ke, X.; Van Tendeloo, G.; Núñez, R.; Tobias, G. *Chem. Eur. J.* **2015**, *21*, 16792.

(17) Brynda, J.; Cigler, P.; Grüner, B.; Maloy, R. P.; Marder, P.; Sicha, V.; Bakardjiev, M.; Holub, J.; Dzubak, P.; Hajduch, M. *Carbonic anhydrase inhibitors and method of their production*. Patent PCT/CZ2012/000106, **2013**.

(18) W, K.; Konig, W.; König, W.; Geiger, R. *Chem. Ber.* **1970**, *103*, 788.

(19) El-Faham, A.; Albericio, F. *Chem. Rev.* **2011**, *111*, 6557.

(20) Xue, Y.; Liu, Y.; Lu, F.; Qu, J.; Chen, H.; Dai, L. *J. Phys. Chem. Lett.* **2012**, *3*, 1607.

(21) Il'inchik, E. A.; Volkov, V. V.; Mazalov, L. N. *J. Struct. Chem.* **2005**, *46*, 523.

(22) Stankovich, S.; Dikin, D. A.; Piner, R. D.; Kohlhaas, K. A.; Kleinhammes, A.; Jia, Y.; Wu, Y.; Nguyen, S. T.; Ruoff, R. S. *Carbon* **2007**, *45*, 1558.

(23) Paredes, J. I.; Villar-Rodil, S.; Martínez-Alonso, A.; Tascón, J. M. D. *Langmuir* **2008**, *24*, 10560.

(24) Li, D.; Muller, M. B.; Gilje, S.; Kaner, R. B.; Wallace, G. G. *Nat. Nano* **2008**, *3*, 101.

(25) Sandoval, S.; Kumar, N.; Oro-Solé, J.; Sundaresan, A.; Rao, C. N. R.; Fuertes, A.; Tobias, G. *Carbon* **2016**, *96*, 594.

(26) Núñez, R.; Juárez-Pérez, E. J.; Teixidor, F.; Santillan, R.; Farfán, N.; Abreu, A.; Yépez, R.; Viñas, C. *Inorg. Chem.* **2010**, *49*, 9993.

CONCLUSIONES

9. CONCLUSIONES

Capítulo 3:

1. Se han sintetizado mediante reacciones de Heck y con buen rendimiento *trans*-estilbenos sustituidos con 1 y 2 derivados del *o*-carborano y *m*-carborano enlazados sobre el primer C_c, y con -Me o -Ph sobre el segundo C_c sobre el segundo C_c (**15**-**22**). Fue necesario sintetizar previamente los precursores que contienen el grupo estirenil (**7**-**10**). Todos los compuestos han sido caracterizados por RMN, IR MALDI-TOF, análisis elemental y además, se resolvieron las estructuras cristalinas de **12**, **13**, **15**, **18 19**, **20** y **21** mediante difracción de rayos-X.

2. El estudio fotofísico revela, que los espectros de UV-Vis presentan un patrón similar al fluoróforo que portan (estireno o estilbeno), con ligeras variaciones en la λ_{abs} máxima. tan sólo en derivados de *o*-carborano con el sustituyente *Ph* (**10**, **16** y **20**) se produce un *quenching* de la fluorescencia, atribuido a un proceso de Transferencia de Carga Intermolecular (ICT) hacia el clúster. Además los cálculos DFT predicen claramente este proceso para **10** y en el caso de **16** y **20**, predicen un porcentaje de contribución del grupo *Ph* al orbital LUMO superior al resto de compuestos. Los valores de Φ_F arrojan un resultado de gran relevancia y es que, a excepción de los compuestos mencionados **10**, **16** y **20**, en el resto de los casos la presencia de 1 clúster boro incrementa el Φ_F del estilbeno (Φ_F = 5 %) a valores entre 7.1 y 9.8 %, y la presencia de 2 clústeres, lo incrementa hasta valores entre 16.2 y 19.3 %. Este fenómeno podría deberse a una disminución de la desactivación por fotoisomerización *trans* →*cis* al aumentar la rigidez de la molécula, o a que la presencia de los clústeres evite en cierta medida las interacciones tipo π-π *stacking* entre los estilbenos.

Capítulo 4:

3. Se han sintetizado mediante reacciones SN_2 y de Heck, nuevos derivados de *o*-carborano y *m*-carborano disustituidos con 2 grupos estilbenil en ambos C_c (**29**-**30**). Además en el caso del m-carborano, se prepararon estos compuestos con 1 y 2 átomos de yodo sobre vértices de B (**31**-**32**). Los compuestos han sido totalmente caracterizados por RMN, IR y análisis elemental y. además, se resolvieron mediante difracción de rayos-X las estructuras cristalinas de **28**, **29**, **30** y **32**. En la estructura de **29** los estilbenos se disponen de forma colineal mientras que, en **30** adoptan una orientación *face-to-edge* estabilizada por débiles interacciones intramoleculares CH-π.

4. El estudio fotofísico en disolución no revela grandes diferencias entre los compuestos, con un comportamiento similar al estilbeno libre y Φ_F entre 5-7.7 %. Sin embargo, en estado sólido la emisión del derivado *orto* (**29**) se muestra desestructurada, mientras que los derivados *meta* presentan la estructura típica del estilbeno pero con un gran desplazamiento al rojo. Los Φ_{Abs} son muy superiores en estado sólido, en el rango de 11.6-37.8 % y siguiendo claramente el siguiente orden: de **30**>**31**>**32**>**29**. La gran diferencia en la capacidad de emisión entre los análogos *orto* (**29**) y *meta* (**30**), podría deberse a la limitación de la desactivación por isomerización en **30** debido a las interacciones intramoleculares CH-π. La presencia de vértices B-I producen una disminución del Φ_{Abs} en estado sólido, posiblemente por existir un proceso efectivo de ISC.

5. Los nuevos derivados heterosustituidos, se consideran potenciales precursores en la preparación de agentes teragnósticos, que combinan los fluoróforos en los C_c, la actividad terapéutica de los carboranos y, vértices B-I fáciles de derivatizar a vértices B-R, pudiendo ser R una biomolécula de interés.

Capítulo 5:

6. Se han preparado mediante reacciones de metátesis y Heck, moléculas basadas en un núcleo de octasilsesquioxano, funcionalizado en sus 8 vértices de Si con diferentes carboranos, a través de un grupo vinil-estilbeno (**34**-**37**) y rendimientos entre el 43-65 %. Los compuestos han sido totalmente caracterizados por RMN, IR y análisis elemental.

7. Las propiedades fotofísicas en disolución muestran que tienen una gran intensidad de fluorescencia, con Φ_F entre 21 y 59 %. De nuevo, el sustituyente –H, -Me o -Ph en el segundo C_c del *o*-carborano es capaz de regular la capacidad de emisión fluorescente (**34**>**35**>**36**), mientras que en el derivado de Ph-*m*-carborano (**37**) supone un aumento de fluorescencia respecto a su análogo **36**. En estado sólido, se detecta un gran desplazamiento al rojo de la emisión y una drástica disminución del Φ_F, lo que se ha atribuido a un posible efecto de *Aggregation Cause Quenching* (ACQ).

8. El estudio de estabilidad térmica revela un aumento de la misma entre 200-300 °C respecto al octavinilsilsesquioxano (OVS) de partida.

9. La incorporación de propiedades fotoluminiscentes y la mejora de la estabilidad térmica, podría derivar en nuevos estudios en para la aplicabilidad de estos nuevos silsesquioxanos en cerámicas o polímeros que requieran estas propiedades.

Capítulo 6:

10. Se han preparado y caracterizado dendrímeros de núcleo porfirínico funcionalizados en la periferia con 4, 8, 16 y hasta 32 carboranos. Para ello, se emplearon reacciones de hidrosililación obteniendo los productos finales con altos rendimientos (69-88 %).

11. La presencia de los clústeres de boro no alteran el comportamiento fotofísico de los núcleos de porfirina.

12. Mediante DOSY, se ha podido determinar el radio hidrodinámico (R_H) de los dendrímeros, pudiendo establecer una buena relación matemática entre su peso molecular y el tamaño.

13. Se han realizado los primeros test de citotoxicidad, pero es necesario mejorar la solubilidad de los compuestos, y por ello el estudio continúa tras la encapsulación de los dendrímeros en liposomas que mejoran el grado de solubilidad.

Capítulo 7:

14. Se han sintetizado mediante reacciones de Heck, moléculas con núcleo de OVS, funcionalizado con 8 unidades de los derivados apropiados de cobaltabisdicalballuro y ferrabisdicarbralluro, obteniendo los compuestos **[46]**$^{-8}$ y **[47]**$^{-8}$ con rendimientos del 83 y 46 %, respectivamente. Los dendrímeros finales han sido caracterizados por RMN, IR y análisis elemental y además, se ha corroborado que la funcionalización ha sido completa mediante UV-Vis.

15. El estudio de la voltamperometría cíclica de estos compuestos muestra 1 único proceso redox, por tanto los 8 metalacarboranos de cada compuesto son unidades electroactivas equivalentes. Se ha determinado el R_H de las moléculas, entre 16-17 Å, valor suficientemente pequeño para que se pueda producir el proceso redox en todos los metalacarboranos de la periferia de estos compuestos. Además, se ha demostrado que todos los metalacarboranos sufren el proceso redox realizando una reducción química que fue corroborada mediante el estudio del ^{11}B RMN.

16. Los análisis termogravimétricos (ATG) revelan que, la presencia de los metalacarboranos suponen un aumento de la estabilidad del OVS de 150-200 °C.

17. La aplicabilidad de actual de los silsesquioxanos en ciencia de materiales y los resultados obtenidos en este estudio, nos ha planteado realizar futuros estudios donde se apliquen estos compuestos como aditivos en polímeros conductores.

Capítulo 8:

18. Se han preparado materiales híbridos basados en grafeno y clústeres de boro. Se ha funcionalizado el óxido de grafeno (GO) mediante reacciones de condensación de los ácidos carboxílicos y apertura de ciclos epóxido de esta plataforma, con derivados del cobaltabisdicarballuto y *closo*-dodecaborato que contienen un grupo amino terminal, obteniendo los materiales **Cosane-GO** y **B_{12}-GO**, respectivamente. Los nuevos materiales han sido caracterizados por IR y XPS, corroborando la modificación química del GO. Además, con la técnica de STEM-EDX pudo identificarse la presencia de Co en el caso del **Cosane-GO**, y mediante SAED se confirmó que el *closo*-dodecaborato no se encontraba adsorbido sino que, se une químicamente como unidades independientes. Finalmente destaca la detección de B y C mediante EELS y el mapeado de estos elementos con EFTEM confirma una distribución uniforme de los clústeres sobre la superfice. El grado de funcionalización fue determinado por ATG, con valores del 18.3 y 20.8 % m/m para **B_{12}-GO** y **Cosane-GO**, respectivamente.

19. Es de gran relevancia la mejora obtenida en la estabilidad de las dispersiones en agua de los híbridos respecto al GO, de forma que al cabo de 1 mes se mantienen prácticamente inalteradas. Además, también se comprobó que ambos materiales se dispersan bien en acetona, a diferencia del GO, y que en el caso del **Cosane-GO** también la mejora en THF.

20. Esta mejora de propiedades se considera de enorme relevancia al facilitar posteriores modificaciones químicas del GO y, por la importancia de la dispersabilidad en agua requerida en los estudios celulares que se llevarán a cabo.

ANEXO I: ARTÍCULOS PUBLICADOS

Aprobados para la presentación como compendio de publicaciones por la Comisión de Doctorado en Química de Universidad Autónoma de Barcelona el 7 de marzo de 2016.

Inorganic Chemistry

Article

pubs.acs.org/IC

High-Boron-Content Porphyrin-Cored Aryl Ether Dendrimers: Controlled Synthesis, Characterization, and Photophysical Properties

Justo Cabrera-González,[†,‡] Elba Xochitiotzi-Flores,[§,‡] Clara Viñas,[†] Francesc Teixidor,[†] Héctor García-Ortega,[§] Norberto Farfán,[§] Rosa Santillan,[⊥] Teodor Parella,[∥] and Rosario Núñez*[,†]

[†]Institut de Ciència de Materials de Barcelona (ICMAB-CSIC), Campus UAB, 08193 Bellaterra, Barcelona, Spain

[§]Facultad de Química, Departamento de Química Orgánica, Universidad Nacional Autónoma de México (UNAM), 04510 México D.F., México

[⊥]Departamento de Química, Centro de Investigación y de Estudios Avanzados del IPN, Apartado Postal 14-740, 07000 México D.F., México

[∥]Servei de Ressonància Magnètica Nuclear, Universitat Autònoma de Barcelona (UAB), E-08193 Bellaterra, Barcelona, Spain

Supporting Information

ABSTRACT: The synthesis and characterization of a set of poly(aryl ether) dendrimers with tetraphenylporphyrin as the core and 4, 8, 16, or 32 *closo*-carborane clusters are described. A regioselective hydrosilylation reaction on the allyl-terminated functions with carboranylsilanes in the presence of Karstedt's catalyst leads to different generations of boron-enriched dendrimers. This versatile approach allows the incorporation of a large number of boron atoms in the dendrimers' periphery. Translational diffusion coefficients (D) determined by DOSY NMR experiments permit estimation of the hydrodynamic radius (R_H) and molecular size for each dendrimer. Furthermore, a notable correlation between D and the molecular weight (MW) is found and can be used to predict their overall size and folding properties. The UV−vis and emission behavior are not largely affected by the functionalization, therefore implying that the presence of carboranes does not alter their photoluminescence properties.

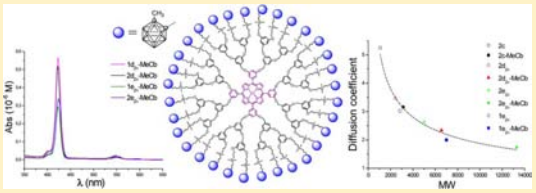

INTRODUCTION

Dendrimers are treelike branched polymers with low polydispersity and a high degree of versatility that tend to adopt globular structures with a well-defined three-dimensional shape.[1] Since the first synthesis reported by Tomalia et al.,[2] these materials have attracted the attention of many research groups because they can be built in a controlled manner, allowing versatility in the nucleus, branching units, or dendrons as well as in the terminal groups.[3] This allows one to change the properties of dendrimers and also to modulate their behavior, with the goal centered on the design and synthesis of dendrimers more specific for certain areas,[4] such as carriers for drug delivery.[5,6] For all of these reasons, they emerged as a new appealing class of particles for nanomedicine.[7] In this respect, boron-enriched dendrimers have been developed for different groups as boron carriers for boron neutron capture therapy (BNCT).[8−10] Our group has also contributed to the search of synthetic strategies for the preparation of high-boron-content neutral dendrimeric systems that incorporate *closo*-carboranes[11,12] and water-soluble polyanionic dendrimers bearing *nido*-carborane[13−15] as well as metallodendrimers containing cobaltabis(dicarbollide) fragments.[16−18] As is well-known, icosahedral carborane derivatives have recently attracted much attention in biomedical and medicinal applications because of their extraordinary characteristics.[19] The hydrophobic character of carboranes can enhance the interactions between pharmaceuticals and their receptors,[20−24] and they have been extensively involved in areas of drug discovery, such as pharmacophores and biologically active compounds.[25−28] During the last decades, several boron-containing porphyrins, with *closo*-carborane[29,30] and *nido*-carborane,[31] have been synthesized and evaluated in vitro and in vivo as promising BNCT agents.[32−35] The combined action of a porphyrin used as a core with dendrons of poly(aryl ether) for the synthesis of dendrimers was first reported by Inoue and collaborators.[36] By using Fréchet's methodology, they prepared an iron porphyrin covalently encapsulated within a large aryl ether dendrimer cage as the first monomolecular model of hemoproteins.[37]

On the basis of both the biocompatibility of porphyrin-cored poly(aryl ether) dendrimers[38−42] and the bioactivity of carborane-containing molecules,[21] in this work our goal is the synthesis and characterization of dendrimers that contain a large number of carborane clusters, in order to obtain biocompatible boron-rich molecules. Synthetic aspects as well as a complete characterization of free-base and zinc-metalated porphyrin-cored dendrimers before and after the incorporation of *closo*-carboranes are discussed. The molecular sizes for these

Received: March 20, 2015
Published: April 29, 2015

DOI: 10.1021/acs.inorgchem.5b00618
Inorg. Chem. 2015, 54, 5021−5031

Scheme 1. Route of the Preparation of Dendrimers 1c−1e and 2c−2e

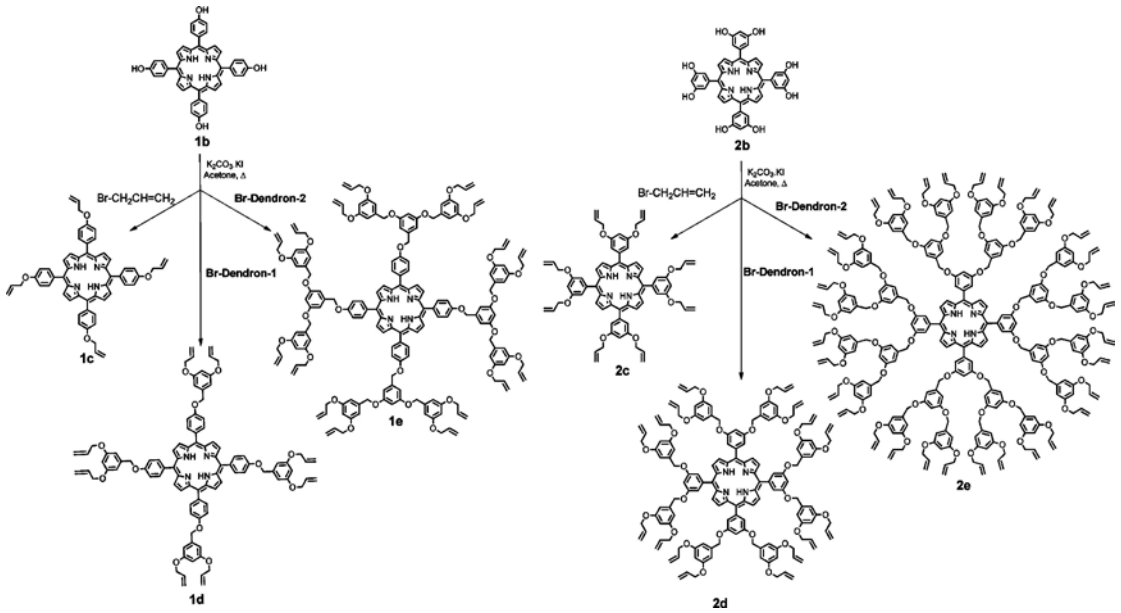

Scheme 2. Metalation of the Porphyrin Core of Dendrimers 1d−1e and 2d−2e with Zinc(II)

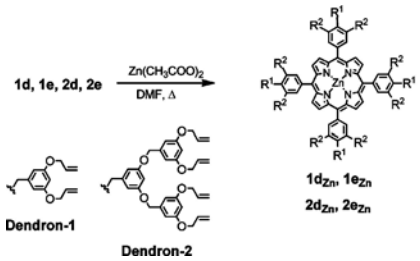

Compound	R^1	R^2
$1d_{Zn}$	Dendron-1	H
$1e_{Zn}$	Dendron-2	H
$2d_{Zn}$	H	Dendron-1
$2e_{Zn}$	H	Dendron-2

kinds of dendrimers were estimated before and after the incorporation of carborane clusters from their hydrodynamic radii (R_H), which were determined using translational diffusion coefficients (D) from DOSY NMR experiments. A comparative study of the absorption and emission properties for all compounds has been carried out, and the influence of the cluster attached to the dendrimer periphery on these photophysical properties has been investigated. We currently focus our research on the study of the biocompatibility and cytotoxicity of these dendrimers for potential biomedical applications.

RESULTS AND DISCUSSION

Synthesis of Carboranyl-Containing Porphyrin-Cored Dendrimers. Different generations of poly(aryl ether) dendrimers with terminal allyl ether groups and a porphyrin as the core have been used as a platform to prepare high-boron-content macromolecules after functionalization with carboranyl fragments. The preparation of the porphyrin macrocycles **1a**[43] and **2a**[44] was carried out from *p*-methoxybenzaldehyde or 3,5-dimethoxybenzaldehyde in the presence of pyrrole and propionic acid as a reaction medium (see the Supporting Information, SI).[45,46] After demethylation with HBr and CH_3COOH,[47] porphyrin cores **1b**[48] and **2b**[49] were obtained (see the SI). On the other hand, Fréchet dendron types, **Br-dendron-1** and **Br-dendron-2**, with allyl groups at the periphery were prepared by esterification of 3,5-dihydroxybenzoic acid in methanol and H_2SO_4, followed by coupling with allyl bromide in the presence of K_2CO_3, KI, and acetone. The subsequent reduction of the ester with $LiAlH_4$ in tetrahydrofuran gave benzylic alcohol, which was treated with $SOCl_2$ and pyridine to generate **Br-dendron-1**.[50−53] From the reaction of 3,5-dihydroxybenzylic alcohol and **Br-dendron-1**, a second derivative of benzylic alcohol was obtained and submitted to a second halogenation to give **Br-dendron-2**.[54,55] The spectroscopic data for dendrons and intermediates are in agreement with those reported in the literature. The reaction of porphyrins **Ib** or **2b** with allyl bromide, **Br-dendron-1**, or **Br-dendron-2** in acetone in the presence of K_2CO_3 and KI leads to the formation of dendrimers with 4 (**1c**),[56] 8 (**1d** and **2c**), 16 (**1e** and **2d**), and 32 (**2e**) allyl groups at the periphery (Scheme 1). Likewise, metalation of the porphyrins in the dendrimers was carried out using *N*,*N*-dimethylformamide (DMF) and $Zn(CH_3COO)_2{\cdot}2H_2O$ (Scheme 2).[46] With

DOI: 10.1021/acs.inorgchem.5b00618
Inorg. Chem. 2015, 54, 5021−5031

Scheme 3. Hydrosilylation Reaction To Obtain Dendrimer $1e_{Zn}$-MeCb

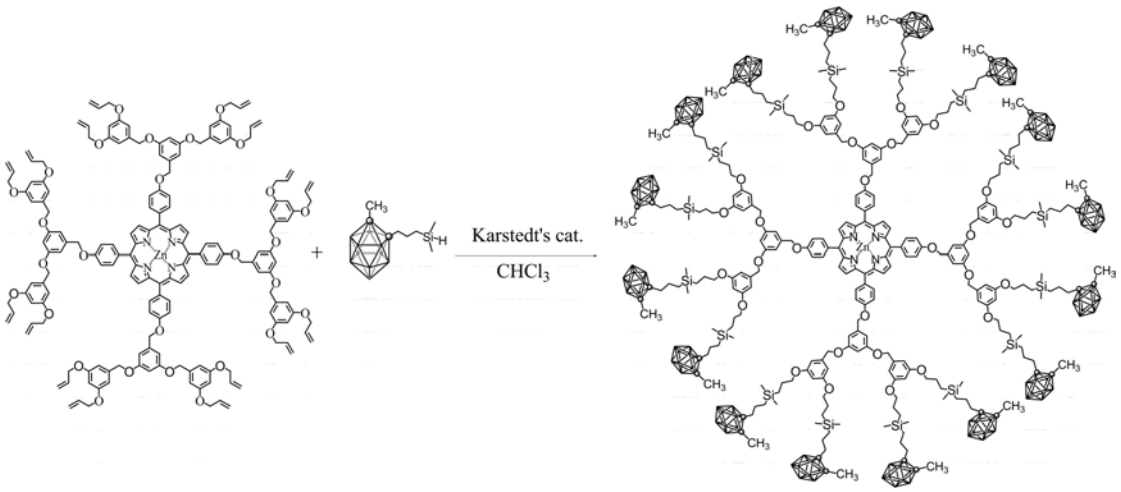

the aim of obtaining high-boron-rich porphyrin-cored dendrimers, we have selected some of these dendritic structures, either free base or zinc porphyrins, to be functionalized with carboranyl derivatives via catalytic hydrosilylation reactions. This approach has already been used before by our group and represents a versatile and efficient methodology to introduce a large number of boron atoms into a molecule.[15] The carboranylsilane 1-CH_3-2-[$CH_2CH_2CH_2(CH_3)_2SiH$]-1,2-*closo*-$C_2B_{10}H_{10}$ was used as the hydrosilylating agent; this is a suitable choice because this precursor is obtained in a fast way and with high yield and has shown to be very efficient in previous hydrosilylation reactions.[12]

To functionalize the periphery of the different generations of porphyrin-cored dendrimers, hydrosilylation reactions of the terminal allyl groups with carboranylsilane were carried out. All reactions were catalyzed by Karstedt's catalyst[57] with the purpose of controlling the regioselectivity of the reaction to obtain the desired β isomers (Scheme 3). Nevertheless, for the different dendrimers, a large number of experiments were performed to find the optima and specific conditions in terms of the stoichiometry, solvent, temperature, and time of reaction. The synthesis of compound **1c-MeCb** (see Figure S1 in the SI) was performed in a minimum volume of CH_2Cl_2, while the syntheses of **1d-MeCb** (Figure 1) and **$1d_{Zn}$-MeCb** were carried out in $CHCl_3$ using a ratio of dendrimer/hydrosilylating agent of 1:1.5 at 50 °C for 5 h in the presence of Karstedt's catalyst (see Scheme 3 as an example of the synthesis of **$1e_{Zn}$-MeCb**). In the case of compound **2c-MeCb**, a higher ratio of carboranylsilane, 1:2, was necessary. To prepare higher generations of dendrimers, **$1e_{Zn}$-MeCb**, **$2d_{Zn}$-MeCb**, and **$2e_{Zn}$-MeCb** (see Figure 1), 1,4-dioxane was used as the solvent because the starting dendrimers were not soluble or the reaction did not work well in other solvents, allowing an increase of the temperature. Besides, a higher ratio of carboranylsilane corresponding to a 100% excess was required for complete hydrosilylation of all terminal allyl groups (16 or 32; Scheme 3).

Hydrosilylation reactions were monitored by ^{1}H NMR spectroscopy to determine completion of the reaction upon the disappearance of the allyl proton resonances of the starting

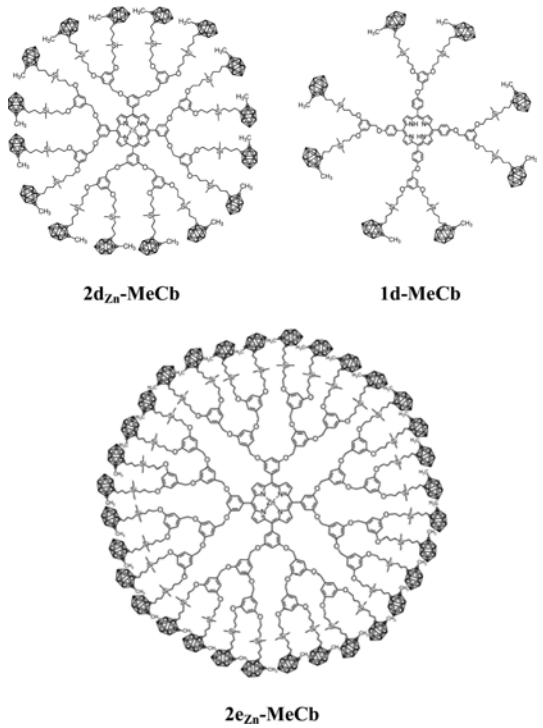

Figure 1. Structural representation of some carboranyl-containing porphyrin-cored dendrimers.

dendrimers; also important is monitoring of the O−CH_2 resonance (H-15 in Figure 2) because after functionalization the signal is shifted to lower frequencies. The preparation of pure compounds is a requirement for the development of compounds especially for biological applications. Therefore, because of the presence of Karstedt's catalyst, a further purification of the functionalized molecules by thin-layer

DOI: 10.1021/acs.inorgchem.5b00618
Inorg. Chem. 2015, 54, 5021−5031

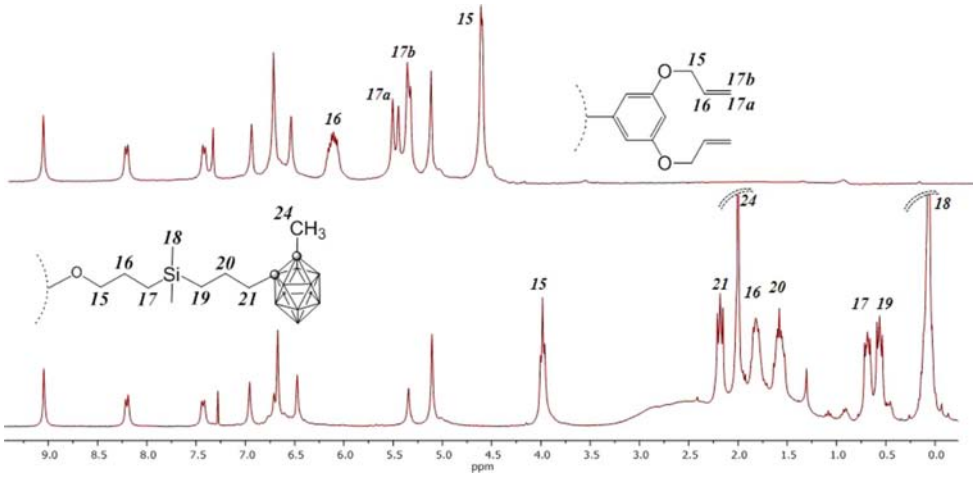

Figure 2. ^{1}H NMR spectra of dendrimer **1e$_{Zn}$-MeCb** before and after functionalization with carborane clusters.

chromatography (TLC) was necessary. This made it possible to recover almost all of the excess carboranylsilane used in the reactions. After that, all carboranyl-containing dendrimers were isolated in excellent yields, in the range 60−88%. Remarkably, reactions with zinc porphyrin cored dendrimers gave higher yields after functionalization with the carboranylsilanes than those from metal-free porphyrins. Indeed, some metal-free porphyrin dendrimer derivatives could not be fully functionalized; however, this could be achieved for the metalated cores. This may be due to coordination of the catalyst to the porphyrinic nitrogen atoms, which produces their partial deactivation.

Characterization of Carboranyl-Containing Porphyrin-Cored Dendrimers. The starting dendrimers were characterized by ^{1}H and ^{13}C NMR, electrospray ionization (ESI-MS), and the signals were assigned from two-dimensional (2D) HSQC experiments. The ^{1}H NMR spectra showed signals assigned to the core (H-β) and NH from 8.85 to 9.00 ppm and from −2.69 to −2.87 ppm, respectively; these NH signals disappear in the corresponding dendrimers with the zinc core, and the allylic signals appear in the range from 5.16 to 6.25 ppm. Likewise, the ^{13}C NMR spectra show signals at 131.2−133.2 ppm (C-β) and 119.9−120.9 ppm (*meso*-C) corresponding to the core. The signals for the allyl groups appear at 69.0−70.5 ppm (CH_2), 133.2−133.6 ppm (CH═CH_2), and 117.9−118.2 ppm (CH═CH_2). The structures of carboranyl-containing dendrimers were established by IR, ^{1}H, ^{13}C{^{1}H}, ^{11}B, and ^{11}B{^{1}H} NMR, and elemental analysis. The IR spectra of the carboranyl-containing dendrimers show the typical ν(B−H) strong bands for *closo* clusters around 2580 cm^{-1}. The absence of a band at 2112 cm^{-1} corresponding to ν(Si−H) from the silane function of the carboranylsilane indicates the total hydrosilylation of the alkene. In the ^{1}H NMR spectra, resonances in the range of 6.25−5.16 ppm due to the allyl protons have disappeared after hydrosilylation reaction, confirming anti-Markovnikov addition of the μ-SiH function to the double bonds and, subsequently, complete peripheral functionalization. In the latter compounds, the presence of new proton resonances in the −CH_2− region corroborates their formation. These resonances correspond to protons H-6 and H-7 in first-generation dendrimers, H-11 and H-12 in the second-generation dendrimers, and H-16 and H-17 in the third-generation dendrimers (see the SI). The ^{1}H NMR spectra for dendrimers bearing *closo* clusters also exhibit resonances at low frequencies, in the −0.11 to −0.08 ppm range for Si-CH_3 protons. In addition, all nonmetalated dendrimers show one resonance near −2.70 ppm due to the two NH protons of the porphyrinic core. The ^{13}C{^{1}H} NMR spectra show resonances attributed to the aromatic signal of the dendron, from 160.5 to 100.0 ppm for all compounds. After functionalization with carboranes, dendrimers show resonances in the region from 84.0 to 74.6 ppm attributed to $C_{cluster}$. The resonances for the Si−CH_3 units bonded to C_c appear around −3.5 ppm, whereas the −CH_2− carbon atoms are displayed in the range from 40.0 to 10.0 ppm.

The ^{11}B{^{1}H} NMR resonances for dendrimers decorated with clusters appear in the characteristic *closo* region, from −6.0 to −11.0 ppm, showing broad overlapped bands with the patterns 2:8. Different mass spectrometry techniques [ESI and matrix-assisted laser desorption ionization time-of-flight (MALDI-TOF)] were also used for characterization of the starting compounds. The formulas of the smaller dendrimers were well established by using ESI-MS showing the molecular ion peak; nevertheless, for the largest dendrimers, neither the ESI nor the MALDI-TOF mass spectra were useful, as important fragmentation was observed. A similar fragmentation had been previously observed for other boron-containing large molecules.[15,17,18]

Experimental Diffusion Coefficients and Estimated Hydrodynamic Radius of Dendrimers. Diffusion NMR experiments have been used to get an estimation of the overall molecular size of a set of six porphyrin-cored aryl ether dendrimers. We have compared dendrimers of different generations before and after functionalization with carboranes (**2c**, **2c-MeCb**, **2d$_{Zn}$**, **2d$_{Zn}$-MeCb**, **2e$_{Zn}$**, and **2e$_{Zn}$-MeCb**). To our knowledge, these are the first boron cluster-containing dendrimers characterized by this technique. Diffusion experiments are displayed using a DOSY (Diffusion-Ordered NMR SpectroscopY) representation, where the chemical shift is plotted versus the diffusion coefficient (D) in a 2D map.[58−60] In addition, diffusion experiments have the advantage of allowing measurement of the diffusion coefficient and

DOI: 10.1021/acs.inorgchem.5b00618
Inorg. Chem. 2015, 54, 5021−5031

estimation of the hydrodynamic radius (R_H) according to the Stokes–Einstein equation over a wide range of molecular weights (MW),[61] being a complementary tool to confirm the successful functionalization of our dendrimers. Figure 3 shows

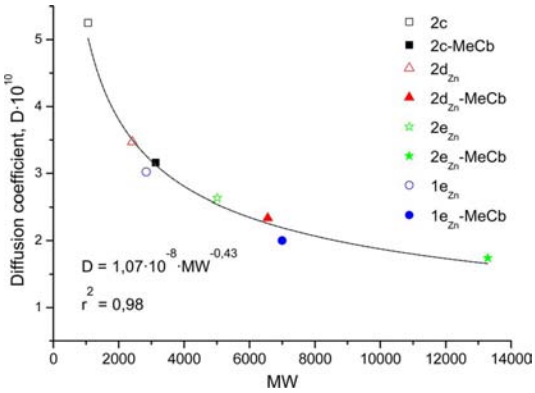

Figure 3. Diffusion coefficients (D) from DOSY experiments versus molecular weights (MW).

the experimental D values of dendrimers as a function of their MW values. The strong correlation between D and MW of the different dendrimers is remarkable, with a rough experimental dependence according to

$$D_A/D_B = (MW_B/MW_A)^a \quad (1)$$

where $a \sim 0.4$–0.5. The simple correlation between D and MW allows for the determination of a calibration curve that could also be applied to a wide range of related compounds under the same conditions of temperature and solvent. To prove this, we have run additional DOSY experiments for dendrimers **1e$_{Zn}$** and **1e$_{Zn}$-MeCb**, which have shown that their D values fit well in the calibration curve (Table 1 and Figure 3). The

Table 1. Diffusion Coefficients and Hydrodynamic Radii Determined by DOSY Experiments for Eight Different Dendrimers

dendrimer	molecular weight (MW)	diffusion coefficient (D)	hydrodynamic radii (R_H, Å)
2c	1063.3	5.25×10^{-10}	7.67
2c-MeCb	3131.1	3.16×10^{-10}	12.7
2d$_{Zn}$	2420.9	3.47×10^{-10}	11.6
2d$_{Zn}$-MeCb	6559.9	2.34×10^{-10}	17.2
2e$_{Zn}$	5014.0	2.63×10^{-10}	15.3
2e$_{Zn}$-MeCb	13290.7	1.74×10^{-10}	23.2
1e$_{Zn}$	2845.1	3.02×10^{-10}	13.3
1e$_{Zn}$-MeCb	6999.4	2.00×10^{-10}	20.2
$CDCl_3$		2.51×10^{-9}	1.60

corresponding R_H values have been calculated assuming that dendrimers are spherical (Table 1). Thus, when R_H for each generation of dendrimer is compared before and after functionalization, it is observed that the R_H value is higher for those dendrimers containing carborane clusters. Obviously, the estimated R_H values also enlarge in a consistent manner when the dendrimer generation is increased. As a general trend, it is observed that full functionalization implies an average increase of the MW by a factor about 2.5–3, a decrease of D by ~60–65%, and an increase of the estimated R_H by ~50–60%. The hydrodynamic radii (R_H) values from this work are in good agreement with the sole result on these parameters obtained for phenyl-terminated porphyrin-cored aryl ether dendrimers from other methodology (global analysis of the fluorescence anisotropy decay).[62] It has been reported that the D value of a given known species or the MW from an unknown compound can be roughly predicted based on the relationship

$$\log(D) = a \log(MW) + b \quad (2)$$

where a and b are two coefficients that depend on the solvent and sample concentration with average values of about $a = -0.62$ and $b = -7.49$ for a $CDCl_3$ solution.[63] In general, eq 2 works well for the smaller dendrimers and shows some deviations for the larger ones, which is attributed to a major relative degree of molecular folding. This is in agreement with our experimental data represented in the curve of Figure 3.

Photophysical Properties of Dendrimers. The UV–vis spectra in $CHCl_3$ of the starting dendrimers are similar to those in tetraphenylporphyrin (TPP),[64] with a maximum absorption for the Soret band from 422 to 423 nm, which is red-shifted by 1–2 nm when the core is metalated (Figure S3 in the SI and Table 2). They show molar extinction coefficients (ε) between

Table 2. Absorption Data of Dendrimers before and after Functionalization with Carborane Clusters

dendrimer	$\varepsilon \times 10^{-5}$	λ Soret band	Q_1 band	Q_2 band
1c	3.43	422	519	556
1d	3.43	423	519	556
1e	3.63	423	519	559
2c	3.80	422	515	548
2d	2.40	423	516	552
2e	2.68	423	517	553
1d$_{Zn}$	4.30	423	550	
1e$_{Zn}$	2.61	424	551	
2d$_{Zn}$	3.03	423	549	
2e$_{Zn}$	3.32	425	550	
1c-MeCb	4.97	423	519	556
1d-MeCb	3.49	422	513	550
2c-MeCb	2.52	422	514	550
2d$_{Zn}$-MeCb	5.18	423	547	
1e$_{Zn}$-MeCb	9.50	424	550	
2e$_{Zn}$-MeCb	3.38	424	550	
1d$_{Zn}$-MeCb	5.64	423	551	

2.40×10^5 and 4.30×10^5 M. Typical Q bands were also observed in all starting dendrimers: the Q_1 band was observed from 515 to 519 nm for free-base porphyrin dendrimers, whereas for metalated porphyrin dendrimers, this band appears between 549 and 551 nm, which is around 33 nm red-shifted (Table 2). As is usual, the Q_2 band was only observed for nonmetalated porphyrin dendrimers, in the range from 548 to 559 nm. The excitation and emission spectra of starting dendrimers in $CHCl_3$ are similar to isolated base-free TTP and zinc tetraphenylporphyrin (Table 3 and Figure 4). When free-base porphyrin dendrimers were irradiated at 422 nm, high-intensity emission bands of around 650–658 nm were observed in the emission spectra, whereas other bands of lower intensity were found to be close to 720 nm. On the other hand, for zinc-metalated porphyrin dendrimers, the emission maximum bands are those of low energy at around 650 nm, while the emission bands near 600 nm exhibit lower intensity. The UV–vis

DOI: 10.1021/acs.inorgchem.5b00618
Inorg. Chem. 2015, 54, 5021–5031

Table 3. Emission Data of Dendrimers before and after Functionalization with Carborane Cages

dendrimer	λ_{max} Em 1	λ_{max} Em 2
1c	657	724
1d	657	723
1e	658	724
2c	650	715
2d	651	716
2e	650	717
1d$_{Zn}$	602	649
1e$_{Zn}$	602	650
2d$_{Zn}$	596	645
2e$_{Zn}$	601	646
1c-MeCb	657	711
1d-MeCb	656	711
2c-MeCb	649	704
2d$_{Zn}$-MeCb	596	643
1e$_{Zn}$-MeCb	604	644
2e$_{Zn}$-MeCb	599	641
1d$_{Zn}$-MeCb	603	645

absorption and emission spectra of carboranyl-containing porphyrin-cored dendrimers in $CHCl_3$ are shown in Figures 5 and 6, respectively. The UV−vis absorption spectra of carboranyl-functionalized dendrimers are similar to those of the noncarboranyl functionalized ones with Soret bands at 422−424 nm, Q_1 bands at 514−550 nm, and Q_2 bands at 550−556 nm, in some cases blue-shifted by 1−6 nm (see Table 2). Neither the Soret nor the Q bands undergo major changes upon an increase in the dendrimer generation or the number of boron clusters on the periphery. Nevertheless, the zinc porphyrin cored dendrimers exhibit absorption maxima at around 423−424 nm, and a small red shift of ∼1−2 nm of the Soret band is observed as the generation number increases. This effect is typical for these kinds of porphyrin-cored dendrimers, for which Aida et al. suggested that the red shift is associated with the encapsulation degree of the porphyrin into the dendrimer,[65] whereas Fréchet et al. proposed that the red shift of the Soret band is an indication of weak interactions between the core and branches.[62] If we compare the emission spectra of carboranyl-containing dendrimers with the unmodified one, it is noticed that no remarkable differences are observed. For nonmetalated dendrimers, emission maxima are observed between 649 and 657 nm, whereas for zinc porphyrin cored dendrimers, two emission bands are observed, with maxima in the range of 596−604 nm, 4−5 nm blue-shifted with respect to the starting dendrimers (Table 3). As was expected, the encapsulation of emitting porphyrins using poly(aryl ether) dendritic structures does not cause an enhancement of their luminescent properties. In the dendrimers reported here, the size of the dendrimer framework has little influence on the fluorescence properties of the core porphyrins,[66] and the fact that the carboranyl-containing dendrimers show a behavior similar to that of the starting ones without boron clusters indicates that the presence of the peripheral carborane units does not have a major influence on the photophysical properties of the porphyrin core.

CONCLUSIONS

A set of new boron-enriched porphyrin-cored aryl ether dendrimers have been obtained by regioselective hydrosilylation of allyl terminal groups with the adequate carboranylsilane. The synthesis of these dendrimers is highly controlled, and the reaction conditions are optimized for each one. Dendrimers have been fully characterized by IR and NMR spectroscopy as well as elemental analysis. In addition, the diffusion coefficients (D) of some dendrimers before and after functionalization with carborane derivatives have been determined by DOSY experiments, and the hydrodynamic radius (R_H) has been calculated using the Stokes−Einstein equation. A notable correlation between D and MW of dendrimers has been found that can be extrapolated to a wide range of related compounds under the same conditions of temperature and solvent to predict their overall size and folding properties. This technique can be used as a complementary tool to confirm the successful functionalization of our dendrimers with carboranes and could possibly be extended to other functionalities. The UV−vis spectra show the characteristic Soret and Q bands for the porphyrin, which are not largely affected by the dendritic branches or the number of carborane clusters. The emission behavior, before and after functionalization of dendrimers, indicates that there are no changes in the photoluminescence (PL) properties after the incorporation of cages, so that the introduction of carborane clusters to the dendrimeric skeleton does not alter their PL behavior, a facet

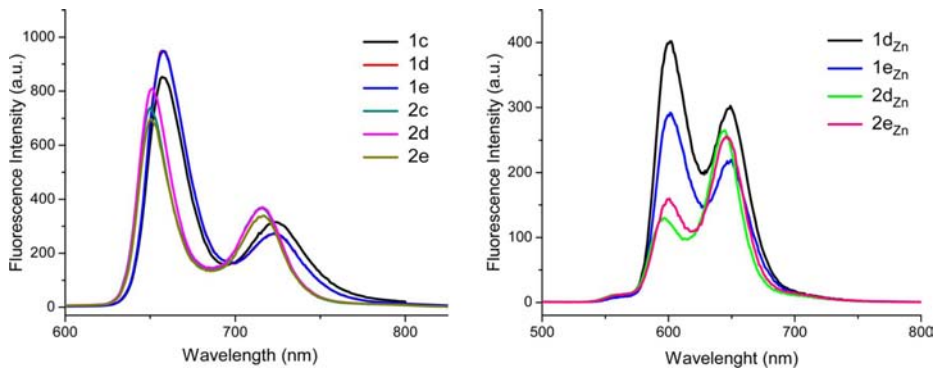

Figure 4. Emission spectra of starting porphyrin-cored dendrimers in $CHCl_3$ (λ_{ex} = 422 nm): free-base dendrimers (left); metalated dendrimers (right).

DOI: 10.1021/acs.inorgchem.5b00618
Inorg. Chem. 2015, 54, 5021−5031

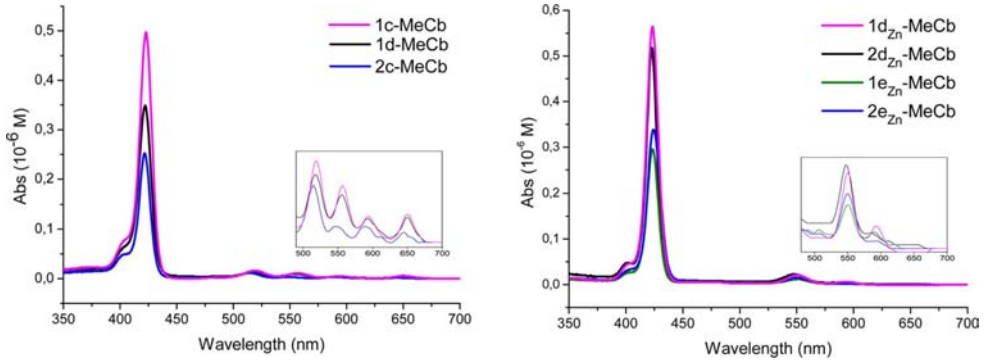

Figure 5. UV−vis spectra in $CHCl_3$ of carboranyl-containing dendrimers: free-base dendrimers (left); metalated dendrimers (right).

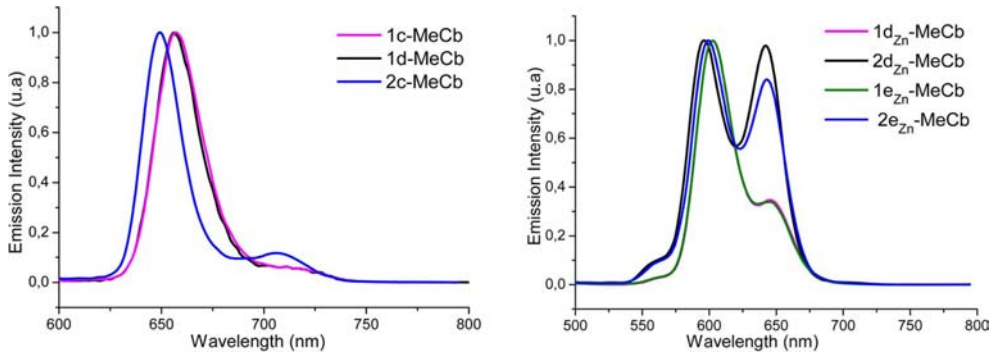

Figure 6. Emission spectra of carboranyl-containing dendrimers in $CHCl_3$ (λ_{ex} = 422 nm): free-base dendrimers (left); metalated dendrimers (right).

that can be important to benefitting from the individual property of the porphyrin and carborane clusters.

EXPERIMENTAL SECTION

Instrumentation. IR spectra were measured on PerkinElmer Spectrum 400 FT-IR/FT-FIR and Shimadzu FTIR-ATR-8300 spectrophotometers (units are reciprocal centimeters). ^{1}H NMR (300.13 and 400 MHz) and $^{13}C\{^1H\}$ (75.47 and 100.5 MHz) spectra were recorded using Varian Unity Inova 400 MHz and Bruker ARX 300 spectrometers. The ^{11}B NMR (96.29 MHz) spectra were recorded on a Bruker ARX 300 spectrometer. All experiments were done with concentrations between 15 and 20 mg/mL at 25 °C. Chemical shifts (ppm) are relative to $Si(CH_3)_4$ for ^{1}H (of residual proton; 7.25 ppm) and ^{13}C (77.23 ppm) in $CDCl_3$. Chemical shift values for ^{11}B NMR spectra were referenced to external $BF_3{\cdot}OEt_2$. Chemical shifts are reported in units of parts per million downfield from the reference, and all coupling constants are reported in Hertz. Mass spectra were obtained from a Thermo-Electron DFS spectrometer instrument by an electron impact (EI) ionization technique, and the AB SCIEX 4800 Plus MALDI TOF/TOF analyzer has the highest sensitivity available in MS and MS/MS mode. UV−vis spectra were recorded on PerkinElmer Lambda 900 and Shimadzu UV-1700 Pharmaspec spectrophotometers using 1.0 cm cuvettes. The fluorescence emission spectra of the starting dendrimers were recorded on a Varian Cary Eclipse fluorescence spectrometer. The fluorescence emission spectra of the carboranyl-containing dendrimers were recorded on a PerkinElmer LS-45 (230 V) fluorescence spectrometer. Samples were prepared in spectroscopic-grade solvents and adjusted to a response within the linear range. No fluorescent contaminants were detected upon excitation in the wavelength region of experimental interest. Elemental analyses were performed using a Carlo Erba EA1108 microanalyzer.

Materials. All reactions were performed under an atmosphere of dinitrogen employing standard Schlenk techniques. The solvents were reagent grade and were purified by distillation from the appropriate drying agents before use. The pyrrole, *p*-$CH_3OC_6H_4CHO$, 3,5-$(CH_3O)_2C_6H_4CHO$, CH_3CH_2COOH, 48% HBr, allyl bromide, $LiAlH_4$, $SOCl_2$, C_5H_5N, and K_2CO_3 were provided by Sigma-Aldrich, glacial CH_3COOH was provided by J. T. Baker, and 1-CH_3-1,2-*closo*-$C_2B_{10}H_{11}$ was supplied by Katchem Ltd. (Prague) and used as received. Karstedt's catalyst (9.21% Pt) was purchased from Johnson Matthey. The *n*-BuLi solution (1.6 M in hexanes) and 1-(CH_3)-2-$[CH_2CH_2CH_2Si(CH_3)_2H]$-1,2-*closo*-$C_2B_{10}H_{10}$ were prepared according to the literature.[12] Compounds **1a**,[43] **2a**,[44] **1b**,[48] **2b**,[49] **Br-dendron-1**,[50−53] and **Br-dendron-2**,[54,55] were prepared following literature processes; in some specific cases, little modification was done (see the SI). UV−vis spectroscopic data for all of these are in agreement with the data reported in the literature.

Procedure for the Preparation of Dendrimers 1c−1e and 2c−2e. A round-bottomed flask equipped with a condenser and a magnetic stirring bar was charged with porphyrin **1b** or **2b**, allyl bromide, or **Br-dendron-1** or **Br-dendron-2**, with K_2CO_3 and a catalytic amount of KI, using acetone as the solvent. The mixture was refluxed for 16 h, monitoring the reaction by TLC. After that, the reaction mixture was filtered and the volatiles were evaporated under vacuum. The solid product was washed with hexane and methanol to remove impurities to obtain dendrimers **1c** with 4, **1d** and **2c** with 8, **1e** and **2d** with 16, and finally **2e** with 32 allyl groups present in the periphery of the dendrimers.

*meso-Tetrakis(4-allyloxyphenyl)porphyrin (**1c**).* The title compound was prepared with **1b** (1.00 g, 1.50 mmol), allyl bromide (1.43 g, 11.70 mmol), K_2CO_3 (2.44 g), and a catalytic amount of KI in

DOI: 10.1021/acs.inorgchem.5b00618
Inorg. Chem. 2015, 54, 5021−5031

acetone. Compound **1c** was obtained as a purple solid (1.07 g, 87% yield). Mp: 250−252 °C. ^{1}H NMR ($CDCl_3$, 300 MHz): δ 8.85 (s, 8H, H-β), 8.09 (d, 8H, J = 8.5 Hz, H-2), 7.26 (d, 8H, J = 8.5 Hz, H-3), 6.25 (ddt, 4H, J = 16.5, 10.5, and 5.1 Hz, H-6), 5.59 (dd, 4H, J = 16.5 and 1.2 Hz, H-7a), 5.43 (dd, 4H, J = 10.5 and 1.5 Hz, H-7b), 4.78 (d, 8H, J = 5.1 Hz, H-5), −2.75 (s, 2H, NH). ^{13}C NMR ($CDCl_3$, 75.5 MHz): δ 158.6 (C-4), 135.8 (C-2), 135.0 (C-1), 133.6 (C-6), 131.2 (C-β), 119.9 (*meso*-C), 118.2 (C-7), 113.2 (C-3), 69.3 (C-5). IR (KBr): ν 3319 (N−H), 1605 (C═C), 1506, 1241 (C−O), 1224, 1175, 803 (C−H), 739 cm^{-1}. MS [m/z (%)]: [M^+ + H] 839 (25), 838 (19), 391 (12), 307 (15), 192 (25), 154 (100), 136 (70), 95 (74), 69 (94). UV−vis ($CHCl_3$): λ_{max} = 422 nm (ε = 342680 M^{-1} cm^{-1}).

*meso-Tetrakis(3,5-diallyloxyphenyl)porphyrin (**2c**).* The title compound was prepared from **2b** (1.00 g, 1.35 mmol), allyl bromide (1.30 g, 10.7 mmol), K_2CO_3 (3.20 g, 23.2 mmol), and KI in acetone. Compound **2c** was obtained as a purple solid, (1.20 g, 84% yield). Mp: 205−207 °C. ^{1}H NMR ($CDCl_3$, 400 MHz): δ 8.93 (s, 8H, H-β), 7.42 (d, 8H, J = 2.4 Hz, H-2), 6.95 (t, 4H, J = 2.4 Hz), 6.14 (ddt, 8H, J = 17.2, 10.5, and 5.3 Hz, H-6), 5.49 (ddt, 8H, J = 17.2, 1.6, and 1.2 Hz, H-7a), 5.33 (ddt, 8H, J = 10.5, 1.5, and 1.2 Hz, H-7b), 4.71 (dt, 16H, J = 5.3 and 1.2 Hz, H-5), −2.85 (s, 2H, NH). ^{13}C NMR ($CDCl_3$, 75.5 MHz): δ 158.0 (C-3), 144.2 (C-1), 133.4 (C-6), 131.3 (C-β), 120.0 (*meso*-C), 118.2 (C-7), 115.0 (C-2), 101.8 (C-4), 69.4 (C-5). IR (KBr): ν 3317 (N−H), 1588 (C═C), 1506, 1290 (C−O) cm^{-1}. MS [m/z (%)]: [M^+ + H] 1063. UV−vis ($CHCl_3$): λ_{max} = 422 nm (ε = 380165 M^{-1} cm^{-1}).

*meso-Tetrakis[4-[3,5-bis(allyloxy)benzyloxy]phenyl]porphyrin (**1d**).* The title compound was obtained from **1b** (0.50 g, 0.74 mmol), **Br-dendron-1** (0.70 g, 2.95 mmol), K_2CO_3 (1.22 g, 8.84 mmol), and KI in acetone. The solid compound was purified by column chromatography using a mixture of hexane/acetone (8:2). The product **1d** was obtained as a purple solid (0.84 g, 77% yield). Mp: 140−144 °C. ^{1}H NMR ($CDCl_3$, 300 MHz): δ 8.86 (s, 8H, H-β), 8.12 (d, 8H, J = 8.6 Hz, H-2), 7.34 (d, 8H, J = 8.6 Hz, H-3), 6.80 (d, 8H, J = 2.2 Hz, H-7), 6.55 (t, 4H, J = 2.2 Hz, H-9), 6.11 (ddt, 8H, J = 17.3, 10.5, and 5.3 Hz, H-11), 5.47 (ddt, 8H, J = 17.3, 1.6, and 1.6 Hz, H-12a), 5.34 (ddt, 8H, J = 10.5, 1.4, and 1.6 Hz, H-12b), 5.27 (s, 8H, H-5), 4.62 (dt, 16H, J = 5.3 and 1.2 Hz, H-10), −2.76 (s, 2H, NH). ^{13}C NMR ($CDCl_3$, 75.5 MHz): δ 160.3 (C-8), 158.8 (C-4), 139.6 (C-6), 135.8 (C-2), 135.2 (C-1), 133.4 (C-11), 131.2 (C-β), 119.9 (*meso*-C), 118.1 (C-12), 113.3 (C-3), 106.6 (C-7), 101.7 (C-9), 70.5 (C-5), 69.2 (C-10). IR (KBr): ν 3316 (N−H), 1597 (C═C), 1506, 1455, 1240, 1171, 1019 (C−O), 802 (C−H), 735 cm^{-1}. MS [m/z (%)]: [M^+ + H] 1487 (68), 1486 (40), 1285 (20), 203 (74), 154 (100), 136 (80), 121 (70), 69 (58). UV−vis ($CHCl_3$): λ_{max} = 423 nm (ε = 343425 M^{-1} cm^{-1}).

*meso-Tetrakis[3,5-[3,5-bis(allyloxy)dibenzyloxy]phenyl]porphyrin (**2d**).* The title compound was obtained from **2b** (0.50 g, 0.74 mmol), **Br-dendron-1** (1.30 g, 5.4 mmol), K_2CO_3 (2.20 g, 16.2 mmol), and KI in acetone. The solid was purified by column chromatography using a mixture of hexane/acetone (8:2). The product **2d** was obtained as a purple oil (0.84 g, 60% yield). ^{1}H NMR ($CDCl_3$, 400 MHz): δ 8.88 (s, 8H, H-β), 7.49 (d, 8H, J = 2.2 Hz, H-2), 7.05 (t, 4H, J = 2.2 Hz, H-4), 6.67 (d, 16H, J = 2.3 Hz, H-7), 6.47 (t, 8H, J = 2.3 Hz, H-9), 5.99 (ddt, 16H, J = 17.3, 10.5, and 5.3 Hz, H-11), 5.35 (ddt, 16H, J = 17.3, 1.6, and 1.6 Hz, H-12a), 5.21 (ddt, 16H, J = 10.5, 1.6, and 1.4 Hz, H-12b), 5.16 (s, 16H, H-5), 4.49 (dt, 32H, J = 5.3 and 1.4 Hz, H-10), −2.87 (s, 2H, NH). ^{13}C NMR ($CDCl_3$, 100 MHz): δ 160.2 (C-8), 158.1 (C-3), 144.2 (C-1), 139.3 (C-6), 133.3 (C-11), 119.9 (*meso*-C), 118.0 (C-12), 115.4 (C-2), 106.5 (C-7), 101.8 (C-4, C-9), 70.5 (C-5), 69.1 (C-10). IR (KBr): ν 3317 (N−H), 1597 (C═C), 1506, 1455, 1295, 1171, 1019 (C−O) cm^{-1}. MS [m/z (%)]: [M^+] 2360. UV−vis ($CHCl_3$): λ_{max} = 423 nm (ε = 240225 M^{-1} cm^{-1}).

*meso-Tetrakis[4-[3,5-bis(3,5-bis(allyloxy)benzyloxy)benzyloxy]-phenyl]porphyrin (**1e**).* The title compound was obtained from **1b** (0.5 g, 0.74 mmol), **Br-dendron-2** (0.86 g, 1.54 mmol), and K_2CO_3 (0.46 g, 3.33 mmol) in the presence of KI in acetone. The solid obtained was purified by column chromatography using a mixture of hexane/acetone (8:2). The product **1e** was obtained as a red solid (0.52 g, 49% yield). Mp: 53−57 °C. ^{1}H NMR ($CDCl_3$, 300 MHz): δ 8.87 (s, 8H, H-β), 8.13 (d, 8H, J = 8.5 Hz, H-2), 7.35 (d, 8H, J = 8.5 Hz, H-3), 6.88 (d, 8H, J = 2.2 Hz, H-7), 6.66 (d, 16H, J = 2.3 Hz, H-12), 6.64 (t, 4H, J = 2.2 Hz, H-9), 6.48 (t, 8H, J = 2.3 Hz, H-14), 6.05 (ddt, 16H, J = 17.3, 10.5, and 5.3 Hz, H-16), 5.41 (ddt, 16H, J = 17.3, 1.6, and 1.5 Hz, H-17a), 5.27 (ddt, 16H, J = 10.5, 1.5, and 1.4 Hz, H-17b), 5.28 (s, 8H, H-5), 5.06 (s, 16H, H-10), 4.54 (dt, 32H, J = 5.3 and 1.5 Hz, H-15), −2.78 (s, 2H, NH). ^{13}C NMR ($CDCl_3$, 75.5 MHz): δ 160.4 (C-8), 160.2 (C-13), 158.8 (C-4), 139.7 (C-6), 139.4 (C-11), 135.9 (C-2), 135.2 (C-1), 133.3 (C-16), 133.2 (C-β), 119.9 (*meso*-C), 118.0 (C-17), 113.3 (C-3), 106.9 (C-7), 106.5 (C-12), 102.0 (C-9), 101.6 (C-14), 70.5 (C-5), 70.4 (C-10), 69.2 (C-15). IR (KBr): ν 3316 (N−H), 1596 (C═C), 1507, 1450, 1240, 1150, 1046 (C−O), 831 (C−H), 802, 731 cm^{-1}. MS (MALDI): m/z 2785. UV−vis ($CHCl_3$): λ_{max} = 423 nm (ε = 362830 M^{-1} cm^{-1}).

*meso-Tetrakis[3,5-[3,5-bis(3,5-bis(allyloxy)benzyloxy)-dibenzyloxy]phenyl]porphyrin (**2e**).* The title compound was obtained from **2b** (0.18 g, 0.24 mmol), **Br-dendron-2** (1.10 g, 1.90 mmol), and K_2CO_3 (81.00 g, 5.8 mmol) in the presence of KI in acetone. The solid obtained was purified by column chromatography using a mixture of hexane/acetone (8:2). Compound **2e** was obtained as a deep-purple oil (0.52 g, 58% yield). ^{1}H NMR ($CDCl_3$, 400 MHz): δ 8.91 (s, 8H, H-β), 7.49 (s, 8H, H-2), 7.05 (s, 4H, H-4), 6.73 (s, 16H, H-7), 6.54 (s, 8H, H-9), 6.51 (s, 32H, H-12), 6.37 (s, 16H, H-14), 5.93 (ddt, 32H, J = 17.3, 10.5, and 5.2 Hz, H-16), 5.29 (dt, 32H, J = 17.3 and 1.3 Hz, H-17a), 5.17 (dt, 32H, J = 10.5 and 1.1 Hz, H-17b), 5.12 (s, 16H, H-5), 4.91 (s, 32H, H-10), 4.40 (d, 64H, J = 5.2 Hz, H-15), −2.83 (s, 2H, NH). ^{13}C NMR ($CDCl_3$, 100 MHz): δ 160.3 (C-8), 160.1 (C-13), 158.2 (C-3), 139.3 (C-11), 136.8 (C-6), 133.3 (C-16), 117.9 (C-17), 115.3 (C-2), 106.9 (C-7), 106.3 (C-12), 102.1 (C-4, C-9), 101.6 (C-14), 70.5 (C-5), 70.2 (C-10), 69.0 (C-15). IR (KBr): ν 3317 (N−H), 1594 (C═C), 1507, 1450, 1296, 1150, 1046 (C−O) cm^{-1}. UV−vis ($CHCl_3$): λ_{max} = 423 nm (ε = 268265 M^{-1} cm^{-1}).

Procedure for the Metalation of Compounds 1d, 1e, 2d, and 2e. Metalation of the porphyrin was carried out using conditions reported previously.[46] A round-bottomed flask equipped with a condenser and a magnetic stirring bar was charged with **1d** (or **1e**, **2d**, or **2e**) and $Zn(CH_3COO)_2{\cdot}2H_2O$ (the same amount in grams as the porphyrin) in 70 mL of DMF, and the mixture was refluxed for 30 min. After cooling to room temperature, the solid was precipitated by the addition of cold water and washed with methanol to remove traces of DMF.

*[meso-Tetrakis[4-[3,5-bis(allyloxy)benzyloxy]phenyl]-porphyrinato]zinc(II) (**1d$_{Zn}$**).* The title compound was obtained from **1b** (0.70 g, 0.47 mmol) and $Zn(CH_3COO)_2{\cdot}2H_2O$ (0.70 g, 3.19 mmol). Compound **1d$_{Zn}$** was obtained as a purple solid (0.61 g, 83% yield). Mp: 139−141 °C. ^{1}H NMR ($CDCl_3$, 400 MHz): δ 8.97 (s, 8H, H-β), 8.12 (d, 8H, J = 8.3 Hz, H-2), 7.33 (d, 8H, J = 8.3 Hz, H-3), 6.78 (s, 8H, H-7), 6.52 (s, 4H, H-9), 6.10 (ddt, 8H, J = 17.3, 10.5, and 5.3 Hz, H-11), 5.46 (d, 8H, J = 17.3 Hz, H-12a), 5.33 (d, 8H, J = 10.5 Hz, H-12b), 5.26 (s, 8H, H-5), 4.59 (d, 16H, J = 5.3 Hz, H-10). ^{13}C NMR ($CDCl_3$, 100.5 MHz): δ 160.3 (C-8), 158.6 (C-4), 150.7 (C-α), 139.7 (C-6), 135.8 (C-1), 135.7 (C-2), 133.4 (C-11), 132.1 (C-β), 120.9 (*meso*-C), 118.1 (C-12), 113.2 (C-3), 106.6 (C-7), 101.7 (C-9), 70.5 (C-5), 69.2 (C-10). IR (KBr): ν 1595 (C═C), 1506, 1453, 1220, 1161, 1148, (C−H), 994, 796 cm^{-1}. UV−vis ($CHCl_3$): λ_{max} = 423 nm (ε = 430265 M^{-1} cm^{-1}).

*[meso-Tetrakis[3,5-[3,5-bis(allyloxy)dibenzyloxy]phenyl]-porphyrinato]zinc(II) (**2d$_{Zn}$**).* The title compound was obtained from **2d** (0.60 g, 0.25 mmol) and $Zn(CH_3COO)_2{\cdot}2H_2O$ (0.60 g, 2.73 mmol). Compound **2d$_{Zn}$** was obtained as a purple solid (0.52 g, 85% yield). Mp: 65−67 °C. ^{1}H NMR ($CDCl_3$, 400 MHz): δ 8.99 (s, 8H, H-β), 7.49 (s, 8H, H-2), 7.03 (s, 4H, H-4), 6.66 (s, 16H, H-7), 6.45 (s, 8H, H-9), 5.99 (ddt, 16H, J = 17.2, 10.0, and 5.2 Hz, H-11), 5.34 (d, 16H, J = 17.2 Hz, H-12a), 5.21 (d, 16H, J = 10.0 Hz, H-12b), 5.14 (s, 16H, H-5), 4.49 (d, 32H, J = 5.2 Hz, H-10). ^{13}C NMR ($CDCl_3$, 100.5 MHz): δ 160.2 (C-8), 158.0 (C-3),150.2 (C-α) 144.9 (C-1), 139.4 (C-6), 133.3 (C-11), 132.2 (C-β), 120.9 (*meso*-C), 118.0 (C-12), 115.3 (C-2), 106.5 (C-7), 102.2 (C-4), 101.7 (C-9), 70.5 (C-5), 69.1 (C-10). IR (KBr): ν 1587 (C═C), 1449, 1294, 1145, 1049 (C−O), 1000, 923 cm^{-1}. UV−vis ($CHCl_3$): λ_{max} = 424 nm (ε = 303005 M^{-1} cm^{-1}).

DOI: 10.1021/acs.inorgchem.5b00618
Inorg. Chem. 2015, 54, 5021−5031

*[meso-Tetrakis[4-[3,5-bis[3,5-bis(allyloxy)benzyloxy]benzyloxy]-phenyl]porphyrinato]zinc(II) (**1e**$_{Zn}$).* The title compound was obtained from **1e** (0.50 g, 0.22 mmol) and $Zn(CH_3COO)_2{\cdot}2H_2O$ (0.50 g, 2.73 mmol). Compound **1e**$_{Zn}$ was obtained as a purple solid (0.52 g, 85% yield). Mp: 76−78 °C. ^{1}H NMR ($CDCl_3$, 400 MHz): δ 8.98 (s, 8H, H-β), 8.13 (d, 8H, J = 7.9 Hz, H-2), 7.33 (d, 8H, J = 7.9 Hz, H-3), 6.82 (s, 8H, H-7), 6.60 (s, 16H, H-12), 6.58 (s, 4H, H-9), 6.43 (s, 8H, H-14), 6.02 (ddt, 16H, J = 17.3, 10.5, and 3.4 Hz, H-16), 5.39 (d, 16H, J = 17.3 Hz, H-17a), 5.26 (d, 16H, J = 10.5 Hz, H-17b), 5.22 (s, 16H, H-5), 4.99 (s, 16H, H-10), 4.50 (d, 32H, J = 3.4 Hz, H-15). ^{13}C NMR ($CDCl_3$, 100.5 MHz): δ 160.3 (C-8), 160.1 (C-13), 158.6 (C-4), 150.6 (C-α), 139.6 (C-6), 139.3 (C-11), 135.9 (C-1), 135.7 (C-2), 133.3 (C-16), 132.1 (C-β), 120.8 (*meso*-C), 117.9 (C-17), 113.1 (C-3), 106.9 (C-7), 106.4 (C-12), 102.0 (C-9), 101.6 (C-14), 70.4 (C-5), 70.2 (C-10), 69.1 (C-15). IR (KBr): ν 1592 (C═C), 1447, 1242, 1144, 1042 (C−O), 993, 829 cm^{-1}. UV−vis ($CHCl_3$): λ_{max} = 423 nm (ε = 260520 M^{-1} cm^{-1}).

*[meso-Tetrakis[3,5-[3,5-bis[3,5-bis(allyloxy)benzyloxy]-dibenzyloxy]phenyl]porphyrinato]zinc(II) (**2e**$_{Zn}$).* The title compound was obtained from **2e** (0.48 g, 0.1 mmol) and $Zn(CH_3COO)_2{\cdot}2H_2O$ (0.48 g, 2.19 mmol). Compound **2e**$_{Zn}$ was obtained as a purple solid (0.390 g, 80% yield). Mp: 59−61 °C. ^{1}H NMR ($CDCl_3$, 400 MHz): δ 9.01 (s, 8H, H-β), 7.50 (d, 8H, J = 2.3 Hz, H-2), 7.05 (t, 4H, J = 2.3 Hz, H-4), 6.73 (d, 16H, J = 2.1 Hz, H-7), 6.54 (t, 8H, J = 2.1 Hz, H-9), 6.49 (d, 32H, J = 2.2 Hz, H-12), 6.34 (t, 16H, J = 2.2 Hz, H-14), 5.91 (ddt, 32H, J = 17.2, 10.5, and 5.3 Hz, H-16), 5.28 (dt, 32H, J = 17.2 and 1.6 Hz, H-17a), 5.16 (dt, 32H, J = 10.5 and 1.3 Hz, H-17b), 5.12 (s, 16H, H-5), 4.91 (s, 32H, H-10), 4.38 (dt, 64H, J = 5.3 and 1.4 Hz, H-15). ^{13}C NMR ($CDCl_3$, 100.5 MHz): δ 160.3 (C-8), 160.0 (C-13), 158.0 (C-3), 150.1 (C-α), 144.9 (C-1), 139.4 (C-6), 139.2 (C-11), 133.2 (C-16), 132.2 (C-β), 120.8 (*meso*-C), 117.8 (C-17), 115.2 (C-2), 106.8 (C-7), 106.3 (C-12), 101.9 (C-4 and C-9), 101.5 (C-14), 70.5 (C-5), 70.2 (C-10), 69.0 (C-15). IR (KBr): ν 1591 (C═C), 1447, 1295, 1146, 1047 (C−O), 1046, 1001, 830 cm^{-1}. UV−vis ($CHCl_3$): λ_{max} = 425 nm (ε = 331535 M^{-1} cm^{-1}).

1c-MeCb. A 5 mL round-bottomed flask was charged with **1c** (60 mg, 0.072 mmol) and 1-CH_3-2-[$CH_2CH_2CH_2(CH_3)_2SiH$]-1,2-*closo*-$C_2B_{10}H_{10}$ (111 mg, 0.430 mmol) and dried under vacuum for 15 min. The mixture was dissolved in 1 mL of dry CH_2Cl_2, and 12 μL of Karstedt's catalyst was added and refluxed for 5 h under nitrogen. The volatiles were removed under pressure to obtain a brown-purple oil, which was purified by preparative TLC (1:1 dichloromethane/hexane) and precipitated with 1:1 dichloromethane/ethanol, giving a purple solid (95 mg, 71% yield). ^{1}H NMR ($CDCl_3$, 300 MHz): δ 8.91 (s, 8H, H-β), 8.16 (d, 8H, ^3J(H,H) = 9 Hz, H-2), 7.30 (d, 8H, ^3J(H,H) = 12 Hz, H-3), 4.24 (t, 16H, ^3J = 6 Hz, H-5), 2.26 (t, 16H, ^3J = 9 Hz, H-11), 2.05 (s, 24H, H-14), 1.99 (m, 16H, H-6), 1.67 (m, 16H, H-10), 0.84 (t, 16H, ^3J = 9 Hz, H-7), 0.66 (t, 16H, ^3J = 9 Hz, H-9), 0.16 (s, 48H, H-8), −2.69 (br s, 2H, NH). ^{11}B NMR ($CDCl_3$, 96.7 MHz): δ −5.86 (d, 8B, $^1J_{B,H}$ = 147 Hz), −10.79 (d, 32B, $^1J_{B,H}$ = 142 Hz). ^{13}C{^{1}H} NMR ($CDCl_3$, 75.5 MHz): δ 158.91 (C-4), 135.66 (C-2), 134.47 (C-1), 131.07 (C-β), 119.80 (*meso*-C), 112.76 (C-3), 78.11 (C-12), 74.66 (C-13), 70.72 (C-5), 39.04 (C-11), 24.30 (C-10), 24.00 (C-6), 23.19 (C-14), 15.29 (C-7), 11.32 (C-9), −3.42 (C-8). FTIR-ATR: ν 2579 (i, B−H str) cm^{-1}. Elem anal. Calcd for $C_{88}H_{150}B_{40}N_4O_4Si_4$: C, 56.43; H, 8.07; N, 2.99. Found: C, 56.82; H, 8.40; N, 2.90.

1d-MeCb. The title compound was obtained from **1d** (30 mg, 0.020 mmol), 1-CH_3-2-[$CH_2CH_2CH_2(CH_3)_2SiH$]-1,2-*closo*-$C_2B_{10}H_{10}$ (63 mg, 0.244 mmol), and 10 μL of Karstedt's catalyst in 1 mL of $CHCl_3$ stirred at 50 °C for 5 h. The reaction mixture was purified by preparative TLC (acetonitrile) and precipitated with 1:1 ether/ethanol, giving a purple solid (46 mg, 64% yield). ^{1}H NMR ($CDCl_3$, 300 MHz): δ 8.92 (s, 8H, H-β), 8.18 (d, 8H, ^3J = 6 Hz, H-2), 7.41 (d, 8H, ^3J = 6 Hz, H-3), 6.82 (s, 8H, H-7), 6.54 (s, 4H, H-9), 5.32 (s, 8H, H-5), 4.05 (t, 16H, ^3J = 6 Hz, H-10), 2.21 (t, 16H, ^3J = 7.5 Hz, H-16), 2.02 (s, 24H, H-19), 1.87 (m, 16H, H-11), 1.61 (m, 16H, H-15), 0.73 (t, 16H, ^3J = 9 Hz, H-12), 0.60 (t, 16H, ^3J = 9 Hz, H-14), 0.10 (s, 48H, H-13), −2.70 (br s, 2H, NH). ^{11}B NMR ($CDCl_3$, 96.7 MHz): δ −5.91 (d, 16B, $^1J_{B,H}$ = 148 Hz), −10.78 (d, 64B, $^1J_{B,H}$ = 140 Hz). ^{13}C{^{1}H} NMR ($CDCl_3$, 75.5 MHz): δ 160.6 (C-8), 158.7 (C-4), 139.4 (C-6), 135.7 (C-2), 135.0 (C-1), 131.2 (C-β), 119.7 (*meso*-C), 113.2 (C-3), 106.0 (C-7), 101.0 (C-9), 78.1 (C-17), 74.6 (C-18), 70.7 (C-10), 70.5 (C-5), 39.0 (C-16), 24.3 (C-15), 23.9 (C-11), 23.1 (C-19), 15.3 (C-12), 11.2 (C-14), −3.4 (C-13). FTIR-ATR: ν 2578 (i, B−H str) cm^{-1}. Elem anal. Calcd for $C_{160}H_{294}B_{80}N_4O_{12}Si_8$: C, 54.05; H, 8.33; N, 1.58. Found: C, 54.00; H, 8.00; N, 1.55.

2c-MeCb. The title compound was obtained from **2c** (60 mg, 0.056 mmol), 1-CH_3-2-[$CH_2CH_2CH_2(CH_3)_2SiH$]-1,2-*closo*-$C_2B_{10}H_{10}$ (231 mg, 0.896 mmol), and 15 μL of Karstedt's catalyst in 1 mL of $CHCl_3$ stirred at 50 °C for 5 h. The reaction mixture was purified by preparative TLC (1:1 dichloromethane/hexane) and precipitated with 1:1 dichloromethane/ethanol, giving a purple solid (127 mg, 72% yield). ^{1}H NMR ($CDCl_3$, 300 MHz): δ 8.96 (s, 8H, H-β), 7.38 (s, 8H, H-2), 6.91 (s, 4H, H-4), 4.11 (t, 16H, ^3J = 6 Hz, H-7), 2.14 (t, 16H, ^3J = 7.5 Hz, H-13), 1.91 (s, 24H, H-16), 1.87 (m, 16H, H-8), 1.54 (m, 16H, H-12), 0.69 (t, 16H, ^3J = 7.5 Hz, H-9), 0.55 (t, 16H, ^3J = 7.5 Hz, H-11), 0.05 (s, 64H, H-10), −2.82 (br s, 2H, NH). ^{11}B NMR ($CDCl_3$, 96.7 MHz): δ −5.87 (d, 16B, $^1J_{B,H}$ = 145 Hz), −10.77 (d, 64B, $^1J_{B,H}$ = 138 Hz). ^{13}C{^{1}H} NMR ($CDCl_3$, 75.5 MHz): δ 158.3 (C-3), 143.9 (C-1), 131.2 (C-β), 119.9 (*meso*-C), 114.4 (C-2), 101.1 (C-4), 78.1 (C-14), 74.6 (C-15), 70.8 (C-7), 38.9 (C-13), 24.3 (C-12), 23.9 (C-8), 23.1 (C-16), 15.2 (C-9), 11.2 (C-11), −3.5 (C-10). FTIR-ATR: ν 2578 (i, B−H str) cm^{-1}. Elem anal. Calcd for $C_{132}H_{270}B_{80}N_4O_8Si_8$: C, 50.63; H, 8.69; N, 1.79. Found: C, 51.60; H, 9.04; N, 1.65.

1d$_{Zn}$-MeCb. The title compound was obtained from **1d**$_{Zn}$ (31 mg, 0.020 mmol), 1-CH_3-2-[$CH_2CH_2CH_2(CH_3)_2SiH$]-1,2-*closo*-$C_2B_{10}H_{10}$ (62 mg, 0.240 mmol), and 15 μL of Karstedt's catalyst in 1 mL of $CHCl_3$ stirred at 50 °C for 5 h. The reaction mixture was purified by preparative TLC (acetonitrile) and precipitated with 1:1 dichloromethane/ethanol, giving a purple solid (59 mg, 82% yield). ^{1}H NMR ($CDCl_3$, 300 MHz): δ 9.01 (s, 8H, H-β), 8.17 (d, 8H, ^3J = 9 Hz, H-2), 7.39 (d, 8H, ^3J = 6 Hz, H-3), 6.80 (s, 8H, H-7), 6.51 (s, 4H, H-9), 5.31 (s, 8H, H-5), 4.03 (t, ^3J = 6 Hz, 16H, H-10), 2.20 (t, ^3J = 7.5 Hz, 16H, H-16), 2.02 (s, 24H, H-19), 1.86 (m, 16H, H-11), 1.60 (m, 16H, H-15), 0.72 (t, 16H, ^3J = 9 Hz, H-12), 0.59 (t, 16H, ^3J = 9 Hz, H-14), 0.09 (s, 48H, H-13). ^{11}B NMR ($CDCl_3$, 96.7 MHz): δ −5.88 (d, 16B, $^1J_{B,H}$ = 146 Hz), −10.75 (d, 64B, $^1J_{B,H}$ = 139 Hz). ^{13}C{^{1}H} NMR ($CDCl_3$, 75.5 MHz): δ 160.6 (C-8), 158.6 (C-4), 150.5 (C-α), 140.4 (C-1), 139.4 (C-6), 135.5 (C-2), 131.9 (C-β), 120.8 (*meso*-C), 106.0 (C-7), 101.1 (C-9), 78.1 (C-17), 74.6 (C-18), 70.7 (C-5), 70.7 (C-10), 39.0 (C-16), 24.3 (C-15), 23.9 (C-11), 23.1 (C-19), 15.3 (C-14), 11.2 (C-12), −3.4 (C-13). FTIR-ATR: ν 2578 (i, B−H str) cm^{-1}. Elem anal. Calcd for $C_{160}H_{292}B_{80}N_4O_{12}Si_8Zn$: C, 53.10; H, 8.13; N, 1.55. Found: C, 53.38; H, 8.18; N, 1.45.

2d$_{Zn}$-MeCb. The title compound was obtained from **2d**$_{Zn}$ (40 mg, 0.0165 mmol), 1-CH_3-2-[$CH_2CH_2CH_2(CH_3)_2SiH$]-1,2-*closo*-$C_2B_{10}H_{10}$ (137 mg, 0.531 mmol), and 15 μL of Karstedt's catalyst in 1 mL of 1,4-dioxane stirred at 55 °C for 5 h. The reaction mixture was purified by preparative TLC (70:30 acetonitrile/ethyl acetate) and precipitated with 1:1 dichloromethane/ethanol, giving a purple solid (95 mg, 88% yield). ^{1}H NMR ($CDCl_3$, 300 MHz): δ 9.09 (s, 8H, H-β), 7.56 (s, 8H, H-2), 7.10 (s, 4H, H-4), 6.67 (s, 16H, H-7), 6.44 (s, 8H, H-9), 5.16 (s, 16H, H-5), 3.93 (br s, 32H, H-10), 2.13 (t, 32H, ^3J = 7.5 Hz, H-16), 1.95 (s, 48H, H-19), 1.77 (m, 16H, H-11), 1.53 (m, 16H, H-15), 0.62 (br s, 16H, H-12), 0.51 (br s, 16H, H-14), 0.01 (s, 96H, H-13). ^{11}B NMR ($CDCl_3$, 96.7 MHz): δ −5.94 (d, 32B, $^1J_{B,H}$ = 153 Hz), −10.70 (d, 128B, $^1J_{B,H}$ = 130 Hz). ^{13}C{^{1}H} NMR ($CDCl_3$, 75.5 MHz): δ 160.5 (C-8), 158.1 (C-3), 150.1 (C-α), 144.7 (C-1), 1389.0 (C-6), 132.0 (C-β), 120.8 (*meso*-C), 114.9 (C-2), 106.0 (C-7), 101.5 (C-4), 101.0 (C-9), 78.1 (C-17), 74.6 (C-18), 70.6 (C-5), 70.6 (C-10), 38.9 (C-16), 24.2 (C-15), 23.8 (C-11), 23.1 (C-19), 15.2 (C-12), 11.1 (C-14), −3.5 (C-13). FTIR-ATR: ν 2578 (i, B−H str) cm^{-1}. Elem anal. Calcd for $C_{276}H_{556}B_{160}N_4O_{24}Si_{16}Zn$: C, 50.53; H, 8.54; N, 0.85. Found: C, 51.03; H, 8.67; N, 0.78.

1e$_{Zn}$-MeCb. The title compound was obtained from **1e**$_{Zn}$ (25 mg, 0.0088 mmol), 1-CH_3-2-[$CH_2CH_2CH_2(CH_3)_2SiH$]-1,2-*closo*-$C_2B_{10}H_{10}$ (72 mg, 0.279 mmol), and 20 μL of Karstedt's catalyst in 1 mL of 1,4-dioxane stirred at 60 °C for 5 h. The reaction mixture was purified by preparative TLC (acetonitrile) and precipitated with 1:1 dichloromethane/ethanol, giving a purple solid (42 mg, 69% yield). ^{1}H

DOI: 10.1021/acs.inorgchem.5b00618
Inorg. Chem. 2015, 54, 5021−5031

NMR ($CDCl_3$, 300 MHz): δ 9.05 (s, 8H, H-β), 8.21 (d, 8H, ^3J = 9 Hz, H-2), 7.43 (d, 8H, ^3J = 6 Hz, H-3), 6.96 (s, 8H, H-7), 6.71 (s, 4H, H-9), 6.67 (s, 16H, H-12), 6.47 (s, 8H, H-14), 5.34 (s, 8H, H-5), 5.11 (s, 16H, H-10), 3.98 (t, 32H, ^3J = 6 Hz, H-15), 2.18 (t, 32H, ^3J = 9 Hz, H-21), 2.00 (s, 48H, H-24), 1.82 (m, 32H, H-16), 1.58 (m, 32H, H-20), 0.69 (t, 32H, ^3J = 9 Hz, H-17), 0.56 (t, 32H, ^3J = 9 Hz, H-19), 0.07 (s, 96H, H-18). ^{11}B NMR ($CDCl_3$, 96.7 MHz): δ −5.89 (d, 32B, $^1J_{B,H}$ = 148 Hz), −10.77 (d, 128B, $^1J_{B,H}$ = 140 Hz). $^{13}C\{^1H\}$ NMR ($CDCl_3$, 75.5 MHz): δ 160.5 (C-13), 160.4 (C-8), 158.6 (C-4), 150.5 (C-α), 139.6 (C-6), 139.1 (C-11), 135.7 (C-1), 135.5 (C-2), 1312.0 (C-β), 120.8 (*meso*-C), 113.0 (C-3), 106.7 (C-7), 106.0 (C-12), 101.8 (C-9), 101.0 (C-14), 78.2 (C-22), 74.7 (C-23), 70.6 (C-15), 70.3 (C-10), 70.3 (C-5), 39.0 (C-21), 24.3 (C-20), 23.8 (C-16), 23.1 (C-24), 15.2 (C-17), 11.2 (C-19), −3.4 (C-18). FTIR-ATR: ν 2580 (i, B−H str) cm^{-1}. Elem anal. Calcd for $C_{305}H_{583}B_{160}N_4O_{28}Si_{16}Zn$: C, 52.34; H, 8.40; N, 0.80. Found: C, 53.06; H, 8.53; N, 0.75.

***2e*$_{Zn}$*-MeCb*.** The title compound was obtained from **2e**$_{Zn}$ (38 mg, 0.0076 mmol), 1-CH_3-2-$[CH_2CH_2CH_2(CH_3)_2SiH]$-1,2-*closo*-$C_2B_{10}H_{10}$ (109 mg, 0.422 mmol), and 17 μL of Karstedt's catalyst in 1 mL of 1,4-dioxane stirred at 60 °C for 5 h. The reaction mixture was purified by preparative TLC (acetonitrile) and precipitated with 1:1 dichloromethane/ethanol, giving a purple solid (74 mg, 74% yield). ^{1}H NMR ($CDCl_3$, 300 MHz): δ 9.11 (s, 8H, H-β), 7.56 (s, 8H, H-2), 7.12 (s, 4H, H-4), 6.80 (s, 16H, H-7), 6.55 (s, 8H, H-9), 6.53 (s, 32H, H-12), 6.36 (s, 8H, H-14), 5.17 (br s, 8H, H-5), 4.95 (br s, 32H, H-10), 3.85 (br s, 64H, H-15), 2.11 (br s, 64H, H-21), 1.93 (s, 96H, H-24), 1.71 (m, 64H, H-16), 1.52 (m, 64H, H-20), 0.58 (br s, 64H, H-17), 0.50 (br s, 64H, H-19), −0.01 (s, 192H, H-18). ^{11}B NMR ($CDCl_3$, 96.7 MHz): δ −6.01 (d, 64B, $^1J_{B,H}$ = 153 Hz), −10.69 (d, 256B, $^1J_{B,H}$ = 123 Hz). $^{13}C\{^1H\}$ NMR ($CDCl_3$, 75.5 MHz): δ 160.4 (C-13), 158.7 (C-8), 158.0 (C-3), 150.1 (C-α), 139.3 (C-6), 139.0 (C-11), 132.2 (C-β), 107.5 (C-2), 106.7 (C-7), 105.9 (C-12), 102.2 (C-4), 101.7 (C-9), 100.9 (C-14), 78.2 (C-22), 74.7 (C-23), 71.5 (C-5), 70.5 (C-15), 70.2 (C-10), 38.9 (C-21), 24.3 (C-20), 23.8 (C-16), 23.1 (C-24), 15.1 (C-17), 11.1 (C-19), −3.5 (C-18). FTIR-ATR: ν 2580 (i, B−H str) cm^{-1}. Elem anal. Calcd for $C_{564}H_{1132}B_{320}N_4O_{56}Si_{32}Zn$: C, 50.97; H, 8.58; N, 0.42. Found: C, 51.30; H, 8.61; N, 0.44.

Diffusion NMR. All DOSY NMR experiments were carried out on dilute $CDCl_3$ solutions.[67,68] Similar concentrations (about 2 mg of product dissolved in 0.6 mL of $CDCl_3$ into a 5 mm NMR tube) were used to minimize the effect of different solution viscosities for different samples, which were confirmed from the diffusion coefficient of the residual $CDCl_3$ signal taken as an internal reference. After introduction of the sample into the magnet, 10 min were allowed to pass to achieve a general temperature stabilization and regulation along the entire NMR tube. This is important to minimize convection effects highly probable in a nonviscous solvent such as $CDCl_3$.

DOSY experiments were performed at 298 K on a Bruker AVANCE 500 NMR spectrometer operating at 500.13 MHz and equipped with a cryoprobe *z*-gradient inverse probehead capable of producing gradients in the *z* direction with a maximum strength of 53.5 G cm^{-1}. To check for the presence and effective suppression of deleterious convection effects, a test LEDBP experiment was recorded for the first sample with and without sample rotation, and the results were compared to data obtained from double-stimulated echo sequence. Thus, we decided to run DOSY experiments for all samples using the double-stimulated echo sequence incorporating bipolar gradient pulses and a longitudinal eddy current delay (dstegp3s in the Bruker library).

The gradient strength was linearly incremented in 16 steps from 2% up to 95% of the maximum gradient strength. Diffusion times and gradient pulse durations were optimized for each experiment in order to achieve a 95% decrease in the resonance intensity at the largest gradient amplitude; typically, diffusion times between 100 and 150 ms and bipolar rectangular gradient pulses between 1.0 and 2.0 ms were employed. The longitudinal eddy current delay was held constant to 5 ms, whereas the gradient pulse recovery time was set to 100 μs. After Fourier transformation followed by the same phase and baseline correction of each 1D data set, the diffusion dimension of the 2D DOSY spectra was obtained by using the DOSY protocol included into the Bruker *TOPSPIN* software package (version 1.3).

■ ASSOCIATED CONTENT

Supporting Information

Procedures, ^{1}H, ^{13}C, and HSQC NMR spectra for starting dendrimers, ^{1}H and ^{13}C NMR spectra for carboranyl-containing dendrimers, molecular structures for carboranyl-containing dendrimers, UV−vis spectra for starting dendrimers, and 2D DOSY spectra for dendrimers. This material is available free of charge via the Internet at http://pubs.acs.org.

■ AUTHOR INFORMATION

Corresponding Author

*E-mail: rosario@icmab.es. Fax: (+34) 935805729.

Notes

The authors declare no competing financial interest.

‡J.C.-G. is enrolled in the UAB Ph.D. program, and E.X.-F. is enrolled in the UNAM Ph.D. program.

■ ACKNOWLEDGMENTS

This work has been supported by the Junta de Andalucía, programa Proyectos de Excelencia (P11-FQM-8229) and Ministerio de Economía y Competitividad (CTQ2013-44670-R and CTQ2012-32436). J.C.-G. thanks the CSIC for an Intramural grant. E.X.-F. thanks CONACYT for a Ph.D. fellowship (211329) and Programa de Cooperación Científica UNAM-CSIC and CONACYT for financial support.

■ REFERENCES

(1) Bosman, A. W.; Janssen, H. M.; Meijer, E. W. *Chem. Rev.* **1999**, *99*, 1665−1688.
(2) Tomalia, D. A.; Baker, H.; Dewald, J.; Hall, M.; Kallos, G.; Matin, S.; Roeck, J.; Ryder, J.; Smith, P. *Polymer J.* **1985**, *17*, 117−132.
(3) Walter, M. V.; Malkoch, M. *Chem. Soc. Rev.* **2012**, *41*, 4593−4609.
(4) Astruc, D.; Boisselier, E.; Ornelas, C. *Chem. Rev.* **2010**, *110*, 1857−1959.
(5) Menjoge, A. R.; Kannan, R. M.; Tomalia, D. A. *Drug Discovery Today* **2010**, *15*, 171−185.
(6) Cheng, Y. *Dendrimer-Based Drug Delivery Systems: From Theory to Practice*; Wiley: New York, 2012; ISBN 978-1-118-27522-1.
(7) Khandare, J.; Calderón, M.; Diaga, N. M.; Haag, R. *Chem. Soc. Rev.* **2012**, *41*, 2824−2848.
(8) Skukla, S.; Gong, W.; Chatterjee, M.; Yang, W.; Sekido, M.; Diop, L. A.; Müller, R.; Sudimack, J. J.; Lee, R. J.; Barth, R. F.; Tjarks, W. *Bioconjugate Chem.* **2003**, *14*, 158−167.
(9) Barth, R. F.; Coderre, J. A.; Vicente, M. G. H.; Blue, T. E. *Clin. Cancer Res.* **2005**, *11*, 3987−4002.
(10) Parrott, M. C.; Marchington, E. B.; Valliant, J. F.; Adronov, A. J. *J. Am. Chem. Soc.* **2005**, *127*, 12081−12089.
(11) Núñez, R.; González-Campo, A.; Viñas, C.; Teixidor, F.; Sillanpää, R.; Kivekäs, R. *Organometallics* **2005**, *24*, 6351−6357.
(12) González-Campo, A.; Viñas, C.; Teixidor, F.; Núñez, R.; Kivekäs, R.; Sillanpää, R. *Macromolecules* **2007**, *40*, 5644−5652.
(13) Lerouge, F.; Viñas, C.; Teixidor, F.; Núñez, R.; Abreu, A.; Xochitiotzi, E.; Santillan, R.; Farfán, N. *Dalton Trans.* **2007**, 1898−1903.
(14) Lerouge, F.; Ferrer-Ugalde, A.; Viñas, C.; Teixidor, F.; Abreu, A.; Xochitiotzi, E.; Farfán, N.; Santillan, R.; Sillanpää, R.; Núñez, R. *Dalton Trans.* **2011**, *40*, 7541−7550.
(15) González-Campo, A.; Ferrer-Ugalde, A.; Viñas, C.; Teixidor, F.; Sillanpää, R.; Rodríguez-Romero, J.; Santillan, R.; Farfán, N.; Núñez, R. *Chem.—Eur. J.* **2013**, *19*, 6299−6312.
(16) Juárez Pérez, E. J.; Viñas, C.; Teixidor, F.; Núñez, R. *Organometallics* **2009**, *28*, 5550−5559.

DOI: 10.1021/acs.inorgchem.5b00618
Inorg. Chem. 2015, 54, 5021−5031

(17) Juárez-Pérez, E. J.; Viñas, C.; Teixidor, F.; Santillan, R.; Farfán, N.; Abreu, A.; Yépez, R.; Núñez, R. *Macromolecules* **2010**, *43*, 150−159.
(18) Núñez, R.; Juárez-Pérez, E. J.; Teixidor, F.; Santillan, R.; Farfán, N.; Abreu, A.; Yépez, R.; Viñas, C. *Inorg. Chem.* **2010**, *49*, 9993−10000.
(19) Grimes, R. N. *Carboranes*, 2nd ed.; Academic Press: London, 2011.
(20) Julius, R. L.; Farha, O. K.; Chiang, J.; Perry, L. J.; Hawthorne, M. F. *Proc. Natl. Acad. Sci. U. S. A.* **2007**, *104*, 4808−4813.
(21) Scholz, M.; Blobaum, A. L.; Marnett, L. J.; Hey-Hawkins, E. *Bioorg. Med. Chem.* **2012**, *20*, 4830−4837.
(22) Brynda, J.; Mader, P.; Šícha, V.; Fábry, M.; Poncová, K.; Bakardiev, M.; Grüner, B.; Cígler, P.; Řezáčová, P. *Angew. Chem., Int. Ed.* **2013**, *52*, 13760−13763.
(23) Issa, F.; Kassiou, M.; Rendina, L. M. *Chem. Rev.* **2011**, *111*, 5701−5722.
(24) Bednarska, K.; Olejniczak, A. B.; Klink, M.; Sułowska, Z.; Leśnikowski, Z. J. *Bioorg. Med. Chem. Lett.* **2014**, *24*, 3073−3078.
(25) Armstrong, A. F.; Valliant, J. F. *Dalton Trans.* **2007**, 4240−4251.
(26) Scholz, M.; Hey-Hawkins, E. *Chem. Rev.* **2011**, *111*, 7035−7062.
(27) Calabrese, G.; Nesnas, J. J.; Barbu, E.; Fatouros, D.; Tsibouklis, J. *Drug Discovery Today* **2012**, *17*, 153−159.
(28) Hosmane, N. *Boron Science. New Technologies and Applications*; CRC Press, Taylor & Francis Group: Boca Raton, FL, 2012.
(29) Bhupathiraju, N. V. S. D. K.; Vicente, M. G. H. *Bioorg. Med. Chem.* **2013**, *15*, 485−495.
(30) Ol'shevskaya, V. A.; Zaitsev, A. V.; Luzgina, V. N.; Kondratieva, T. T.; Ivanov, O. G.; Kononova, E. G.; Petrovskii, P. V.; Minonov, A. F.; Kalinin, V. N.; Hofmann, J.; Shtil, A. A. *Bioorg. Med. Chem.* **2006**, *14*, 109−120.
(31) Kawabata, S.; Yang, W.; Barth, R. F.; Wu, G.; Huo, T.; Binns, P. J.; Riley, K. J.; Ongayi, O.; Gottumukkala, V.; Vicente, M. G. H. *J. Neurooncol.* **2011**, *103*, 175−185.
(32) Bregadze, V. I.; Sivaev, I. B.; Gabel, D.; Wöhrle, D. *J. Porphyrins Phthalocyanines* **2001**, *5*, 767−781.
(33) Kreimann, E. L.; Miura, M.; Itoiz, M. E.; Heber, E.; Garavaglia, R. N.; Batistoni, D.; Jiménez-Rebagliati, R.; Roberti, M. J.; Micca, P. L.; Coderre, J. A.; Schwint, A. E. *Arch. Oral Biol.* **2003**, *48*, 223−232.
(34) Vicente, M. G. H.; Edwards, B. F.; Shetty, S. J.; Hou, Y.; Boggan, J. E. *Bioorg. Med. Chem.* **2002**, *10*, 481−492.
(35) Pietrangeli, D.; Rosa, A.; Ristori, S.; Salvati, A.; Altieri, S.; Ricciardi, G. *Coord. Chem. Rev.* **2013**, *257*, 2213−2231.
(36) Jin, R. H.; Aida, T.; Inoue, S. *J. Chem. Soc., Chem. Commun.* **1993**, 1260−1262.
(37) Jiang, D.-L.; Aida, T. *Chem. Commun.* **1996**, 1523−1524.
(38) Zhang, G.-D.; Harada, A.; Nishiyama, N.; Jiang, D.-L.; Koyama, H.; Aida, T.; Kataoka, K. *J. Controlled Release* **2003**, *93*, 141−150.
(39) Nishiyama, N.; Stapert, H. R.; Zhang, G.-D.; Takasu, D.; Jiang, D.-L.; Nagano, T.; Aida, T.; Kataoka, K. *Bioconjugate Chem.* **2003**, *14*, 58−66.
(40) Jang, W.-D.; Nishiyama, N.; Zhang, G.-D.; Harada, A.; Jiang, D.-L.; Kawauchi, S.; Morimoto, Y.; Kikuchi, M.; Koyama, H.; Aida, T.; Kataoka, K. *Angew. Chem., Int. Ed.* **2005**, *44*, 419−423.
(41) Nishiyama, N.; Nakagishi, Y.; Morimoto, Y.; Lai, P.-S.; Miyazaki, K.; Urano, K.; Horie, S.; Kumagai, M.; Fukushima, S.; Cheng, Y.; Jang, W.-D.; Kikuchi, M.; Kataoka, K. *J. Controlled Release* **2009**, *133*, 245−251.
(42) Li, W.-S.; Aida, T. *Chem. Rev.* **2009**, *109*, 6047−6076.
(43) Singh, K.; Sharma, A.; Behal, S.; Kaur, P. *Lett. Org. Chem.* **2007**, *4*, 374−377.
(44) Tamiaki, H.; Matsumoto, N.; Unno, S.; Shinoda, S.; Tsukube, H. *Inorg. Chim. Acta* **2000**, *300*−*302*, 243−249.
(45) Adler, A. D.; Longo, F. R.; Finarelli, J. D.; Goldmacher, J.; Assour, J.; Korsakoff, L. *J. Org. Chem.* **1967**, *32*, 476−476.
(46) León-Cedeño, F.; Menes-Arzate, M.; García-Ortega, H. *Rev. Cubana Quim.* **2006**, *18*, 140−143.
(47) Landini, D.; Montanari, F.; Rolla, F. *Synthesis* **1978**, *10*, 771−773.
(48) Rojkiewicz, M.; Kús, P.; Kozub, P.; Kempa, M. *Dyes Pigm.* **2013**, *99*, 627−635.
(49) Nardis, S.; Pomarico, G.; Tortora, L.; Capuano, R.; D'Amico, A.; Natale, C. D.; Paolesse, R. *J. Mater. Chem.* **2011**, *21*, 18638−18644.
(50) Haba, O.; Haga, K.; Ueda, M.; Morikawa, O.; Konishi, H. *Chem. Mater.* **1999**, *11*, 427−432.
(51) Yamakawa, Y.; Ueda, M.; Nagahata, R.; Takeuchi, K.; Asai, M. *J. Chem. Soc., Perkin Trans. 1* **1998**, 4135−4139.
(52) Lu, K.; Wu, Y. J.; Wang, H. X.; Zhou, Z. X. *Polyhedron* **1999**, *18*, 1153−1158.
(53) Percec, V.; Dulcey, A.; Peterca, M.; Ilies, M.; Miura, Y.; Edlund, U.; Heiney, P. A. *Aust. J. Chem.* **2005**, *58*, 472−482.
(54) Uda, M.; Momotake, A.; Arai, T. *Tetrahedron Lett.* **2005**, *46*, 3021−3024.
(55) Elmer, S. L.; Zimmerman, S. C. *J. Org. Chem.* **2004**, *69*, 7363−7366.
(56) Lindsey, J. S.; Schreiman, I. C.; Hsu, P. H. C.; Kearney, C.; Marguerettaz, A. M. *J. Org. Chem.* **1987**, *52*, 827−836.
(57) Wu, W.; Zhang, X. Y.; Kang, S. X.; Gao, Y. M. *Chin. Chem. Lett.* **2010**, *21*, 312−316.
(58) Macchioni, A.; Ciancaleoni, G.; Zuccaccia, C.; Zuccaccia, D. *Chem. Soc. Rev.* **2008**, *37*, 479−489.
(59) Pregosin, P. S.; Kumar, P. G. A.; Fernandez, I. *Chem. Rev.* **2005**, *105*, 2977−2998.
(60) Cohen, Y.; Avram, L.; Frish, L. *Angew. Chem., Int. Ed.* **2005**, *44*, 520−554.
(61) Morris, K. F.; Johnson, C. S., Jr. *J. Am. Chem. Soc.* **1992**, *114*, 3139−3141.
(62) Matos, M. S.; Hofkens, J.; Verheijen, W.; De Schryver, F. C.; Hecht, S.; Pollak, K. W.; Fréchet, J. M. J.; Forier, B.; Daen, W. *Macromolecules* **2000**, *33*, 2967−2973.
(63) Li, D.; Kagan, G.; Hopson, R.; Williard, P. G. *J. Am. Chem. Soc.* **2009**, *131*, 5627−5634.
(64) Dolphin, D. *The Porphyrins*; Academic Press: New York, 1978.
(65) Sadamoto, R.; Tomioka, N.; Aida, T. *J. Am. Chem. Soc.* **1996**, *118*, 3978−3979.
(66) Harth, E. M.; Hecht, S.; Helms, B.; Malmstrom, E. E.; Fréchet, J. M. J.; Hawker, C. J. *J. Am. Chem. Soc.* **2002**, *124*, 3926−3938.
(67) Morris, G. A. *Encyclopedia of Nuclear Magnetic Resonance*; Grant, D. M., Harris, R. K., Eds.; Wiley: New York, 2002; Vol. 9, pp 35−44.
(68) Johnson, C. S., Jr. *Prog. Nucl. Magn. Reson. Spectrosc.* **1999**, *34*, 203−256.

DOI: 10.1021/acs.inorgchem.5b00618
Inorg. Chem. 2015, 54, 5021−5031

ChemPubSoc Europe

DOI: 10.1002/chem.201505044

CHEMISTRY
A European Journal
Communication

Graphene Oxide

Highly Dispersible and Stable Anionic Boron Cluster–Graphene Oxide Nanohybrids

Justo Cabrera-González,[a] Laura Cabana,[a] Belén Ballesteros,[b] Gerard Tobias,*[a] and Rosario Núñez*[a]

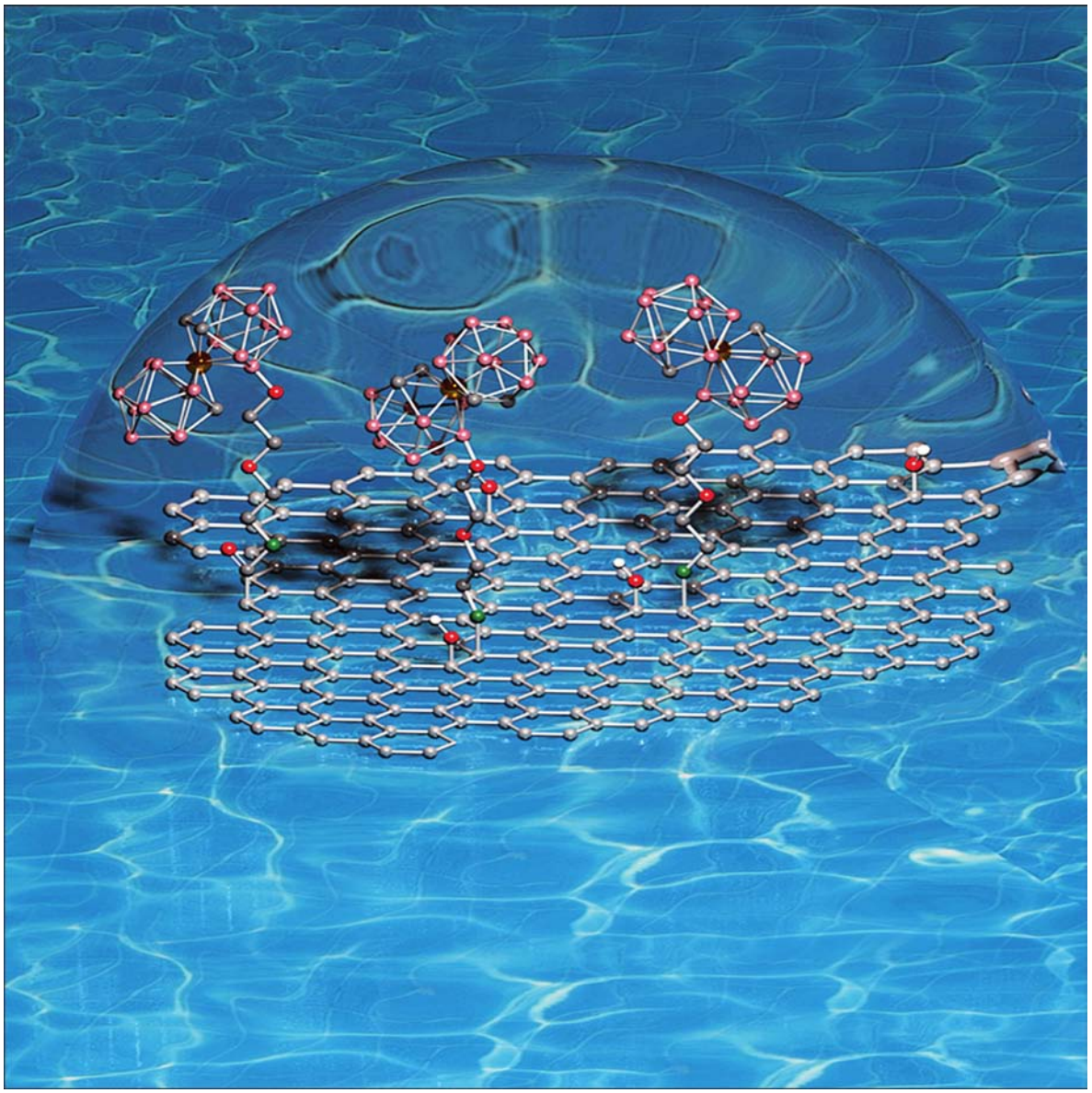

Abstract: An efficient process to produce boron cluster–graphene oxide nanohybrids that are highly dispersible in water and organic solvents is established for the first time. Dispersions of these nanohybrid materials in water were extraordinarily stable after one month. Characterization of hybrids after grafting of appropriate cobaltabisdicarbollide and *closo*-dodecaborate derivatives onto the surface of graphene oxide (GO) was done by FT-IR, XPS, and UV/Vis. Thermogravimetric analysis (TGA) clearly shows a higher thermal stability for the modified-GO nanohybrids compared to the parent GO. Of particular note, elemental mapping by energy-filtered transmission electron microscopy (EFTEM) reveals that a uniform decoration of the graphene oxide surface with the boron clusters is achieved under the reported conditions. Therefore, the resulting nanohybrid systems show exceptional physico-chemical and thermal properties, paving the way for an enhanced processability and further expanding the range of application for graphene-based materials.

In the last decade, graphene has been making a profound impact in many areas of science and technology due to its exceptional and unique chemical and physical properties.[1] The strong van der Waals interactions between graphene sheets lead to aggregation and poor solution processability, being a major drawback for many of the envisaged applications. To overcome these limitations, chemical modification of the graphitic structure has been widely employed. One of the most conventional methods consists of the treatment of graphite with strong oxidizing acids, thus leading to the formation of graphene oxide (GO).[2] The presence of oxygen-containing functional groups not only renders graphene water dispersible but also makes it an excellent starting point for further derivatisation.[3] The formation of these carbon-based hybrid materials is an efficient way not only to exploit the synergies of both constituent elements but it can also lead to unique properties,[4] which open the way to applications in nanodevices[5] and biomedicine,[6] among others.

Recent advances in the preparation of boron cluster-based materials for nanotechnology and drug design have greatly expanded their potential use in these fields.[7] From the large group of boron cluster compounds, the cobaltabisdicarbollide anion (or cosane), [3,3′-Co($C_2B_9H_{11}$)$_2$]$^-$, and the dodecahydro-*closo*-dodecaborate, also referred to as *closo*-dodecaborate dianion [$B_{12}H_{12}$]$^{2-}$, are receiving increased interest. The [3,3′-Co($C_2B_9H_{11}$)$_2$]$^-$ has exceptional chemical and thermal stability, as well as uncommon physico-chemical properties in water, owing to its self-assembling capacity,[8] inducing the ability to assemble into micelles and monolayer vesicles.[9] This anion can be accumulated in vitro within living cells[10] and after radiolabeling the cosane with ^{125}I and ^{124}I, it can be visualized in vivo by positron emission tomography–computed tomography (PET-CT).[11] Moreover, the [$B_{12}H_{12}$]$^{2-}$ shows high chemical and hydrolytic stability, high solubility in water as sodium salt, a better surfactant behaviour than the cosine,[12] and low toxicity, which are significant features for the design of pharmaceuticals, making this anion and its derivatives ideal candidates for cancer treatment with boron neutron capture therapy (BNCT).[13] Additionally, the [$B_{12}H_{12}$]$^{2-}$ finds application as molecular motors and actuators capable of delivering useful work to nano-devices for photochemical or electrochemical power sources.[14] Despite their exceptional properties, the functionalization of surfaces with cosane[15] and [$B_{12}H_{12}$]$^{2-}$ anions has been scarcely explored. Due to the uniqueness of these boron cluster anions, we are convinced that the modification of GO with them is of crucial importance to develop new materials for medical applications and devices.

Here we report an easy and efficient covalent functionalization of GO with the appropriate amine derivatives of *closo*-dodecaborate and cosane anions. The attachment of these boron clusters has been corroborated by FT-IR, UV/Vis, XPS, and TGA analysis. Although neutral boron cluster detection by electron energy loss spectroscopy (EELS) was established,[16] herein an anionic boron cluster was detected and mapped by EFTEM for the first time. Furthermore, we report here the first example of the covalent attachment of *closo*-dodecaborate on a surface.

Starting from boron clusters [3,3′-Co(8-$C_4H_8O_2$-1,2-$C_2B_9H_{10}$)(1′,2′-$C_2B_9H_{11}$)] (**1**) and [$B_{12}H_{11}$($C_4H_8O_2$)]$^-$ (**2**) (see Scheme 1 a), their respective derivatives, [8-NH_2-$C_4H_8O_2$-3,3′-Co(1,2-$C_2B_9H_{10}$)(1′,2′-$C_2B_9H_{11}$)]$^-$ (**3**) and [1-(8-NH_2-$C_4H_8O_2$)-$B_{12}H_{11}$]$^{2-}$ (**4**), were obtained by using the procedure earlier described.[15b,17] GO was prepared by a modified Hummer's method from graphite powder.[18] The boron clusters were covalently grafted onto the graphene oxide sheets through an amide and amine formation between **3** and **4** and oxygen-containing groups (e.g., carboxyl groups and epoxy) of GO.[3b] The functionalization reaction was performed by adding *N*,*N*-dicyclohexylcarbodimide (DCC) and 1-hydroxybenzotriazole (HOBt) to a dispersion of GO in dry *N*,*N*-dimethylformamide (DMF). This mixture was stirred for 30 min, followed by the addition of **3** or **4**. The reaction was performed at 40 °C over 72 h, to give **Cosane-GO** and **B_{12}-GO** hybrids, respectively (Scheme 1 b).

Characterization of the hybrid materials by FT-IR spectroscopy points out structural changes after functionalization of the GO (Figure 1). For **B_{12}-GO** and **Cosane-GO** hybrids, the ν(B–H) vibration band appears at around 2487 and 2541 cm^{-1}, respectively, which is in a similar range to a previously described neutral carborane cluster–GO hybrid.[19] After the grafting reaction, relative changes of the C=O stretching band (from carboxylic groups at 1730 cm^{-1}) and the C–O band (from epoxy groups at 1226 cm^{-1}), with respect to the C=C stretching band

[a] *J. Cabrera-González, Dr. L. Cabana, Dr. G. Tobias, Dr. R. Núñez*
Institut de Ciència de Materials de Barcelona (ICMAB-CSIC), Campus UAB
08193 Bellaterra, Barcelona (Spain)
E-mail: gerard.tobias@icmab.es
rosario@icmab.es

[b] *Dr. B. Ballesteros*
Catalan Institute of Nanoscience and Nanotechnology (ICN2), CSIC and The Barcelona Institute of Science and Technology
Campus UAB 08193 Bellaterra, Barcelona (Spain)

Supporting information and the ORCID identification numbers for some of the authors of this article can be found under http://dx.doi.org/10.1002/chem.201505044.

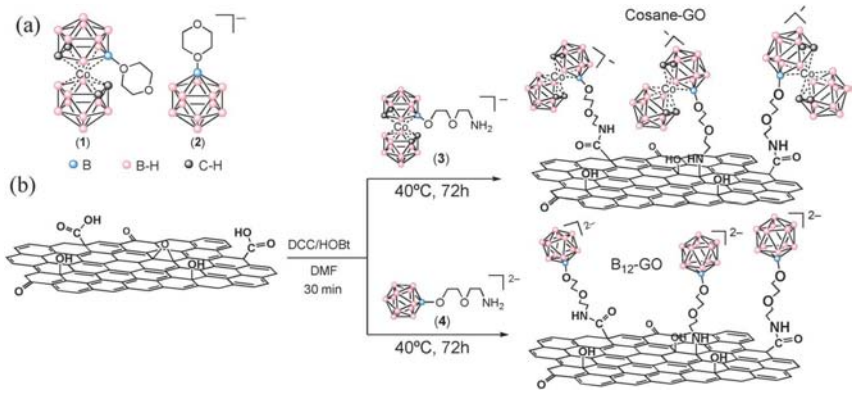

Scheme 1. a) Starting oxonium-derivative boron clusters. b) Chemical functionalization of GO with anionic boron clusters.

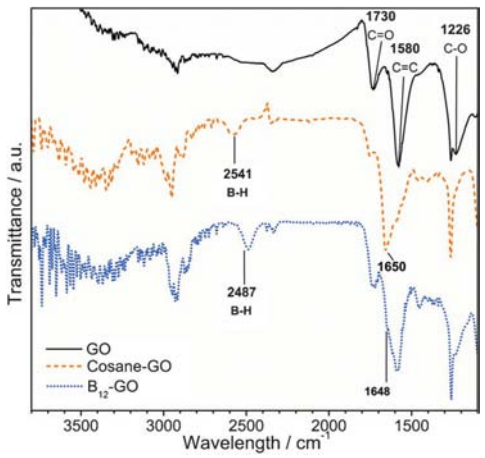

Figure 1. Infrared spectra of starting GO and modified-GO materials.

(1580 cm^{-1}) are detected.[19,20] Additionally, a shoulder at $\approx$1650 cm^{-1} from the stretching ν(NC=O) vibration is observed[21] for **B_{12}-GO** and **Cosane-GO** hybrids.

The modification of the GO surface by boron clusters was also quantitatively determined by conducting thermogravimetric analysis (TGA) in air (Figures S1–S3 in the Supporting Information). GO shows a remarkable weight loss at 220 °C due to the elimination of oxygen-bearing functionalities, and the sample is completely combusted at about 600 °C. For **B_{12}-GO** and **Cosane-GO**, the complete oxidation of the hybrid takes place at higher temperatures between 600 and 720 °C, owing to the presence of highly thermally stable borane clusters.[22] The degree of functionalization can be determined from the residue after the complete combustion of the different samples. During the process all the carbon from the GO and the organic part from the boron cluster compounds get oxidized. Hence, the solid residue obtained comes from inorganic materials and the oxidized boron cluster compounds. As expected, the residual mass after the complete combustion at 900 °C is higher for both **B_{12}-GO** and **Cosane-GO** compared to GO (see the Supporting Information). Therefore, we can establish that **Cosane-GO** and **B_{12}-GO** hybrids contain around 20.8 wt% and 18.3 wt% of the respective boron cluster derivatives. This indicates that the degree of functionalization of the GO with **3** and **4** is 484 $\mu mol\,g^{-1}$ for **Cosane-GO** and 375 $\mu mol\,g^{-1}$ for **B_{12}-GO**. Considering that the main components of the hybrids are carbon and the boron clusters, this degree of functionalization would correspond to one *closo*-dodecaborate cluster every 187 C atoms for **B_{12}-GO** and one cosane cluster every 136 C atoms for **Cosane-GO**. These levels of functionalization are similar to the recent report on the functionalization of graphene with carborane.[23] As a result, the presence of boron clusters covalently grafted to the graphene oxide surface causes an enhancement of the thermal stability of the nanohybrid materials.

X-ray photoelectron spectroscopy (XPS) analysis directly confirmed the covalent bonding of **3** and **4** onto GO. For **Cosane-GO** hybrid, B and Co can be detected in the general survey scan as well as in the high resolution XPS over the B 1s and Co 2p regions (Figure S4 in the Supporting Information). Moreover, the ratio between the two elements was determined to be 21:1, in agreement with the stoichiometry of the cosane used for the synthesis. On the other hand, for **B_{12}-GO** boron was detected in the general survey scan and high resolution XPS (Figure S5 in the Supporting Information). High resolution of the C 1s region clearly reveals the chemical modification of GO with boron cluster compounds. By doing the deconvolution, we can observe the different functionalities present on the structure of GO (Figure 2a). For **B_{12}-GO** (Figure 2b) and **Cosane-GO** (Figure 2c) hybrids, the intensities of C–O/C–O–C, at 285.8 and 285.5 eV respectively, have dramatically decreased, as well as the C=O signal from starting GO at 288.6 eV. Moreover, a new deconvolution curve attributed to C–N appears from 286.0 to 286.4.[24] This further confirms the covalent functionalization of the GO with the chosen boron clusters.

Moreover, the selected area electron diffraction (SAED) pattern of **B_{12}-GO** shows well-defined diffraction spots that corre-

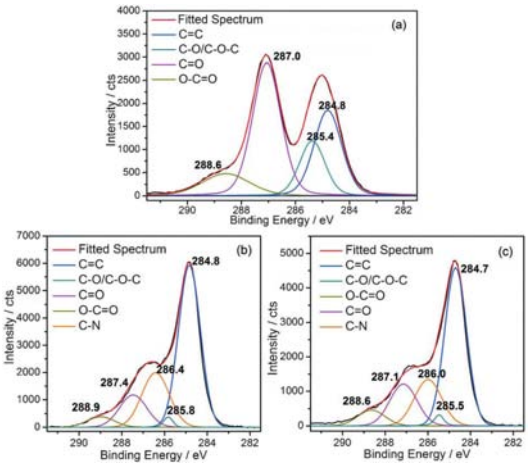

Figure 2. High resolution XPS spectra in the C 1s region for a) GO, b) **B_{12}-GO**, and c) **Cosane-GO**.

spond to the crystalline structure of the graphene (Figure S7 in the Supporting Information). In this SAED pattern of **B_{12}-GO** it is no longer possible to observe the crystalline structure of compound **4** (Figure S6 in the Supporting Information), confirming the attachment of the boron cluster as individual entities onto the surface of GO.

With regard to **Cosane-GO**, STEM-EDX (scanning transmission electron microscopy/energy-dispersive X-ray spectroscopy) was used to identify the cobalt atoms from cosane clusters. The signals at 6.924 and 0.776 keV, which belong to the energy dispersive X-ray signal from cobalt, confirm the presence of **3**, hence the functionalization of GO (Figure S8 in the Supporting Information).

In the case of **B_{12}-GO**, STEM-EDX was not useful to confirm the success of the functionalization because detection of light elements (such as B or C) presents a challenge for EDX. Instead, EELS and energy filtered transmission electron microscopy (EFTEM) were used. EELS analysis on a graphene flake shows the B-K and C-K edges, together with the O-K and N-K also present in the sample (Figure S9 in the Supporting Information). The corresponding EFTEM elemental distribution maps taken on the K-ionization edges of B and C are shown in Figure 3. Carbon is found both on the graphene flake and the carbon support film, whereas the boron map only shows bright intensity on the graphene flake (see Figures S10 and S11 in the Supporting Information for additional EFTEM maps).

UV/Vis spectra were next acquired to assess the dispersibility of GO and GO functionalized with cosane and *closo*-dodecaborate anions in H_2O. The resulting spectra of as-prepared dispersions in water for the tree samples (1 mg mL^{-1}) are exhibited in Figure 4 a. The functionalized samples were compared with GO because it is well-known that this material presents a high dispersibility in water.[3a] The UV/Vis spectrum of GO shows a characteristic maximum absorption peak at around 240 nm attributed to the π–π^* transition of aromatic C–C bonds.[25] In the modified-GO hybrids with anionic boron clusters, this absorption band is redshifted about 15–30 nm when the supernatant liquid is analyzed, which confirms the chemical modification of GO.[25,26] In the **Cosane-GO** dispersions the band around 305 nm is characteristic of the cosane anion.[27] The absorbance at $\lambda = 240$ nm was analyzed to assess the relative degree of dispersion. For ease of comparison, the absorbance of GO at 240 nm was set as 100 %. The as-prepared dispersions of GO and **B_{12}-GO** present a similar degree of dispersibility, whereas

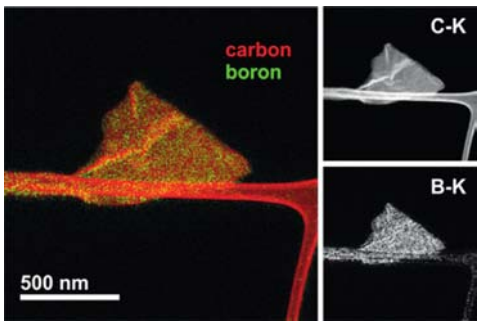

Figure 3. EFTEM elemental distribution maps of carbon and boron on sample **B_{12}-GO**.

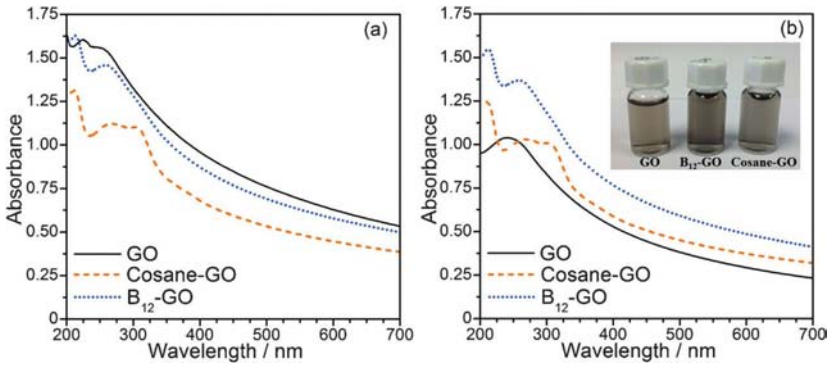

Figure 4. UV/Vis absorption spectra of GO, **Cosane-GO**, and **B_{12}-GO** dispersed in water a) as-prepared and b) after 1 month.

Cosane-GO turns out to be around 28% less dispersible. This could be due to the different surfactant behaviour of $[B_{12}H_{12}]^{2-}$ versus cosane, as was previously reported by Teixidor and co.[12] This can account for better dispersibility of **B_{12}-GO** with respect to **cosane-GO**. Remarkably, after 1 month (Figure 4b) the water dispersibility of GO decreased by 33% and both boron cluster-modified–GO hybrid dispersions remain almost unaltered; **B_{12}-GO** shows about 32% more dispersibility than GO and **Cosane-GO** preserves its degree of dispersibility, which now is slightly higher than GO. A picture of the analyzed dispersions is included in the inset of Figure 4b. Noticeably, this indicates that the chemical modification of GO with these anionic boron clusters resulted in an improved stability of the aqueous dispersions. It becomes clear that covalent bonding of boron clusters onto graphene oxide changes the chemical and physical characteristics of the graphene surface. Thus, we have analyzed as-prepared dispersions of the different materials in THF by UV/Vis and in acetone by visual inspection, owing to its strong absorption below 340 nm. An evident increase of dispersibility was observed for THF dispersions of **Cosane-GO** hybrids with respect to GO (Figure S12 in the Supporting Information). In acetone (Figure S13 in the Supporting Information), the GO dispersion is not stable[25] but the supernatant liquid of **Cosane-GO** and **B_{12}-GO** shows noteworthy color intensity after one hour. Consequently, these boron clusters play a crucial role in the dispersibility properties of the hybrid materials to markedly improve the stability of dispersions both in water and organic solvents. To the best of our knowledge, these are the first examples of boron modified-GO hybrids that show this feature, which is of great interest for further processing and applications.

To summarize, we have covalently grafted amine-functionalized cosane and $[B_{12}H_{12}]^{2-}$ anions onto the surface of graphene oxide. The efficient covalent grafting was corroborated by FT-IR and XPS. TGA showed different weight loss for boron cluster compounds grafted onto graphene oxide compared to unmodified graphene, the former being more thermally stable. Remarkably, chemical modification of graphene oxide with these anionic boron clusters results in nanohybrids with an enhanced dipersibility both in water and in organic solvents, as well as highly stable aqueous dispersions, as assessed by UV/Vis. Notably, EFTEM imaging has provided elemental maps confirming the uniform distribution of the boron clusters on the graphene oxide flakes. In conclusion, the combination of cobaltabisdicarbollide and *closo*-dodecaborate anions with graphene oxide leads to new high-boron-content materials with exceptional physico-chemical and thermal properties. The development of applications for these nanohybrids is currently in progress.

Acknowledgements

This work has been supported by Ministerio de Economía y Competitividad, (MINECO; CTQ2013-44670-R, MAT2014-53500-R) and Generalitat de Catalunya (2014/SGR/149). J.C.-G. thanks the CSIC for an intramural grant. ICMAB and ICN2 acknowledge financial support from the Spanish Ministry of Economy and Competitiveness, through the "Severo Ochoa" Programme for Centres of Excellence in R&D (SEV- 2015-0496 and SEV-2013-0295). J.C.G. is enrolled in the UAB Ph.D. program.

Keywords: boron clusters · dispersibility · electron microscopy · graphene oxide

[1] a) A. K. Geim, K. S. Novoselov, *Nat. Mater.* **2007**, *6*, 183–191; b) A. K. Geim, *Science* **2009**, *324*, 1530–1534; c) X. Huang, Z. Yin, S. Wu, X. Qi, Q. He, Q. Zhang, Q. Yan, F. Boey, H. Zhang, *Small* **2011**, *7*, 1876–1902.

[2] P. Wick, A. E. Louw-Gaume, M. Kucki, H. F. Krug, K. Kostarelos, B. Fadeel, K. A. Dawson, A. Salvati, E. Vázquez, L. Ballerini, M. Tretiach, F. Benfenati, E. Flahaut, L. Gauthier, M. Prato, A. Bianco, *Angew. Chem. Int. Ed.* **2014**, *53*, 7714–7718; *Angew. Chem.* **2014**, *126*, 7846–7850.

[3] a) D. Chen, H. Feng, J. Li, *Chem. Rev.* **2012**, *112*, 6027–6053; b) V. Georgakilas, M. Otyepka, A. B. Bourlinos, V. Chandra, N. Kim, K. C. Kemp, P. Hobza, R. Zboril, K. S. Kim, *Chem. Rev.* **2012**, *112*, 6156–6214; c) D. Bitounis, H. Ali-Boucetta, B. H. Hong, D.-H. Min, K. Kostarelos, *Adv. Mater.* **2013**, *25*, 2258–2268.

[4] a) C. J. Shearer, A. Cherevan, D. Eder, *Adv. Mater.* **2014**, *26*, 2295–2318; b) L. Cabana, B. Ballesteros, E. Batista, C. Magén, R. Arenal, J. Oró-Solé, R. Rurali, G. Tobias, *Adv. Mater.* **2014**, *26*, 2016–2021; c) L. Shao, X. Huang, D. Teschner, W. Zhang, *ACS Catal.* **2014**, *4*, 2369–2373.

[5] S. J. Kim, K. Choi, B. Lee, Y. Kim, B. H. Hong, *Annu. Rev. Mater. Res.* **2015**, *45*, 63–84.

[6] a) C. Chung, Y.-K. Kim, D. Shin, S.-R. Ryoo, B. H. Hong, D.-H. Min, *Acc. Chem. Res.* **2013**, *46*, 2211–2224; b) K. Kostarelos, K. S. Novoselov, *Science* **2014**, *344*, 261–263; c) A. Servant, A. Bianco, M. Prato, K. Kostarelos, *Bioorg. Med. Chem. Lett.* **2014**, *24*, 1638–1649.

[7] a) R. N. Grimes, in *Carboranes (Second Edition)* (Ed.: R. N. Grimes), Academic Press, Oxford, **2011**, pp. 1053–1082; b) N. S. Hosmane, *Boron Science: New Technologies and Applications*, CRC Press, Taylor & Francis, Boca Raton, **2011**; c) R. Kaplánek, P. Martásek, B. Grüner, S. Panda, J. Rak, B. S. S. Masters, V. Král, L. J. Roman, *J. Med. Chem.* **2012**, *55*, 9541–9548; d) M. Scholz, E. Hey-Hawkins, *Chem. Rev.* **2011**, *111*, 7035–7062.

[8] P. Matějíček, P. Cígler, A. B. Olejniczak, A. Andrysiak, B. Wojtczak, K. Procházka, Z. J. Lesnikowski, *Langmuir* **2008**, *24*, 2625–2630.

[9] P. Bauduin, S. Prevost, P. Farràs, F. Teixidor, O. Diat, T. Zemb, *Angew. Chem. Int. Ed.* **2011**, *50*, 5298–5300; *Angew. Chem.* **2011**, *123*, 5410–5412.

[10] M. Tarrés, E. Canetta, C. Viñas, F. Teixidor, A. J. Harwood, *Chem. Commun.* **2014**, *50*, 3370–3372.

[11] K. B. Gona, A. Zaulet, V. Gómez-Vallejo, F. Teixidor, J. Llop, C. Viñas, *Chem. Commun.* **2014**, *50*, 11415–11417.

[12] C. Viñas, M. Tarrès, P. González-Cardoso, P. Farràs, P. Bauduin, F. Teixidor, *Dalton Trans.* **2014**, *43*, 5062–5068.

[13] a) S. Tachikawa, T. Miyoshi, H. Koganei, M. E. El-Zaria, C. Viñas, M. Suzuki, K. Ono, H. Nakamura, *Chem. Commun.* **2014**, *50*, 12325–12328; b) M. Neumann, U. Kunz, H. Lehmann, D. Gabel, *J. Neuro-Oncol.* **2002**, *57*, 97–104.

[14] M. W. Lee, O. K. Farha, M. F. Hawthorne, C. H. Hansch, *Angew. Chem. Int. Ed.* **2007**, *46*, 3018–3022; *Angew. Chem.* **2007**, *119*, 3078–3082.

[15] a) E. J. Juárez-Pérez, P. H. Mutin, M. Granier, F. Teixidor, R. Núñez, *Langmuir* **2010**, *26*, 12185–12189; b) E. J. Juárez-Pérez, M. Granier, C. Viñas, P. H. Mutin, R. Núñez, *Chem. Asian J.* **2012**, *7*, 277–281; c) L. Cabana, A. González-Campo, X. Ke, G. Van Tendeloo, R. Núñez, G. Tobias, *Chem. Eur. J.* **2015**, *21*, 16792–16795.

[16] D. A. Morgan, J. Sloan, M. L. H. Green, *Chem. Commun.* **2002**, 2442–2443.

[17] A. Semioshkin, E. Nizhnik, I. Godovikov, Z. Starikova, V. Bregadze, *J. Organomet. Chem.* **2007**, *692*, 4020–4028.

[18] S. Sandoval, N. Kumar, A. Sundaresan, C. N. R. Rao, A. Fuertes, G. Tobias, *Chem. Eur. J.* **2014**, *20*, 11999–12003.

[19] V. Štengl, S. Bakardjieva, M. Bakardjiev, B. Štíbr, M. Kormunda, *Carbon* **2014**, *67*, 336–343.

[20] Y. Xue, Y. Liu, F. Lu, J. Qu, H. Chen, L. Dai, *J. Phys. Chem. Lett.* **2012**, *3*, 1607–1612.

[21] S. Niyogi, E. Bekyarova, M. E. Itkis, J. L. McWilliams, M. A. Hamon, R. C. Haddon, *J. Am. Chem. Soc.* **2006**, *128*, 7720 – 7721.
[22] A. González-Campo, B. Boury, F. Teixidor, R. Núñez, *Chem. Mater.* **2006**, *18*, 4344 – 4353.
[23] J. U. Kahlert, A. Rawal, J. M. Hook, L. M. Rendina, M. Choucair, *Chem. Commun.* **2014**, *50*, 11332 – 11334.
[24] S. Stankovich, D. A. Dikin, R. D. Piner, K. A. Kohlhaas, A. Kleinhammes, Y. Jia, Y. Wu, S. T. Nguyen, R. S. Ruoff, *Carbon* **2007**, *45*, 1558 – 1565.
[25] J. I. Paredes, S. Villar-Rodil, A. Martínez-Alonso, J. M. D. Tascón, *Langmuir* **2008**, *24*, 10560 – 10564.
[26] S. Sandoval, N. Kumar, J. Oro-Solé, A. Sundaresan, C. N. R. Rao, A. Fuertes, G. Tobias, *Carbon* **2016**, *96*, 594 – 602.
[27] R. Núñez, E. J. Juárez-Pérez, F. Teixidor, R. Santillan, N. Farfán, A. Abreu, R. Yépez, C. Viñas, *Inorg. Chem.* **2010**, *49*, 9993 – 10000.

Received: December 15, 2015
Published online on ■■ ■■, 0000

ANEXO II:
ARTÍCULOS EN PREPARACIÓN O PENDIENTES DE PUBLICACIÓN

Carborane-stilbene dyads: Influence of substituents and isomers on the photoluminescent properties

Albert Ferrer-Ugalde,[a] Justo Cabrera-González,[a] Emilio José Juárez-Pérez,[a] Clara Viñas,[a] Francesc Teixidor[a], Ezequiel Pérez-Inestrosa,[b] Jose María Montenegro,[b] Reijo Sillanpää,[c] Matti Haukka,[c] Rosario Núñez*[a]

[a] Institut de Ciència de Materials de Barcelona (ICMAB-CSIC), Campus U.A.B., 08193, Bellaterra, Barcelona, Spain. E-mail: rosario@icmab.es

[b] Department of Organic Chemistry, Faculty of Sciences, University of Málaga, Málaga, Spain.

[c] Department of Chemistry, University of Jyväskylä, FIN-40014, Jyväskylä, Finland

 # J. Cabrera-González is enrolled in the UAB PhD program.

Introduction

Functionalized stilbenes (1,2-diphenylethylene) have attracted immense attention over the past decades, being widely used in the manufacture of dyes, dye lasers, optical brighteners and other materials.[1] Stilbene exists as two possible isomers, *trans*- and *cis*-1,2-diphenylethylene, the latter being much less stable due to steric hindrance between the aromatic rings, forcing them to be out-of-plane, breaking their conjugation. *Trans*-stilbene derivatives are usually thermally and chemically stable compounds, possessing unique photoluminescence properties that are convenient for monitoring by relevant optical techniques. *Trans*-Stilbene isomerizes to *cis*-stilbene under the influence of light, whereas the reverse path can be induced by heat or light. For this reason, the fluorescence of *trans*-stilbene derivatives is generally complex, leading to weak emissions in diluted aqueous solutions or typical organic solvents due to the formation of a twisted intermediate.[2] The role of many different stilbene derivatives in photochemistry and photophysics has been exhaustively reviewed,[3] leading to a progressive interest of researchers in applying these molecules in a wide diversity of

applications such as biomedicine,[4] lasers,[5] electro-optic materials,[6] LEDs,[7] non-linear optics[8] and scintillators.[9]

Dicarba-*closo*-dodecaboranes, or simply known as carboranes ($C_2B_{10}H_{12}$), are electron-deficient boron clusters with a three-dimensional delocalization of the electrons inside the cage. Depending on the relative positions of the two carbon atoms within the boron structure, there exists three different possible isomers, *ortho* (1,2-$C_2B_{10}H_{12}$), *meta* (1,7-$C_2B_{10}H_{12}$), and *para* (1,12-$C_2B_{10}H_{12}$). They all possess □-bond interactions, which allow them to interact electronically with □-conjugated systems, leading to relevant changes in the final photophysical properties of the latter.[10] However, very different electronic properties between the three isomers have been reported, especially their electron-withdrawing capacity, which has been found to be much larger for the *ortho*- isomer when compared to its *meta*- and *para*-counterparts.[11] These differences can be explained by a better electronic delocalization and a lower distortion of the cage in the following order: *para* ≈ *meta* >>> *ortho*.[12] This particular electronic behavior of the *ortho* isomer has led to extensive studies about its role in the photoluminescence properties of different systems incorporating *o*-carboranes. It has been widely reported that when a particular fluorophore is directly attached to at least one of the $C_{cluster}$ (C_c) atoms of the cage, an efficient quenching of the fluorescence is generally observed.[11c, 13] It is generally accepted that the quenching takes place due to a rapid photoinduced electron-transfer (PET) process, in which the fluorophore, gives an electron from its S_1 excited state to the lower energy excited state S_x of the cluster, and then relaxed to the ground state in a non-radiative way.[14] At the same time, a significant enlargement of the Cc-Cc bond length is commonly observed for *o*-carborane derivatives, making a possible correlation between this fact and the PET process.[15] Therefore, a sharp increase on the research of new carborane-based photoluminescent materials has been observed in the last years, as exemplified by the deployment of these compounds in different applications such as sensors of nucleophilic anions,[16] dyads in optoelectronic devices such as organic field-effect transistors (OFETs),[17] or light-emitting diodes (OLEDs, PLEDs, PHOLEDs),[18] and their use in microscopy imaging, especially in two-photon absorption (TPA) for biomedicine purposes.[19]

In a previous work in our laboratory, the synthesis and the fluorescence of *o*-carboranyl-functionalized Fréchet-type poly(aryl-ether) derivatives exhibiting intense blue emission under UV irradiation in different solvents at room temperature was reported.[20] To the best of our knowledge, this was the first example of fluorescent molecules bearing *o*-carboranyl fragments. In addition, we recently reported the synthesis and the photophysical behavior of small molecules based on *o*-carboranyl-substituted styrenes, anthracenes and fluorenes,[13a, 15b] and also larger molecules such as dendrimers or octasilsesquioxanes functionalized with up to 9 clusters per molecule.[21] In many of these compounds, the donor group is generally linked to the carborane cage through a methylene spacer. We demonstrated the key role of the substituent attached to the adjacent Cc atom as well as the nature of the cluster in determining the fluorescence intensity. In these systems, the introduction of an aromatic group attached to the carborane cage was found to quench efficiently the fluorescence of the fluorophore due to a PET process.

Therefore, the aim of this work has been focused on the design, synthesis and study of the photoluminescence properties of novel stilbene-containing *ortho* and *meta*-carborane derivatives. Although different types of approaches can be used to synthesize stilbenes,[1] the method chosen to prepare the new compounds was the Heck coupling, due to their high selectivity and ease of synthesis. All the compounds were properly characterized and the crystal structures of seven stilbene- substituted carboranes have been determined by X-ray diffraction analysis and reported herein. Experimental and theoretical comparative studies of the photoluminescent (PL) properties between the *ortho* and *meta*-carborane derivatives and the influence of the substituents on the adjacent cluster carbon atom have also been carried out.

Instrumentation. Elemental analyses were performed using a Carlo Erba EA1108 microanalyzer. IR spectra were recorded from KBr pellets on a Shimadzu FTIR-8300 spectrophotometer. The ^{1}H NMR (300.13 MHz), $^{11}B\{^{1}H\}$ and ^{11}B NMR (96.29 MHz) and $^{13}C\{^{1}H\}$ NMR (75.47 MHz) spectra were recorded on a Bruker ARX 300 spectrometer. All NMR spectra were recorded in $CDCl_3$ or CD_3COCD_3 solutions at 25ºC. Chemical shift values for $^{11}B\{^{1}H\}$ NMR spectra were referenced to external $BF_3{\cdot}OEt_2$, and those for ^{1}H

and $^{13}C\{^1H\}$ NMR were referenced to $SiMe_4$. Chemical shifts are reported in units of parts per million downfield from reference, and all coupling constants are reported in Hertz. MALDI-TOF-MS mass spectra were recorded in the negative ion mode using a Bruker Biflex MALDI-TOF [N2 laser; λexc 337 nm (0.5 ns pulses); voltage ion source 20.00 kV (Uis1) and 17.50 kV (Uis2)]. UV-vis spectra were recorded on Shimadzu UV-1700 Pharmaspec spectrophotometer, using 0.1 cm cuvettes. The concentration of the compounds was 10^{-4} mol·L^{-1} The fluorescence emission spectra were recorded in a JASCO FP-750 spectrofluorometer and a FLS 920 from Edinburgh Instruments using a 450W Xe lamp as excitation source. Samples were prepared in spectroscopic grade solvents and adjusted to a response within the linear range. No fluorescent contaminants were detected on excitation in the wavelength region of experimental interest. Fluorescence quantum yields were determined by comparison with styrene or stilbene as reference, and corrected for the refractive index of the solvent, cyclohexane for styrene (n = 1.426) and methylcyclohexane for stilbene (n = 1.422). Samples were prepared in such a way as to obtain an absorbance of 0.1–0.2 at the excitation wavelength. The quantum yield for *i* was determined by $\Phi_i = [(F_i \cdot A_R \cdot n_i^2)/ (F_R \cdot A_i \cdot n_R^2)] \cdot \Phi_R$ where $f_i = 1\text{-}10^{-Ai}$, F are the integrated intensities, A the absorbances and n the refractive indices.

Materials. All reactions were performed under an atmosphere of dinitrogen employing standard Schlenk techniques. Tetrahydrofuran and 1,4-dioxane were purchased from Merck and distilled from sodium benzophenone previously to use. DMF was purchased from Aldrich and distilled over anhydrous calcium oxide prior use. Commercial grade diethyl ether, ethyl acetate, hexane, chloroform and dichloromethane were used without further purification. Compounds 1-C_6H_5-1,2-*closo*-$C_2B_{10}H_{11}$ and 1-CH_3-1,2-*closo*-$C_2B_{10}H_{11}$ were supplied by Katchem Ltd. (Prague) and used as received. 1-CH_3-1,7-*closo*-$C_2B_{10}H_{11}$ and 1-C_6H_5-1,7-*closo*-$C_2B_{10}H_{11}$ were obtained by thermal isomerization following the literature procedure.[22] 4-vinylbenzyl chloride, *n*-BuLi solution (1.6 M in hexane), 4-iodobenzyl bromide, $Pd_2(dba)_3$ and $Pd(t\text{-}Bu_3P)_2$ were purchased from Aldrich. Iodobenzene was purchased from Alfa Aesar and NCy_2Me from Acros. Compounds **1, 2** and **5** were obtained using literature procedures.[13a, 23]

X-ray Structure Determinations. The crystals of **6**, **7**, **9**, **12**, **13**, **14**, and **15** were immersed in cryo-oil, mounted in MiTeGen loops, and measured at 120-123 K. The X-ray diffraction data were collected on a Rigaku Oxford Diffraction Supernova diffractometer using Cu Kα (λ = 1.54184 Å) radiation or on a Nonius Kappa ApexII diffractometer using Mo Kα (λ = 0.71073 Å) radiation. The Denzo/Scalepack[24] or CrysAlisPro[25] program packages were used for cell refinements and data reductions. The structures were solved by direct methods or by charge flipping method using the SHELXS-97[26] or Superflip[27] programs. A multi-scan or Gaussian absorption correction (SADABS[28] or CrysAlisPro[25]) was applied to structural data of **6**, **7**, **12**, **14**, and **15**. Structural refinements were carried out using SHELXL-97 or SHELXL-2014[26] programs. The unit cell of structures **9** and **12** contained two independent molecules. In structure **9**, carbon atoms in the double bond between the aromatic rings in one of the stilbene ligands were disordered over two sites. Structure **12** was refined as a racemic twin. The BASF value was refined to 0.017. In all structures the hydrogen atoms were positioned geometrically and constrained to ride on their parent atoms with C-H = 0.95-0.99 Å, B-H 1.12 Å, and U_{iso} = 1.2-1.5·U_{eq}(parent atom). Crystallographic details are summarized in Table 2 and selected bond lengths in Table S1.

Calculations. Ground-state calculations were carried out by using hybrid DFT (B3LYP functional) and Ahlrichs def2-TZV basis set[29] as implemented in the ORCA 3.0.1 package.[30] Partial density of state (PDOS) of the fragments fluorophore (styrenyl or stilbenyl), carboranyl substituent (methyl or phenyl) and carborane cage (*ortho*-, *meta* or *para*-carborane) and their orbital composition analysis (Mulliken type with 0.5 eV of FWHM) were obtained using Multiwfn 3.3.7.[31] Probabilty (60 %) isodensity for the HOMO – LUMO 3D contour plots of the compounds were obtained using Gabedit.[32]

Compound 3.- A dry 25 mL round-bottomed flask equipped with a condenser and a magnetic stirring bar was charged under nitrogen with a solution of 1-CH_3-1,7-$C_2B_{10}H_{11}$ (0.520 g, 3.30 mmol) in THF (10 mL) at 0°C. Then, a solution of *n*BuLi 1.6M in hexanes (2.3 mL, 3.70 mmol) was added dropwise to the mixture, which was allowed to stir for 1 h at room temperature and cooled again at 0°C. Then, [4-(CH_2=CH)-C_6H_4-CH_2]Cl (0.57 mL, 3.60 mmol) was added rapidly to the mixture under vigorous stirring and it was

reflux overnight. After that, the solvent was removed under vacuum and the oily residue was extracted with Et_2O (3x10 mL), transferred to a separating funnel and washed with H_2O (3 x 15 mL). The organic layer was dried over $MgSO_4$ and the volatiles were reduced under vacuum. The yellowish oil residue was purified by preparative layer chromatography (dichloromethane/hexane 1:1) to give **3** as colorless oil. Yield: 0.604 g, 67 %. ^{1}H NMR ($CDCl_3$, TMS), δ(ppm): 7.38 (d, 2H, ^3J(H,H) = 9 Hz, C_6H_4), 7.09 (d, 2H, ^3J(H,H) = 9 Hz, C_6H_4), 6.73 (dd, 1H, ^3J(H,H) = 18 Hz, ^3J(H,H) = 9 Hz, C*H*=CH_2), 5.77 (d,1H, ^3J(H,H) = 18 Hz, CH=CH_2), 5.28 (d, 1H, ^3J(H,H) = 9 Hz, CH=CH_2), 3.19 (s, 2H, CH_2), 1.66 (s, 3H, CH_3); ^{1}H{^{11}B} NMR ($CDCl_3$, TMS), δ(ppm): 7.38 (d, 2H, ^3J(H,H) = 6 Hz, C_6H_4), 7.09 (d, 2H, ^3J(H,H) = 9 Hz, C_6H_4), 6.73 (dd, 2H, ^3J(H,H) = 18 Hz, ^3J(H,H) = 9 Hz, 1H, C*H*=CH_2), 5.77 (d, 1H, ^3J(H,H) = 18 Hz, CH=CH_2), 5.28 (d, 1H, ^3J(H,H) = 9Hz, CH=CH_2), 3.20 (s, 2H, CH_2), 2.62 (s, 2H, B-*H*), 2.21 (s, 6H, B-*H*), 2.07 (s, 2H, B-*H*), 1.66 (s, 3H, CH_3); ^{11}B NMR (CD_3COCD_3,BF_3·Et_2O), δ(ppm): -5.09 (d, 1B, ^1J(B,H) = 162 Hz), -6.78 (d, 1B, ^1J(B,H) = 224 Hz), -9.46 (d, 6B, ^1J(B,H) = 165 Hz), -11.43 (d, 2B, ^1J(B,H) = 188 Hz); ^{13}C{^{1}H} NMR (CD_3COCD_3, TMS), δ(ppm): 136.89 (s, CH-C_6H_4), 136.79 (s, CH_2-C_6H_4), 136.47 (s, *C*H=CH_2), 130.17 (s, C_6H_4), 126.13 (s, C_6H_4), 113.45 (s, CH=*C*H_2), 77.28 (s, C_c-CH_2), 71.15 (s, C_c-CH_3), 42.09 (s, *C*H_2), 23.86 (s, C_c-*C*H_3); ATR (ν_{max}/cm^{-1}): 3089 (w, C-H st), 3007 (w, C-H st), 2937 (w, C-H st), 2586 (s, B-H st); Anal.Calcd. for $C_{12}H_{22}B_{10}$: C, 52.52; H, 8.08. Found: C, 52.80; H, 8.22.

Compound 4.- The procedure was the same as for **3**, but using a solution of 1-C_6H_5-1,7-$C_2B_{10}H_{11}$ (0.218 g, 0.99 mmol) in Et_2O (3 mL), *n*BuLi 1.6M in hexanes (0.68 mL, 1.10 mmol) and a solution of [4-(CH_2=CH)-C_6H_4-CH_2]Cl (0.17 mL, 1.09 mmol) in THF (2 mL). After work-up, the yellowish oil residue was purified by preparative layer chromatography (dichloromethane/hexane 2:3) to give **4** as colorless oil. Yield: 0.133 g, 40 %. ^{1}H NMR ($CDCl_3$, TMS), δ(ppm): 7.41-7.38 (m, 4H, C_6H_4 and C_6H_5), 7.30-7.25 (m, 3H, C_6H_5), 7.13 (d, 2H, ^3J(H,H) = 9 Hz, C_6H_4), 6.74 (dd, 1H, ^3J(H,H) = 18 Hz, ^3J(H,H) = 9 Hz, C*H*=CH_2), 5.79 (d, 1H, ^3J(H,H) = 18 Hz, CH=CH_2), 5.29 (d, 1H, ^3J(H,H) = 9 Hz, CH=CH_2), 3.29 (s, 2H, CH_2); ^{1}H{^{11}B} NMR ($CDCl_3$, TMS), δ(ppm): 7.41-7.38 (m, 4H, C_6H_4 and C_6H_5), 7.30-7.25 (m, 3H, C_6H_5), 7.13 (d, 2H, ^3J(H,H) = 9 Hz, C_6H_4), 6.74 (dd, 2H, ^3J(H,H) = 18 Hz, ^3J(H,H) = 9 Hz, 1H, C*H*=CH_2), 5.79 (d, 1H, ^3J(H,H) = 18 Hz, CH=CH_2), 5.29 (d, 1H, ^3J(H,H) =

9 Hz, CH=CH_2), 3.29 (s, 2H, CH_2), 2.93 (s, 2H, B-*H*), 2.53 (s, 3H, B-*H*), 2.41 (s, 1H, B-*H*), 2.34 (s, 2H, B-*H*), 2.22 (s, 2H, B-*H*); ^{11}B NMR ($CDCl_3$, $BF_3{\cdot}Et_2O$), δ (ppm): -6.04 (d, 1B, ^1J(B,H) = 101 Hz), -6.83 (d, 1B, ^1J(B,H) = 111 Hz), -10.79 (d, 6B, ^1J(B,H) = 154 Hz), -13.63 (d, 2B, ^1J(B,H) = 175 Hz); ^{13}C{^{1}H} NMR (CD_3COCD_3, TMS), δ (ppm): 136.88 (s, CH-C_6H_4), 136.40 (s, CH_2-C_6H_4), 136.33 (s, *C*H=CH_2), 135.28 (s, C_c-C_6H_5), 130.06 (s, C_6H_4), 128.54 (s, C_6H_5), 128.25 (s, C_6H_5), 127.78 (s, C_6H_5), 126.28 (s, C_6H_4), 114.08 (s, CH=*C*H_2), 78.15 (s, C_c-C_6H_5), 76.27 (s, C_c-CH_2), 42.93 (s, *C*H_2); ATR (ν_{max}/cm^{-1}): 3029 (m, C-H st), 2928 (m, C-H st), 2854 (w, C-H st), 2585 (s, B-H st); Anal.Calcd. for $C_{17}H_{24}B_{10}$: C, 60.68; H, 7.19. Found: C, 60.92; H, 7.46.

Compound 5.- Following the literature procedure, compound **5** was obtained in 65% from 1-CH_3-1,2-$C_2B_{10}H_{11}$ (0.325 g, 2.06 mmol) and 4-iodobenzyl bromide (0.606 g, 1.98 mmol) in THF. ^{1}H NMR ($CDCl_3$, TMS), δ(ppm): 7.70 (d, 2H, ^3J(H,H) = 9 Hz, C_6H_4), 6.95 (d, 2H, ^3J(H,H) = 9 Hz, C_6H_4), 3.42 (s, 2H, CH_2), 2.17 (s, 3H, CH_3); ^{1}H{^{11}B} NMR ($CDCl_3$, TMS), δ(ppm): 7.70 (d, 2H, ^3J(H,H) = 9 Hz, C_6H_4), 6.95 (d, 2H, ^3J(H,H) = 9 Hz, C_6H_4), 3.42 (s, 2H, CH_2), 2.29 (s, 3H, B-*H*), 2.19 (s, 2H, B-*H*), 2.17 (s, 3H, CH_3), 2.10 (s, 3H, B-*H*), 2.05 (s, 2H, B-*H*); ^{11}B NMR ($CDCl_3$, $BF_3{\cdot}Et_2O$), δ(ppm): -4.15 (d, 1B, ^1J(B,H) = 150 Hz), -5.78 (d, 1B, ^1J(B,H) = 154 Hz), -9.91 (d, 4B, ^1J(B,H) = 100 Hz), -10.55 (d, 4B, ^1J(B,H) = 117 Hz); ^{13}C{^{1}H} NMR ($CDCl_3$, TMS), δ(ppm): 137.79 (s, C_6H_4), 134.54 (s, C_6H_4), 132.15 (s, C_6H_4), 93.85 (s, *C*-I), 74.81 (s, C_c-CH_3), 40.75 (*C*H_2), 23.66 (s, C_c-*C*H_3); ATR (ν_{max}/cm^{-1}): 3058 (w, C-H st), 2924 (m, C-H st), 2852 (w, C-H st), 2604 (s, B-H st), 2566 (s, B-H st); Anal.Calcd. for $C_{10}H_{19}B_{10}I$: C, 32.09; H, 5.12. Found: C, 33.12; H, 5.15.

Compound 6.- A dry 25 mL round-bottomed flask equipped with a magnetic stirring bar was charged under nitrogen with a solution of 1-C_6H_5-1,2-$C_2B_{10}H_{11}$ (200 g, 0.909 mmol) in THF (5 mL) , at 0°C. Then, a solution of *n*BuLi 1.6M in hexane (0.63 mL, 1 mmol) was added dropwise to the mixture, which was allowed to stir for 1 h at room temperature and then cooled to -84°C. After this, a solution of 4-iodobenzyl bromide (293 g, 0.937 mmol) in THF (5 mL) was added dropwise to the mixture under vigorous stirring and allowed to react at room temperature overnight. After that, the solvent was removed under vacuum and the orange residue was extracted with ethyl acetate (3 x 10 mL), transferred to a separating funnel and washed with a saturated aqueous solution

of NaCl (3 x 10 mL). The organic layer was dried over $MgSO_4$ and the volatiles were reduced under vacuum. The orange oil residue was purified by preparative layer chromatography (ethyl acetate/hexane 15:85) leading to **6** as a colorless solid. Yield: 218 g, 55%. A diethyl ether solution of **6** gave crystals suitable for X-ray analysis. ^{1}H NMR ($CDCl_3$, TMS), δ(ppm): 7.72 (d, 2H, ^3J(H,H) = 6 Hz, C_6H_5), 7.58 (d, 2H, ^3J(H,H) = 9 Hz, C_6H_4), 7.45-7.55 (m, 3H, C_6H_5), 6.57 (d, 2H, ^3J(H,H) = 9 Hz, C_6H_4), 3.06 (s, 2H, CH_2); ^{1}H{^{11}B} NMR ($CDCl_3$, TMS), δ(ppm): 7.72 (d, 2H, ^3J(H,H) = 6 Hz, C_6H_5), 7.58 (d, 2H, ^3J(H,H) = 9 Hz, C_6H_4), 7.45-7.55 (m, 3H, C_6H_5), 6.57 (d, 2H, ^3J(H,H) = 9 Hz, C_6H_4), 3.06 (s, 2H, CH_2), 2.71 (s, 2H, B-*H*), 2.42 (s, 3H, B-*H*), 2.33 (s, 1H, B-*H*), 2.25 (s, 2H, B-*H*), 2.21 (s, 2H, B-*H*); ^{11}B NMR ($CDCl_3$, BF_3·Et_2O), δ(ppm): -3.55 (d, 2B, ^1J(B,H) = 143 Hz), -10.15 (d, 8B, ^1J(B,H) = 120 Hz); ^{13}C{^{1}H} NMR ($CDCl_3$, TMS), δ(ppm): 137.52 (s, C_6H_4), 134.74 (s, C_6H_4), 131.92 (s, C_6H_4), 131.48 (s, C_6H_5), 130.97 (s, C_6H_5), 130.71 (s, C_6H_5), 129.13 (s, C_6H_5), 93.67 (s, *C*-I), 83.72 (s, C_c-C_6H_5), 81.36 (s, C_c-CH_2), 40.50 (s, CH_2); ATR-IR (ν_{max}/cm^{-1}): 3059 (w, C-H st), 2928 (w, C-H st), 2580 (s, B-H st), 2554 (s, B-H st); MALDI-TOF-MS (m/z): Calcd: 436.34. Found: 434.67 [M-2]; Anal.Calcd. for $C_{15}H_{21}B_{10}I$: C, 41.29; H, 4.85. Found: C, 41.33; H, 4.89.

Compound 7.- A dry 10 mL round-bottomed flask equipped with a magnetic stirring bar was charged under nitrogen with a solution of 1-CH_3-1,7-$C_2B_{10}H_{11}$ (0.200 g, 1.27 mmol) in THF (3.5 mL) at 0°C. Then, a solution of *n*BuLi 1.6M in hexanes (0.87 mL, 1.39 mmol) was added dropwise to the mixture, which was allowed to stir for 1 h at room temperature and cooled again at 0°C. Then, a solution of 4-iodobenzyl bromide (0.400 g, 1.31 mmol) in THF (3 mL) was added dropwise to the mixture under vigorous stirring. Then it was equilibrated at 0°C for 1 hour and then allowed to react at room temperature overnight. After that, the solvent was removed under vacuum and the residue was extracted with dichloromethane (3 x 10 mL), transferred to a separating funnel and washed with a saturated aqueous solution of NaCl (3 x 10 mL). The organic layer was dried over $MgSO_4$ and the volatiles were reduced under vacuum. The orange oil residue was purified by preparative layer chromatography (dichloromethane/hexane 15:85) to give **7** as a colorless solid. Yield: 0.346 g, 74 %. A diethyl ether solution of **7** gave crystals suitable for X-ray analysis. ^{1}H NMR ($CDCl_3$,

TMS), δ(ppm): 7.67 (d, 2H, ^{3}J(H,H) = 9 Hz, C_6H_4), 6.87 (d, 2H, ^{3}J(H,H) = 9 Hz, C_6H_4), 3.15 (s, 2H, CH_2), 1.66 (s, 3H, CH_3); $^{1}H\{^{11}B\}$ NMR ($CDCl_3$, TMS), δ(ppm): 7.67 (d, 2H, ^{3}J(H,H) = 9 Hz, C_6H_4), 6.87 (d, 2H, ^{3}J(H,H) = 9 Hz, C_6H_4), 3.15 (s, 2H, CH_2), 2.60 (s, 2H, B-*H*), 2.27 (s, 1H, B-*H*), 2.18 (s, 5H, B-*H*), 2.07 (s, 2H, B-*H*),1.66 (s, 3H, CH_3); ^{11}B NMR ($CDCl_3$, $BF_3{\cdot}Et_2O$), δ(ppm):-6.42 (d, 1B, ^{1}J(B,H) = 170 Hz), -8.25 (d, 1B, ^{1}J(B,H) = 241 Hz), -10.67 (d, 6B, ^{1}J(B,H) = 156 Hz), -13.33 (d, 2B, ^{1}J(B,H) = 191 Hz); $^{13}C\{^{1}H\}$ NMR ($CDCl_3$, TMS), δ(ppm): 137.56 (s, C_6H_4), 136.50 (s, C_6H_4), 131.78 (s, C_6H_4), 93.16 (s, *C*-I), 75.98 (s, C_c-CH_2), 70.84 (s, C_c-CH_3), 42.42 (CH_2), 24.49, (s, C_c-CH_3); ATR (ν_{max}/cm^{-1}): 3063 (w, C-H st), 2932 (m, C-H st), 2852 (w, C-H st), 2586 (s, B-H st); Anal.Calcd. for $C_{10}H_{19}B_{10}I$: C, 32.09; H, 5.12. Found: C, 32.32; H, 5.21.

Compound 8.- The procedure was the same as for **7**, but using a solution of 1- C_6H_5-1,7-$C_2B_{10}H_{11}$ (0.218 g, 0.99 mmol) in THF (3 mL), *n*BuLi 1.6M in hexanes (0.68 mL, 1.10 mmol) and a solution of 4-iodobenzyl bromide (0.315 g, 1.01 mmol) in THF (2 mL). After work-up, the orange oil residue was purified by preparative layer chromatography (ethyl acetate/hexane 10:90) and the white layer was extracted and purified again by preparative layer chromatography (dichloromethane/hexane 1:1) to give **8** as a colorless solid. Yield: 0.262 g, 60%. ^{1}H NMR ($CDCl_3$, TMS), δ(ppm): 7.68 (d, 2H, ^{3}J(H,H) = 9 Hz, C_6H_4), 7.38 (d, 2H, ^{3}J(H,H) = 6 Hz, C_6H_5), 7.33-7.23 (m, 3H, C_6H_5), 6.90 (d, 2H, ^{3}J(H,H) = 9 Hz, C_6H_4), 3.24 (s, 2H, CH_2); $^{1}H\{^{11}B\}$ NMR ($CDCl_3$, TMS), δ(ppm): 7.68 (d, 2H, ^{3}J(H,H) = 9 Hz, C_6H_4), 7.39 (d, 2H, ^{3}J(H,H) = 6 Hz, C_6H_5), 7.33-7.23 (m, 3H, C_6H_5), 6.90 (d, 2H, ^{3}J(H,H) = 9 Hz, C_6H_4), 3.24 (s, 2H, CH_2), 2.90 (s, 2H, B-*H*), 2.53 (s, 3H, B-*H*), 2.37 (s, 1H, B-*H*), 2.31 (s, 2H, B-*H*), 2.22 (s, 2H, B-*H*); ^{11}B NMR ($CDCl_3$, $BF_3{\cdot}Et_2O$), δ(ppm): -6.16 (d, 2B, ^{1}J(B,H) = 104 Hz), -10.71 (d, 6B, ^{1}J(B,H) = 153 Hz), -13.62 (d, 2B, ^{1}J(B,H) = 175 Hz); $^{13}C\{^{1}H\}$ NMR ($CDCl_3$, TMS), δ(ppm): 137.65 (s, C_6H_4), 136.40 (s, C_6H_4), 135.15 (s, C_6H_5), 131.81 (s, C_6H_4), 128.65 (s, C_6H_5), 128.33 (s, C_6H_5), 127.78 (s, C_6H_5), 93.32 (s, *C*-I), 78.37 (s, C_c-C_6H_5), 75.55 (s, C_c-CH_2), 42.88 (s, CH_2); ATR (ν_{max}/cm^{-1}): 3055 (w, C-H st), 2925 (m, C-H st), 2581 (s, B-H st);. Anal.Calcd. for $C_{15}H_{21}B_{10}I$: C, 41.29; H, 4.85. Found: C, 42.28; H, 5.09.

Compound 9.- A dry 5 mL round-bottomed flask equipped with a condenser and a magnetic stirring bar was charged under nitrogen with a solution of **1** (100 mg, 0.36

mmol), iodobenzene (82 mg, 0.40 mmol), $Pd_2(dba)_3$ (3 mg, 0.004 mmol), $Pd(t\text{-}Bu_3P)_2$ (3 mg, 0.006 mmol) and NCy_2Me (0.1 mL, 0.48 mmol) in 2 mL of 1,4-dioxane. The solution was stirred and refluxed at 100°C overnight. After that, the solution was filtered through 1 cm of Celite, which was washed with 10 mL of THF. The solvent mixture was removed in vacuo and then the residue was dissolved in 2 mL of THF. The solution was precipitated with 50 mL of methanol and filtered to give **9** as a white solid. Yield: 112 mg, 88 %. A diethyl ether solution of **9** gave crystals suitable for X-ray analysis. ^{1}H NMR ($CDCl_3$, TMS), δ (ppm): 7.57-7.50 (m, 4H, C_6H_5 + C_6H_4), 7.40 (dd, 2H, ^{3}J(H,H)= 9 Hz, ^{3}J(H,H)= 7.5 Hz, C_6H_5), 7.32 (d, 1H, ^{3}J(H,H)= 7.5 Hz, C_6H_5), 7.21 (d, 2H, ^{3}J(H,H)= 9 Hz, C_6H_4), 7.14 (d, 2H, ^{3}J(H,H)= 3 Hz, C*H*=C*H*), 3.49 (s, 2H, CH_2), 2.19 (s, 3H, -CH_3); ^{1}H{^{11}B} NMR ($CDCl_3$, TMS), δ (ppm): 7.57-7.50 (m, 4H, C_6H_5 + C_6H_4), 7.40 (dd, 2H, ^{3}J(H,H)= 9 Hz, ^{3}J(H,H)= 7.5 Hz, C_6H_5), 7.32 (d, 1H, ^{3}J(H,H)= 7.5 Hz, C_6H_5), 7.21 (d, 2H, ^{3}J(H,H)= 9 Hz, C_6H_4), 7.14 (d, 2H, ^{3}J(H,H)= 3 Hz, C*H*=C*H*), 3.49 (s, 2H, CH_2), 2.32 (s, B-*H*), 2.27 (s, B-*H*), 2.19 (s, 3H, -CH_3), 2.12 (s, B-*H*). ^{11}B NMR ($CDCl_3$, $BF_3{\cdot}Et_2O$), δ (ppm): -4.22 (d, 1B, ^{1}J(B, H)= 143 Hz), -5.76 (d, 1B, ^{1}J(B,H)= 150 Hz), -10.47 (d, 8B, ^{1}J(B,H)= 132 Hz); ^{13}C{^{1}H} NMR ($CDCl_3$, TMS), δ (ppm): 137.21 (s, C_6H_4), 134.08 (s, C_6H_4), 130.72 (s, C_6H_4), 129.51 (s, C_6H_5), 128.77 (s, CH=*C*H), 127.89 (s, *C*H=CH), 126.65 (s, C_6H_4 and C_6H_5), 74.65 (s, *Cc*-CH_3), 41.03 (s, *C*H_2), 23.71 (s, -*C*H_3); ATR (ν_{max}/cm^{-1}): 3025 (w, C-H st), 2919 (m, C-H st), 2850 (w, C-H st), 2572 (s, B-H st); MALDI-TOF-MS (m/z): Calcd: 350.51. Found: 348.76 [M-2]; Anal. Calcd. for $C_{18}B_{10}H_{26}$: C, 61.68; H, 7.48. Found: C, 61.36; H, 7.47.

Compound 10.- The procedure was the same as for **9**, using **2** (100 mg, 0.30 mmol), iodobenzene (67 mg, 0.33 mmol), $Pd_2(dba)_3$ (3 mg, 0.004 mmol), $Pd(t\text{-}Bu_3P)_2$ (3 mg, 0.006 mmol) and NCy_2Me (0.1 mL, 0.48 mmol) in 2 mL of 1,4-dioxane. After workup compound **10** was obtained as a pure white solid. Yield: 95 mg, 78 %. ^{1}H NMR ($CDCl_3$, TMS), δ (ppm): 7.75 (d, 2H, ^{3}J(H,H)= 9 Hz, C_6H_5), 7.55-7.46 (m, 5H, C_c-C_6H_5), 7.41-7.35 (m, 4H, , C_c-C_6H_5 + C_6H_5), 7.30 (d, 1H, ^{3}J(H,H)= 3 Hz, C_6H_5), 7.08 (d, 2H, ^{3}J(H,H)= 3 Hz, C*H*=C*H*), 6.83 (d, 2H, ^{3}J(H,H)= 6 Hz, C_6H_4), 3.11 (s, 2H, CH_2); ^{1}H{^{11}B} NMR ($CDCl_3$, TMS), δ (ppm): 7.75 (d, 2H, ^{3}J(H,H)= 9 Hz, C_6H_5), 7.55-7.46 (m, 5H, C_c-C_6H_5), 7.41-7.35 (m, 4H, C_c-C_6H_5 + C_6H_5), 7.30 (d, 1H, ^{3}J(H,H)= 3 Hz, C_6H_5), 7.08 (d, 2H, ^{3}J(H,H)= 3 Hz, C*H*=C*H*), 6.83 (d, 2H, ^{3}J(H,H)= 6 Hz, C_6H_4), 3.11 (s, 2H, CH_2), 2.74 (s, B-H), 2.41 (s, B-H), 2.32 (s, B-

H), 2.24 (s, B-H); ^{11}B NMR ($CDCl_3$, $BF_3{\cdot}Et_2O$), δ (ppm): -3.68 (d, 2B, ^{1}J(B, H)= 146 Hz), -10.30 (d, 8B, ^{1}J(B,H)= 134 Hz); ^{13}C{^{1}H} NMR ($CDCl_3$, TMS), δ (ppm): 137.17 (s, C_6H_4 and C_6H_5), 136.95 (s, CH_2-C_6H_4), 134.49(s, C_c-C_6H_5), 131.53 (s, C_c-C_6H_5), 130.87 (s, C_c-C_6H_5), 130.40 (s, C_c-C_6H_5), 129.26 (s, C_6H_5), 129.07 (s, C_6H_4), 128.72 (s, C_6H_5), 127.96 (s, CH=*C*H), 127.79 (s, *C*H=CH), 126.56 (s, C_6H_4), 126.41 (s, C_6H_5), 83.72 (s, C_c-C_6H_5), 82.06 (s, C_c-CH_2), 40.73 (s, *C*H_2); ATR (ν_{max}/cm^{-1}): 2988 (m, C-H st), 2902 (m, C-H st), 2582 (s, B-H st), 2559 (s, B-H st); MALDI-TOF-MS (m/z): Calcd: 412.58. Found: 410.81 [M-2]. Anal. Calcd. for $C_{23}B_{10}H_{28}$: C, 66.96; H, 6.84. Found: C, 66.53; H, 7.05.

Compound 11.- The procedure was the same as for **9**, but using **3** (110 mg, 0.40 mmol), iodobenzene (84 mg, 0.42 mmol), $Pd_2(dba)_3$ (3 mg, 0.004 mmol), Pd(t-$Bu_3P)_2$ (3 mg, 0.006 mmol) and NCy_2Me (0.1 mL, 0.48 mmol) in 1,4-dioxane (2 mL). After workup compound **11** was obtained as a pure white solid. Yield: 87 mg, 62 %.^{1}H NMR ($CDCl_3$, TMS), δ(ppm): 7.55-7.47 (m, 4H, C_6H_5 + C_6H_4), 7.41-7.36 (m, 2H, C_6H_5), 7.30 (d, 1H, ^3J(H,H) = 6 Hz, C_6H_5), 7.13 (s, 2H, C*H*=C*H*), 7.12 (d, 2H, ^3J(H,H) = 6 Hz, C_6H_4), 3.22 (s, 2H, CH_2), 1.66 (s, 3H, CH_3); ^{1}H{^{11}B} NMR ($CDCl_3$, TMS), δ(ppm): 7.55-7.47 (m, 4H, C_6H_5 + C_6H_4), 7.41-7.36 (m, 2H, C_6H_5), 7.30 (d, 1H,^3J(H,H) = 6 Hz, C_6H_5), 7.13 (s, 2H, C*H*=C*H*), 7.12 (d, 2H, ^3J(H,H) = 6 Hz, C_6H_4), 3.22 (s, 2H, CH_2), 2.64 (s, 2H, B-*H*), 2.22 (s, 6H, B-*H*), 2.08 (s, 2H, B-*H*), 1.66 (s, 3H, CH_3); ^{11}B NMR ($CDCl_3$, $BF_3{\cdot}Et_2O$), δ(ppm): -6.52 (d, 1B, ^1J(B,H) = 155 Hz), -8.21 (d, 1B, ^1J(B,H) = 154 Hz), -10.77 (d, 6B, ^1J(B,H) = 151 Hz), -13.32 (d, 2B, ^1J(B,H) = 175 Hz); ^{13}C{^{1}H} NMR ($CDCl_3$, TMS), δ (ppm): 137.27 (s, C_6H_4), 136.62 (s, C_6H_4), 136.40 (s, C_6H_5), 130.22 (s, C_6H_4), 129.00 (s, C_6H_5), 128.69 (s, C_6H_5), 128.14 (s, CH=*C*H), 127.69 (s, *C*H=CH), 126.51 (s, C_6H_4 and C_6H_5), 70.74 (s, C_c-CH_3), 42.72 (s, *C*H_2), 24.53 (s, *C*H_3); ATR (ν_{max}/cm^{-1}): 3026 (m, C-H st), 2942 (m, C-H st), 2852 (w, C-H st), 2584 (s, B-H st);); MALDI-TOF-MS (m/z): Calcd: 350.51. Found: 351.34 [M+1]; Anal.Calcd. for $C_{18}H_{26}B_{10}$: C, 61.68; H, 7.48. Found: C, 61.73; H, 7.77.

Compound 12.- The procedure was the same as for **9**, but using **4** (90 mg, 0.27 mmol), iodobenzene (57 mg, 0.28 mmol), $Pd_2(dba)_3$ (3 mg, 0.004 mmol), Pd(t-$Bu_3P)_2$ (3 mg, 0.006 mmol) and NCy_2Me (0.1 mL, 0.48 mmol) in 1,4-dioxane (2 mL). After workup compound **12** was obtained as a pure white solid. Yield: 52 mg, 47 %. A THF/methanol solution of **12** gave crystals suitable for X-ray analysis. ^{1}H NMR ($CDCl_3$, TMS), δ(ppm):

7.55-7.48 (m, 4H, C_6H_5 + C_6H_4), 7.41-7.37 (m, 4H, C_6H_5 + C_c-C_6H_5), 7.30 (d, 1H, ^3J(H,H) = 6 Hz, C_6H_5), 7.28-7.24 (m, 3H, C_c-C_6H_5), 7.15 (d, 2H, ^3J(H,H) = 6 Hz, C_6H_4), 7.13 (s, 2H, C*H*=C*H*), 3.30 (s, 2H, CH_2); ^{1}H{^{11}B} NMR ($CDCl_3$, TMS), δ(ppm): 7.55-7.48 (m, 4H, C_6H_5 + C_6H_4), 7.41-7.37 (m, 4H, C_6H_5 + C_c-C_6H_5), 7.30 (d, 1H, ^3J(H,H) = 6 Hz, C_6H_5), 7.28-7.24 (m, 3H, C_c-C_6H_5), 7.15 (d, 2H, ^3J(H,H) = 6 Hz, C_6H_4), 7.13 (s, 2H, C*H*=C*H*), 3.30 (s, 2H, CH_2), 2.93 (s, 2H, B-*H*), 2.52 (s, 3H, B-*H*), 2.41 (s, 1H, B-*H*), 2.35 (s, 2H, B-*H*), 2.21 (s, 2H, B-*H*); ^{11}B NMR ($CDCl_3$, BF_3·Et_2O), δ(ppm): -6.24 (d, 2B, ^1J(B,H) = 65 Hz), -10.90 (d, 6B, ^1J(B,H) = 153 Hz), -13.73 (d, 2B, ^1J(B,H) = 170 Hz); ^{13}C{^{1}H} NMR ($CDCl_3$, TMS), δ (ppm): 137.26 (s, C_6H_4), 136.69 (s, C_6H_4), 136.27 (s, C_6H_5), 135.29 (s, C_c-C_6H_5), 130.24 (s, C_6H_4), 129.05 (s, C_6H_5), 128.70 (s, C_6H_5), 128.57 (s, C_c-C_6H_5), 128.27 (C_c-C_6H_5), 128.11 (s, CH=*C*H), 127.79 (s, C_c-C_6H_5), 127.72 (s, *C*H=CH), 126.55 (s, C_6H_4 and C_6H_5), 78.11 (s, C_c-C_6H_5), 76.26 (s, C_c-CH_2), 42.95 (s, *C*H_2); ATR (ν_{max}/cm^{-1}): 3029 (m, C-H st), 3922 (w, C-H st), 2850 (w, C-H st), 2585 (s, B-H st); MALDI-TOF-MS (m/z): Calcd: 412.58 Found: 412.42; Anal.Calcd. for $C_{23}H_{28}B_{10}$: C, 66.96; H, 6.84. Found: C, 66.63; H, 7.02.

Compound 13.- The procedure was the same as for **9**, but using **1** (90 mg, 0.27 mmol), **5** (136 mg, 0.36 mmol), $Pd_2(dba)_3$ (5 mg, 0.006 mmol), Pd(t-$Bu_3P)_2$ (5 mg, 0.01 mmol) and NCy_2Me (0.2 mL, 0.96 mmol) in 2 mL of 1,4-dioxane. After workup compound **13** was obtained as a pure white solid. Yield: 101 mg, 53 %. A dichloromethane solution of **13** gave crystals suitable for X-ray analysis. ^{1}H NMR ($CDCl_3$, TMS), δ (ppm): 7.51 (d, 4H, ^{3}J(H,H)= 9 Hz, C_6H_4), 7.21 (d, 4H, ^{3}J(H,H)= 9 Hz, C_6H_4), 7.12 (s, 4H, C*H*=C*H*), 3.49 (s, 4H, CH_2), 2.19 (s, 6H, -CH_3); ^{1}H{^{11}B} NMR ($CDCl_3$, TMS), δ (ppm): 7.51 (d, 4H, ^{3}J(H,H)= 9 Hz, C_6H_4), 7.21 (d, 4H, ^{3}J(H,H)= 9 Hz, C_6H_4), 7.12 (s, 4H, C*H*=C*H*), 3.49 (s, 4H, CH_2), 2.30 (s, B-*H*), 2.23 (s, B-*H*), 2.19 (s, 6H, -CH_3), 2.11 (s, B-*H*); ^{11}B NMR ($CDCl_3$, BF_3·Et_2O), δ (ppm): -4.21 (d, 1B, ^{1}J(B, H)= 142 Hz), -5.71 (d, 1B, ^{1}J(B,H)= 148 Hz), -10.41 (d, 8B, ^{1}J(B,H)= 134 Hz); ^{13}C{^{1}H} NMR ($CDCl_3$, TMS), δ (ppm): 136.94 (s, C_6H_4), 134.31 (s, C_6H_4), 130.59 (s, C_6H_4), 128.63 (s, *C*H=*C*H), 126.65 (s, C_6H_4), 74.79 (s, *Cc*-CH_3), 41.00 (s, *C*H_2), 23.75 (s, -*C*H_3); ATR (ν_{max}/cm^{-1}): 3028 (w, C-H st), 2925 (m, C-H st), 2853 (w, C-H st), 2565 (s, B-H st); MALDI-TOF-MS (m/z): Calcd: 520.77. Found: 518.97 [M-2]; Anal. Calcd. for $C_{22}B_{20}H_{40}$: C, 50.74; H,7.74; Found: C, 50.64; H, 7.88.

Compound 14.- The procedure was the same as for **9**, but using **2** (77.5 mg, 0.23 mmol), **6** (100 mg, 0.23 mmol), $Pd_2(dba)_3$ (5 mg, 0.006 mmol), $Pd(t\text{-}Bu_3P)_2$ (5 mg, 0.01 mmol) and NCy_2Me (0.2 mL, 0.96 mmol) in 2 mL of 1,4-dioxane. After workup compound **14** was obtained as a pure white solid. Yield: 79 mg, 53 %. A THF/methanol solution of **14** gave crystals suitable for X-ray analysis. ^{1}H NMR ($CDCl_3$, TMS), δ (ppm): 7.74 (d, 4H, ^3J(H,H) = 9 Hz, C_6H_5), 7.61-7.47 (m, 6H, C_6H_5), 7.37 (d, 4H, 3J(H,H)= 9 Hz, C_6H_4), 7.03 (s, 2H, C*H*=C*H*), 6.82 (d, 4H, 3J(H,H)= 9 Hz, C_6H_4), 3.11 (s, 4H, CH_2); ^{1}H{^{11}B} NMR ($CDCl_3$, TMS), δ (ppm): 7.74 (d, 4H, ^3J(H,H) = 9 Hz, C_6H_5), 7.61-7.47 (m, 6H, C_6H_5), 7.37 (d, 4H, ^{3}J(H,H)= 9 Hz, C_6H_4), 7.03 (s, 2H, C*H*=C*H*), 6.82 (d, 4H, ^{3}J(H,H)= 9 Hz, C_6H_4), 3.11 (s, 4H, CH_2), 2.75 (s, B-H), 2.41 (s, B-H), 2.24 (s, B-H); ^{11}B NMR ($CDCl_3$, $BF_3{\cdot}Et_2O$), δ(ppm): -3.59 (d, 2B, ^{1}J(B, H)= 134 Hz), -10.12 (d, 8B, ^{1}J(B,H)= 125 Hz); ^{13}C{^{1}H} NMR ($CDCl_3$, TMS), δ (ppm): 136.59 (s, *C*H=*C*H), 134.48 (s, C_6H_4), 131.25 (s, C_6H_5), 130.63 (s, C_6H_5), 130.14 (s, C_6H_4), 128.87 (s, C_6H_5), 128.17 (s, C_6H_5), 126.16 (s, C_6H_4), 83.58 (s, C_c-C_6H_5), 81.75 (C_c-CH_2) 40.34 (s, -*C*H_2-). ATR (νmax/cm-1): 3027 (w, C-H st), 2919 (m, C-H st), 2851 (w, C-H st), 2565 (s, B-H st); MALDI-TOF-MS (m/z): Calcd: 644.99. Found: 643.11 [M-2]; Anal. Calcd. for $C_{32}B_{20}H_{44}$: C, 59.60; H, 6.88. Found: C, 59.62; H, 7.17.

Compound 15.- The procedure was the same as for **9**, but using **3** (100 mg, 0.36 mmol), **7** (73.3 mg, 0.36 mmol), Pd_2dba_3 (5 mg, 0.006 mmol), $Pd(t\text{-}Bu_3P)_2$ (5 mg, 0.01 mmol) and NCy_2Me (0.1 mL, 0.95 mmol) in 1,4-dioxane (2 mL). After work-up, compound **15** was obtained as a pure white solid. Yield: 90 mg, 65%. A THF/methanol solution of **15** gave crystals suitable for X-ray analysis. ^{1}H NMR ($CDCl_3$, TMS), δ(ppm): 7.47 (d, 4H, ^3J(H,H) = 9 Hz, C_6H_4), 7.12 (d, 4H, ^3J(H,H) = 9 Hz, C_6H_4), 7.10 (s, 2H, C*H*=C*H*), 3.21 (s, 4H, CH_2), 1.66 (s, 6H, CH_3); ^{1}H{^{11}B} NMR ($CDCl_3$, TMS), δ(ppm): 7.47 (d, 4H, ^3J(H,H) = 9 Hz, C_6H_4), 7.12 (d, 4H, ^3J(H,H) = 9 Hz, C_6H_4), 7.10 (s, 2H, C*H*=C*H*), 3.21 (s, 4H, CH_2), 2.64 (s, 4H, B-*H*), 2.22 (s, 12H, B-*H*), 2.08 (s, 4H, B-*H*), 1.66 (s, 6H, CH_3); ^{11}B NMR ($CDCl_3$, $BF_3{\cdot}Et_2O$), δ(ppm): -6.45 (d, 2B, ^1J(B,H) = 147 Hz), -8.11 (d, 2B, ^1J(B,H) = 148 Hz), -10.66 (d, 12B, ^1J(B,H) = 152 Hz), -13.22 (d, 4B, ^1J(B,H) = 177 Hz); ^{13}C{^{1}H} NMR ($CDCl_3$, TMS), δ(ppm): 136.52 (s, C_6H_4), 130.24 (s, C_6H_4), 128.42 (s, *C*H=*C*H), 126.50 (s, C_6H_4), 76.02 (s, C_c-CH_2), 70.79 (s, C_c-CH_3), 42.72 (s, *C*H_2), 24.52 (C_c-*C*H_3); ATR (ν_{max}/cm^{-1}): 3024 (m, C-H st), 2938 (m, C-H st), 2589 (s, B-H st); MALDI-TOF-MS (m/z): Calcd: 520.77

Found: 521.65 [M+1]; Anal.Calcd. for $C_{22}H_{40}B_{20}$: C, 50.74; H, 7.74. Found: C, 50.86; H, 7.89.

Compound 16.- The procedure was the same as for **9**, but using **4** (68mg, 0.202mmol), **8** (88.2mg, 0.202mmol), Pd_2dba_3 (3 mg, 0.003mmol), $Pd(t\text{-}Bu_3P)_2$ (3 mg, 0.006mmol) and NCy_2Me (0.1 mL, 0.95 mmol) in 1,4-dioxane (2 mL). After work-up, compound **16** was obtained as a pure white solid. Yield: 81 mg, 62%. ^{1}H NMR ($CDCl_3$, TMS), δ(ppm): 7.47 (d, 4H, ^3J(H,H) = 9 Hz, C_6H_4), 7.38 (d, 4H, ^3J(H,H) = 6 Hz, C_6H_5), 7.26-7.21 (m, 6H, C_6H_5), 7.12 (d, 4H, ^3J(H,H) = 9 Hz, C_6H_4), 7.10 (s, 2H, C*H*=C*H*), 3.29 (s, 4H, CH_2); ^{1}H{^{11}B} NMR ($CDCl_3$, TMS), δ(ppm): 7.47 (d, 4H, ^3J(H,H) = 9 Hz, C_6H_4), 7.38 (d, 4H, ^3J(H,H) = 6 Hz, C_6H_5), 7.26-7.21 (m, 6H, C_6H_5), 7.12 (d, 4H, ^3J(H,H) = 9 Hz, C_6H_4), 7.10 (s, 2H, C*H*=C*H*), 3.29 (s, 4H, CH_2), 2.92 (s, 4H, B-*H*), 2.51 (s, 8H, B-*H*), 2.40 (s, 2H, B-*H*), 2.34 (s, 4H, B-*H*), 2.20 (s, 2H, B-*H*); ^{11}B NMR ($CDCl_3$, $BF_3{\cdot}Et_2O$), δ(ppm): -6.01 (d, 4B, ^1J(B,H) = 156 Hz), -10.79 (d, 12B, ^1J(B,H) = 152 Hz), -13.50 (d, 4B, ^1J(B,H) = 196 Hz); ^{13}C{^{1}H} NMR ($CDCl_3$, TMS), δ(ppm): 136.61 (s, C_6H_4), 136.39 (s, C_6H_4), 135.29 (s, C_6H_5), 130.24 (s, C_6H_4), 128.53 (s, C_6H_5), 128.44 (s, C_6H_5), 128.25 s, C_6H_5), 127.77 (s, *C*H=*C*H), 126.56 (s, C_6H_4), 79.57 (s, C_c-C_6H_5), 75.67 (s, C_c-CH_2), 42.96 (s, *C*H_2); ATR (ν_{max}/cm^{-1}): 3024 (m, C-H st), 2928 (m, C-H st), 2854 (m, C-H st), 2592 (s, B-H st), 2557 (s, B-H st); MALDI-TOF-MS (m/z): Calcd: 644.91 Found: 645.73 [M+1]; Anal.Calcd. for $C_{32}H_{44}B_{20}$: C, 59.60; H, 6.88. Found: C, 59.70; H, 7.17.

References

[1] a) B. A. Armitage, P. B. Berget, *Science* **2008**, *319*, 1195-1196; b) G. Likhtenshtein, *Stilbenes: Applications in Chemistry, Life Sciences and Materials Science*, John Wiley & Sons, **2009**.

[2] a) J. Saltiel, Y. P. Sun, in *Photochromism* (Ed.: H. D. Bouas-Laurent), Elsevier Science, Amsterdam, **2003**, pp. 64-164; b) D. H. Waldeck, *Chem. Rev.* **1991**, *91*, 415-436; c) M. Aguiar, L. Akcelrud, M. Pinto, T. Atvars, F. Karasz, J. Saitiel, *J. Photosci.* **2003**, *10*, 149-156

[3] a) H. Meier, *Angew. Chem. Int. Ed.* **1992**, *31*, 1399-1420; b) D. G. Whitten, *Acc. Chem. Res.* **1993**, *26*, 502-509; c) P. Gütlich, Y. Garcia, T. Woike, *Coord. Chem. Rev.* **2001**, *219–221*, 839-879; d) Z. R. Grabowski, K. Rotkiewicz, W. Rettig, *Chem. Rev.* **2003**, *103*, 3899-4032; e) A. Momotake, T. Arai, *J. Photochem. Photobiol. C: Photochem. Rev.* **2004**, *5*, 1-25; f) A. S. Polo, M. K. Itokazu, K. M. Frin, A. O. de Toledo Patrocínio, N. Y. Murakami Iha, *Coord. Chem. Rev.* **2006**, *250*, 1669-1680; g) A. S. Polo, M. K. Itokazu, K. M. Frin, A. O. de Toledo Patrocínio, N. Y. Murakami Iha, *Coord. Chem. Rev.* **2007**, *251*, 255-281; h) K. Xiao, H.-J. Zhang, L.-J. Xuan, J. Zhang, Y.-M. Xu, D.-L. Bai, in *Stud. Nat. Prod. Chem., Vol. Volume 34* (Ed.: R. Atta ur), Elsevier, **2008**, pp. 453-646.

[4] a) D. He, W. Jian, X. Liu, H. Shen, S. Song, *J. Agric. Food. Chem.* **2015**, *63*, 1370-1377; b) M. A. Romero, J. A. González-Delgado, J. F. Arteaga, *Nat. Prod. Comm.* **2015**, *10*, 1257-1262; c) F. Silva, C. Nerín, F. C. Domingues, *Food Control* **2015**, *54*, 66-73; d) Y. Wang, Y. Jiang, X. Fan, H. Tan, H. Zeng, Y. Wang, P. Chen, M. Huang, H. Bi, *Toxicol. Lett.* **2015**, *236*, 82-89; e) D. Ha, Q. Chen, T. Hung, U. Youn, T. Ngoc, P. Thuong, H. Kim, Y. Seong, B. Min, K. Bae, *Arch. Pharmacal Res.* **2009**, *32*, 177-183; f) I. Chrząścik, *Crit. Rev. Anal. Chem.* **2009**, *39*, 70-80

[5] C.-K. Wang, J.-C. Liu, K. Zhao, Y.-P. Sun, Y. Luo, *J. Opt. Soc. Am. B* **2007**, *24*, 2436-2442

[6] I. Fuks-Janczarek, R. Miedziński, E. Gondek, P. Szlachcic, I. V. Kityk, *J. Mater. Sci. Mater. Electron.* **2008**, *19*, 434-441

[7] M. Egawa, H. Osaka, S. Kawakami, N. Ohsawa, S. Seo, R. Nomura, US8704215 B2, **2014**.

[8] V. Kundi, P. P. Thankachan, *Phys. Chem. Chem. Phys.* **2015**, *17*, 12299-12309

[9] F. Ahmadov, G. Ahmadov, X. Abdullaev, A. Garibov, E. Guliyev, S. Khorev, R. Madatov, R. Muxtarov, J. Naghiyev, A. Sadigov, Z. Sadygov, S. Suleymanov, F. Zerrouk, *J. Instrum.* **2015**, *10*, C02041

[10] a) R. N. Grimes, *Carboranes*, Academic Press, **2011**; b) G. A. Olah, G. K. S. Prakash, K. Wade, Á. Molnár, R. E. Williams, *Hypercarbon Chemistry*, John Wiley & Sons, Inc., **2011**.

[11] a) N. Tsuboya, M. Lamrani, R. Hamasaki, M. Ito, M. Mitsuishi, T. Miyashita, Y. Yamamoto, *J. Mater. Chem.* **2002**, *12*, 2701-2705; b) O. Crespo, M. C. Gimeno, A. Laguna, I. Ospino, G. Aullon, J. M. Oliva, *Dalton Trans.* **2009**, 3807-3813; c) L. Weber, J. Kahlert, R. Brockhinke, L. Böhling, A. Brockhinke, H.-G. Stammler, B. Neumann, R. A. Harder, M. A. Fox, *Chem. Eur. J.* **2012**, *18*, 8347-8357

[12] A. V. Okotrub, L. G. Bulusheva, V. V. Volkov, *J. Mol. Struct.* **2000**, *520*, 33-38

[13] a) A. Ferrer-Ugalde, E. J. Juárez-Pérez, F. Teixidor, C. Viñas, R. Sillanpää, E. Pérez-Inestrosa, R. Núñez, *Chem. Eur. J.* **2012**, *18*, 544-553; b) K.-R. Wee, W.-S. Han, D. W. Cho, S. Kwon, C. Pac, S. O. Kang, *Angew. Chem. Int. Ed.* **2012**, *51*, 2677-2680

[14] G. F. Jin, Y.-J. Cho, K.-R. Wee, S. A. Hong, I.-H. Suh, H.-J. Son, J.-D. Lee, W.-S. Han, D. W. Cho, S. O. Kang, *Dalton Trans.* **2015**, *44*, 2780-2787

[15] a) B. Peng, Y. Nie, J. Miao, Z. Zhang, M. Xu, G. Sun, *J. Mol. Struct.* **2012**, *1007*, 214-219; b) A. Ferrer-Ugalde, A. González-Campo, C. Viñas, J. Rodríguez-Romero, R. Santillan, N. Farfán, R. Sillanpää, A. Sousa-Pedrares, R. Núñez, F. Teixidor, *Chem. Eur. J.* **2014**, *20*, 9940-9951

[16] a) M. H. Park, K. M. Lee, T. Kim, Y. Do, M. H. Lee, *Chem. - Asian J.* **2011**, *6*, 1362-1366; b) K. C. Song, H. Kim, K. M. Lee, Y. S. Lee, Y. Do, M. H. Lee, *Dalton Trans.* **2013**, *42*, 2351-2354

[17] a) M. Eo, H. J. Bae, M. Hong, Y. Do, S. Cho, M. H. Lee, *Dalton Trans.* **2013**, *42*, 8104-8112; b) J. Marshall, J. Hooton, Y. Han, A. Creamer, R. S. Ashraf, Y. Porte, T. D. Anthopoulos, P. N. Stavrinou, M. A. McLachlan, H. Bronstein, P. Beavis, M. Heeney, *Polym. Chem.* **2014**, *5*, 6190-6199

[18] a) K.-R. Wee, Y.-J. Cho, S. Jeong, S. Kwon, J.-D. Lee, I.-H. Suh, S. O. Kang, *J. Am. Chem. Soc.* **2012**, *134*, 17982-17990; b) A. R. Davis, J. J. Peterson, K. R. Carter, *ACS Macro Lett* **2012**, *1*, 469-472; c) E. G. Cansu-Ergun, A. Cihaner, *Mater. Chem. Phys.* **2013**, *143*, 387-392

[19] a) R. Bernard, D. Cornu, P. L. Baldeck, J. Caslavsky, J. M. Letoffe, J. P. Scharff, P. Miele, *Dalton Trans.* **2005**, 3065-3071; b) R. Bernard, D. Cornu, J.-P. Scharff, R. Chiriac, P. Miele, P. L. Baldeck, J. Čáslavský, *Inorg. Chem.* **2006**, *45*, 8743-8748; c) R. Bernard, C. Barsu, P. L. Baldeck, C. Andraud, D. Cornu, J.-P. Scharff, P. Miele, *Chem. Commun.* **2008**, 3765-3767; d) J.-F. Nicoud, F. Bolze, X.-H. Sun, A. Hayek, P. Baldeck, *Inorg. Chem.* **2011**, *50*, 4272-4278; e) L. Zhu, W. Lv, S. Liu, H. Yan, Q. Zhao, W. Huang, *Chem. Commun.* **2013**, *49*, 10638-10640

[20] a) F. Lerouge, C. Viñas, F. Teixidor, R. Nuñez, A. Abreu, E. Xochitiotzi, R. Santillan, N. Farfan, *Dalton Trans.* **2007**, 1898-1903; b) F. Lerouge, A. Ferrer-Ugalde, C. Viñas, F. Teixidor, R. Sillanpaa, A. Abreu, E. Xochitiotzi, N. Farfan, R. Santillan, R. Nuñez, *Dalton Trans.* **2011**, *40*, 7541-7550

[21] a) A. González-Campo, A. Ferrer-Ugalde, C. Viñas, F. Teixidor, R. Sillanpää, J. Rodríguez-Romero, R. Santillan, N. Farfán, R. Núñez, *Chem. Eur. J.* **2013**, *19*, 6299-6312; b) A. Ferrer-Ugalde, E. J. Juárez-Pérez, F. Teixidor, C. Viñas, R. Núñez, *Chem. Eur. J.* **2013**, *19*, 17021-17030

[22] M. F. Hawthorne, D. C. Young, P. M. Garrett, D. A. Owen, S. G. Schwerin, F. N. Tebbe, P. A. Wegner, *J. Am. Chem. Soc.* **1968**, *90*, 862-868

[23] E. Hao, B. Fabre, F. R. Fronczek, M. G. H. Vicente, *Chem. Mater.* **2007**, *19*, 6195-6205

[24] Z. Otwinowski, W. Minor, *Methods Enzymol.* **1997**, *276*, 307-326

[25] Rigaku Oxford Diffraction, *CrysAlisPro*, **2015**, Yarnton, Oxfordshire, England

[26] G. M. Sheldrick, *Acta Crystallogr., Sect. A* **2008**, *64*, 112-122

[27] L. Palatinus, G. Chapuis, *J. Appl. Crystallogr.* **2007**, *40*, 786-790

[28] SADABSBruker AXS Inc, *G. Sheldrick*, **2012**, Madison, Wisconsin, USA

[29] a) F. Weigend, R. Ahlrichs, *Phys. Chem. Chem. Phys.* **2005**, *7*, 3297-3305; b) A. Schäfer, H. Horn, R. Ahlrichs, *J. Chem. Phys.* **1992**, *97*, 2571-2577

[30] F. Neese, *Wiley Interdiscip. Rev.: Comput. Mol. Sci.* **2012**, *2*, 73-78

[31] a) T. Lu, F. Chen, *J. Comput. Chem.* **2012**, *33*, 580-592; b) L. Tian, C. Feiwu, *Acta Chim. Sinica* **2011**, *69*, 2393-2406

[32] A.-R. Allouche, *J. Comput. Chem.* **2011**, *32*, 174-182

Photoluminescence in carborane-stilbene triads: a combined structural, spectroscopic and computational study

Justo Cabrera-González,[a]# Clara Viñas,[a] Matti Haukka,[c] Santanu Bhattacharyya,[b] Johannes Gierschner,*[b] Rosario Núñez*[a]

[a] Institut de Ciència de Materials de Barcelona (ICMAB-CSIC), Campus U.A.B., 08193, Bellaterra, Barcelona, Spain. E-mail: rosario@icmab.es

[b] Madrid Institute for Advanced Studies, IMDEA Nanoscience, Calle Faraday 9, Campus Cantoblanco, 28049 Madrid, Spain.

[c] Department of Chemistry, University of Jyväskylä, FIN-40014, Jyväskylä, Finland

 # J. Cabrera González is enrolled in the UAB PhD program.

Abstract. A set of triads based on *ortho (o-)* and *metha* (*m-)* carborane clusters bonded to two stilbene units through a $C_{cluster}$-CH_2 have been described, and structures have been confirmed by X-ray diffraction analysis. The study of the influence of both *o*- and *m*-isomers on the absorption and PL emission properties of the stilbene units in solution, confirmed by (TD)DFT, reveals no CT contributions in the lowest excited state. The presence of one or two B-I in *m*-carborane derivatives does not affect the emission properties of stilbenes in solution, probably due to the rather large distance between the iodine and the fluorophore. Nevertheless, a significant red-shift of the PL emission maximum in solid state is observed when is compared to the solution; this can be traced back to PL sensitization most probably by more densely packed stilbene moieties. Remarkably, PL absolute quantum yields in solid state are significantly higher than those obtained in solution, which has been attributed to the restricted environment and the before mentioned sensitization. In conclusion, the bonding of the mentioned carborane clusters to two stilbene units preserves their PL behavior in solution, whereas produces significant changes in solid state. Furthermore, iodinated species

could be considered as promising precursors for theranostic agents, in which it could be possible combine both imaging and therapeutic functions.

Introduction.

Dicarba-*closo*-dodecaboranes ($C_2B_{10}H_{12}$) are highly stable icosahedral boron clusters with a three-dimensional delocalization of the electrons inside the cage. They possess □-bond interactions, which allow them to interact electronically with certain □-conjugated systems, that can lead to relevant changes in the final photophysical properties of compounds, depending in the energetic positions of the highest occupied and lowest unoccupied molecular orbitals (HOMO, LUMO) of the moieties involved.[1] The two isomers, *ortho*-carborane (1,2-$C_2B_{10}H_{12}$) and *meta*-carborane (1,7-$C_2B_{10}H_{12}$) have different electronic properties, especially their electron-withdrawing capacity,[2] which has been found to be much larger for the *ortho* when compared to the *meta*-isomer.[3] We have recently reported the influence of the *ortho*-carborane cluster on the photoluminescent properties of small molecules based on *o*-carboranyl-substituted styrenes, anthracenes and fluorenes,[4] as well as large molecules based on dendrimers functionalized with up to 32 clusters per molecule.[5] Likewise, the use of boron clusters to develop new photoluminescent materials for applications such as organic field-effect transistors (OFETs),[6] light-emitting diodes (OLEDs, PLEDs, PHOLEDs),[7] and their use in microscopy in two-photon absorption (TPA) for biomedicine purposes,[8] among others, has greatly increases during the last years. Moreover, electrophilic iodination of B-H vertices of carboranes[9] has revealed an attractive pathway for functionalization allowing the introduction of a wide range of functional groups and biomolecules through new B-C bond,[10]specially due to the interest of derivatization of boron clusters for biomedicinal applications.[11]

On the other hand, functionalized stilbenes (1,2-diphenylethylene) have attracted great attention over the past decades, due to their use in the production of (laser) dyes, optical brighteners and other materials,[12] as well as important applications in biomedicine.[13] The role of many different stilbene derivatives in photochemistry and photophysics has been exhaustively reviewed.[14] Nevertheless, it is well known that t*rans*-stilbene partly isomerizes to *cis*-stilbene under the influence of light, for that

reason the photophysics of *trans*-stilbene derivatives are generally complex, leading to weak emission in diluted aqueous solutions or typical organic solvents due to the formation of a twisted intermediate.[15]

In the current work, we have designed and synthesized a series of triads based on carborane clusters (*ortho* or *meta*-isomers) bonded to two stilbenes through a -CH_2- to the $C_{cluster}$ atoms. Additionally, iodination of B atoms in *meta* derivatives has been performed to analyze the effect of the iodine in the photophysical properties, but mainly to obtain new fluorescent precursors where the B-I vertices would allow a later derivatization with the desired functional group. All compounds have been characterized and their crystal structures established by X-ray diffraction analysis. Experimental and theoretical comparative studies of the photophysical properties in solution and solid state have been conducted to determine the structure-photophysical properties relationship of the compounds, in particular elucidating the role of the carborane cluster.

Photophysical properties. The optical spectra of compounds **2**, **4**, **6**, **8** in THF solution are very similar to each other and differ only little from what was reported on *trans*-stilbene.[15b] Inspecting for instance compounds **4** and **8** in Figure 7, the absorption spectra are relatively broad and show some vibronic structure, with a maximum at 314 nm, which is 0.09 eV (7 nm) and 0.04 eV (3 nm) red-shifted respect to the *trans*-stilbene (307 nm) and the 4-Methyl-stilbene (311 nm), respectively; but 0.05 eV (4 nm) blue-shifted compared to 4-Methoxy-stilbene (318 nm) in ACN.[16] Only a slight red-shift is observed for **8** compared to its homologous non-iodinated **4**. All compounds show similar molar extinction coefficients (ε). The similarity of absorption maxima and ε values for compounds **2**, **4**, **6** and **8** indicates that neither the carbon atoms position in *ortho* and *meta*-isomers nor the presence of B-I affect the absorption. The photoluminescence (PL) spectra are better structured compared to absorption (Figure 7), which reflects the steeper torsional potential in the first excited singlet state S_1 as compared to the ground state (S_0).[17] The similarity between the spectra of **4** and **8** in solution, with emission maxima at λ_{em} 355 and 352 nm respectively, and to stilbene itself (350 nm), indicates only small electronic interactions between the stilbene units

in the compounds, independently on the type of carborane isomer. Accordingly, the PL kinetics are similar to stilbene, giving small PL quantum yields Φ_F of 5-8% and short lifetimes τ_F of 0.14-0.23 ns (Table 2). It is noted that compounds **6**, **8** are not different from **2**, **4** despite the heavy-atom effect of iodine which is able to promote inter-system crossing (ISC); the apparently low ISC is ascribed to the large distance between iodine and the stilbenes. Due to the analogy to stilbene itself,[14b, 15b] the main non-radiative deactivation pathway in all compounds is assigned to rapid *cis-trans* isomerization. Remarkably, the non-radiative pathway $k_{nr} = (1-\Phi_F)/\tau_F$ are much faster in the *ortho*-compounds as compared to the *meta*-compounds due to geometrical reasons as we will see in the following discussion.

In order to gain deeper insight into the geometrical and spectral properties of the compounds we performed (time-dependent) density functional theory, (TD)DFT, calculations on compounds **2** and **4**. Geometry optimization of **2** gave a collinear arrangement of the stilbene units, see Figure 8, being very similar to the crystal structure analysis; in the crystal, one of the stilbene units is tilted around the $C_{cluster}$-CH_2 bond by 20°, while the other is 0º, in the calculation they are 28º and 14º. In **4**, a somewhat twisted side-by-side arrangement of the stilbene units was found, similar to the crystal structure analysis (Figure 8). The differences of the gas phase optimized structures to those in the crystal are ascribed to packing constraints in the solid. The collinear arrangement of the *ortho*-substituted compound **2** allows for full conformational freedom, whereas the twisted side-by-side arrangement in the *meta*-substituted compound **4** restrict the conformational space, which rationalizes the increased rate for *cis-trans* isomerization in **2**.

MO calculations reveal that both HOMO and LUMO are located in the stilbene moieties; this is very different to carborane-based dyads with smaller chromophores, where the HOMO is localized in the conjugated unit but the LUMO in the carborane unit, so that low-lying charge-transfer (CT) are generated.[3c, 4a] Differently, the LUMO of stilbene (-1.55 eV) is clearly smaller than that of carborane (-0.25 eV) so that the lowest excited singlet transition ($S_0 \rightarrow S_1$), which is formed by a HOMO→LUMO excitation, is determined by stilbene alone. This agrees well with the absorption properties of the

compounds, being very similar to stilbene and without indication for low-lying CT states. Hereby, electronic communication between stilbene and carborane is additionally reduced by the methyl linkers.

The TD-DFT calculations (Figure 9) suggest some slight differences between the **2** and **4** UV/Vis absorption spectra, because of the different electronic situation in both compounds; in fact, coulombic interaction between the $S_0 \rightarrow S_1$ transition dipole moments of each stilbene unit gives rise to (weak) exciton coupling. The collinear arrangement of the stilbene units in **2** provokes weak J-aggregation with an exciton splitting of ca. 0.10 eV, which slightly red-shifts the main absorption band against the calculated spectrum of mono-stilbene carborane (compound **0**; see Figure 9). In contrast, the side-by-side interactions of the stilbenes in **4** gives rise to weak H-aggregation (exciton splitting of 0.22 eV) and a slight blue-shift against **0**. It's interesting that these effects are not visible in experiment although the calculated geometries are reliable (*vide supra*). One possible reason might be due to the fact that the used B3LYP functional tends to somewhat overestimate the coupling, due to its inherent tendency to overestimate delocalization; however, also the long-range corrected ωB97XD functional gives similar values (**2**: 0.07, **4**: 0.13 eV); a further effect might be the neglect of Herzberg-Teller coupling in the calculations. However, the main reason for the difference to experiment is apparently the flexibility around the C_c-CH_2 bond, which leads to a broad distribution of different inter-chromophore orientations at room temperature, which effectively reduces exciton coupling.

Finally, we investigated the PL characteristics in the solid state; thin film spectra of the *meta* derivatives **4**, **6** and **8** are shown in Figure 10. The PL spectra for these compounds, as well as also the single crystal of **4** (see Figure S3) are very similar, showing vibronic structure and a maximum around 460-465 nm (F_L in Figure 10), strongly red-shifted against THF solutions in THF (compound **2** on the other hand shows a structureless and weak PL, see Figure S4). The PL lifetimes for all stilbene compounds in the films are around 1 ns, in all indicating that the emitting species in these compounds are similar in nature. The PL spectra are very heterogeneous with a number of low intensity bands in the 360-420 nm range (F_H). The F_H spectrum has a

different origin than F_L, as it is clearly seen in the absorption spectrum (Figure 10). Also here two ranges are distinctively different; the high energy features A_H at □ < 350 nm are identified as the origin of F_H, whereas the low energy features A_L in the 350-430 nm range are responsible for F_L.[1] The high energy features are bathochromically shifted by ca. 0.25 eV against solution; this agrees with the herringbone (i.e. edge-to-face) arrangement observed for neighboring stilbene units in the x-ray analysis of the compounds (*vide supra*). In fact, similar shifts are found for the solid state herringbone arrangement of distyrylbenzene,[18] and for Langmuir-Blodgett films of stilbenes,[14b] which are expected to arrange as well in such a manner.

The origin of the low energy species is more difficult to assign. It is clearly a minority species as seen in the low optical density of A_L compared to A_H. To investigate whether low lying CT states could be formed in the solid we calculated stacked stilbene-carborane clusters, which however gave no evidence for CT contributions in the lowest excited state. We thus ascribe F_L to effective sensitization; in fact, strong sensitization was observed for distyrylbenzene crystals upon chemical doping with appropriate acceptors at doping levels as low as 0.1 % through efficient thermally activated exciton diffusion.[18-19] A possible source for such acceptor states without invoking contaminations (for which we have indeed no evidence from materials' analysis) are structural misalignments, e.g. more close arrangements of stilbenes, which commonly emit in that spectral range of F_L with similar vibronics and PL lifetimes as reported by Lewis.[20] On the contrary, perfect □-stacks exhibit even stronger bathochromic shifts, longer lifetimes, reduced quantum yields and unstructured spectra.[21] Finally, the absolute quantum yield was measured in powder for compounds **2**, **4**, **6** and **8** (PL spectra in Figure S5). Compounds **4** and **6** show considerably high PL quantum yields in the solid state (**4**: 38%; **6**: 30%), which is much higher than in solution. This is ascribed to a combined effect of the restricted environment in the solid which suppresses isomerization, and effective PL sensitization as discussed above. The quantum yield latter drops to 17% in **8**, which is possibly due to the presence of iodine close to the

[1] The A_H features are little resolved; this is an artifact due to the high optical density of the film.[15] For the same reason, the PL excitation spectrum cannot be evaluated in that range.

stilbene units in the solid state which could open an effective ISC pathway in the excited state.

Conclusion

A set of compounds based on carborane clusters bonded to two stilbene units through C_c-CH_2 have been synthesized and characterized. The bonding of *ortho* or *meta* isomers to the stilbene units do not alter their absorption and emission properties in solution, which is confirmed by (TD)DFT. These results reveal no CT contributions in the lowest excited state, since electronic communication is further diminished by the presence of the CH_2 spacer between the cluster and the stilbenes.

Iodination of boron atoms in *meta*-carborane derivatives does not alter the emission properties of stilbenes in solution, ascribed to the rather large distance between the heavy atom and the fluorophore. Noticeable, in the solid state, a significant red-shift of the PL spectrum with respect to the solution is shown, which can be traced back to PL sensitization most probably by more densely packed stilbene moieties. PL absolute quantum yields in solid state are significantly higher than in solution due to the restricted environment and the before mentioned sensitization. Iodinated compounds show lower PL quantum yields in solid state, ascribed to enhanced ISC in the solid.

Remarkably, our iodinated (B-I) species could be fascinating precursors to hetero-substituted systems, which combine *i.e* fluorescent moieties in the $C_{cluster}$, the therapeutic effect of boron clusters and the possible derivatization by B-coupling reactions with the desired molecules. Current work is being doing in this direction in our laboratory.

Experimental Section.

Instrumentation. Elemental analyses were performed using a Carlo Erba EA1108 microanalyzer. ATR-IR spectra were recorded on a high-resolution spectrometer FT-IR PerkinElmer Spectrum One. The ^{1}H NMR (300.13 MHz), $^{11}B\{^{1}H\}$ and ^{11}B NMR (96.29 MHz) and $^{13}C\{^{1}H\}$ NMR (75.47 MHz) spectra were recorded on a Bruker ARX 300 spectrometer. All NMR spectra were recorded in $CDCl_3$ solutions at 25ºC. Chemical shift values for $^{11}B\{^{1}H\}$ NMR spectra were referenced to external $BF_3{\cdot}OEt_2$, and those for ^{1}H

and $^{13}C\{^1H\}$ NMR were referenced to $SiMe_4$. Chemical shifts are reported in units of parts per million downfield from reference and all coupling constants are reported in Hertz. The UV/Vis absorption spectra were performed in spectroscopic grade THF solution (Sigma-Aldrich) with concentrations ~1.10^{-6} M in normal quartz cuvette having 1 cm path length. Solid state film experiments were performed upon drop casting the THF solutions on quartz surface (thickness having ~100 nm) upon slow solvent evaporation in room temperature. Absorption spectra of both solutions and solid state were measured by a Varian Cary-50 Bio UV/Visible spectrometer after proper base line correction. Fluorescence emission and excitation for both the solution and film were performed by Fluoromax-4 spectrophotometer (Horiba), equipped with a Xenon high pressure lamp source and double monochromators for excitation and emission. The emission and excitation spectra were corrected for the wavelength sensitivity of the PMT, and the excitation source, respectively. For display in the energy scale, the emission spectra were λ^2 corrected for constancy of the integrated area. Fluorescence quantuum yields were determined by relative measurements against quinine sulfate (0.1 M H_2SO_4) with ϕ_F = 0.55. Time resolved fluorescence lifetime measurements for solutions and films were done by the time correlated single photon counting (TCSPC) technique using an Acton SP2500 spectrometer, and low dark current photomultiplier (PMA 06, PicoQuant) for detection. A HydraHarp-400 TCSPC event timer with 1 ps time resolution was used to measure the fluorescence decays. The excitation source was a 337 nm NanoLED (PicoQuant, PLS-8-2-651; 0.5 microwatt power; Trigger level 10 MHz at 90 % intensity) with FWHM ~250 ps. The decay time data was fitted after de-convolution with the IRF data by Fluofit software (PicoQuant). Absolute fluorescence quantum yields were measured in an integrating sphere system (Hamamatsu C9920).

Materials. All reactions were performed under an atmosphere of dinitrogen employing standard Schlenk techniques. Tetrahydrofurane, diethyl ether and 1,4-dioxane were purchased from Merck and distilled from sodium benzophenone previously to use. Commercial grade tetrahydrofurane, methanol, diethyl ether, petroleum ether and dichloromethane were used without further purification. Compound 1,2-*closo*-$C_2B_{10}H_{12}$ was supplied by Katchem Ltd. (Prague) and used as

received. 1,7-*closo*-$C_2B_{10}H_{12}$, compound **1**, 9-I-1,7-dicarba-*closo*-dodecaborane and 9,10-I_2-1,7-dicarba-*closo*-dodecaborane were prepared according to the literature.[1a, 4a, 22] The 4-vinylbenzyl chloride, *n*-BuLi solution (1.6 M in hexane), $Pd_2(dba)_3$ and Pd(t-$Bu_3P)_2$ were purchased from Aldrich. Iodobenzene was purchased from Alfa Aesar and NCy_2Me from Acros.

X-ray Structure Determinations. The crystals of **2**, **4**, **7**, and **8** were immersed in cryo-oil, mounted in a MiTeGen loop, and measured at 120 K. The X-ray diffraction data were collected on an Agilent Supernova diffractometer using Cu Kα (λ = 1.54184 Å) or Mo Kα (λ = 0.71073 Å) radiation. The *CrysAlisPro*[23] program package was used for cell refinements and data reductions. The structures were solved by charge flipping method using the *Superflip*[24] program. A semi-empirical, numerical, or analytical absorption correction (*CrysAlisPro*[24] or *SADABS*[25]) was applied to all data. Structural refinements were carried out using *SHELXL-2014*[26] In all structures the hydrogen atoms were positioned geometrically and constrained to ride on their parent atoms with C-H = 0.95-0.99 Å, B-H 1.12 Å, and U_{iso} = 1.2·U_{eq}(parent atom). The crystal of **2** was found to be twinned (twin matrix [-1.000 0.000 0.000 0.000 -1.000 0.000 0.113 0.000 1.000]) and the BASF value was refined to 0.157. The two components were determined by *PLATON* software.[27] The solvent of crystallization in structure **8** could not be unambiguously resolved and therefore the contribution of the solvent to the calculated structure factors was taken into account by using the SQUEEZE routine of PLATON. [27] In structure **7** the carborane molecule was positioned on a mirror plane and the asymmetric unit contained only half of the molecule. In **8**, the asymmetric unit of consisted of two crystallographically independent molecules. The crystallographic details are summarized in Table 1.

Calculations.

All calculations were done at the (TD)DFT level of theory (in vacuum), employing the B3LYP and ωB97XD functionals, and the 6-311G* basis set as defined in Gaussian 09.[28] The geometry of C2 was optimized both without symmetry (C_1) as well as in the highest possible symmetry C_s. The geometry of C4 was optimized without imposing symmetry (C_1).

Compound 2.- A 5 mL round-bottomed flask under nitrogen was charged with **1** (18 mg, 0.048 mmol), $Pd[P(t\text{-}Bu_3)]_2$ (2 mg, 0.004 mmol), $Pd_2(dba)_3$ (2 mg, 0.002 mmol), iodobenzene (12 μL, 0.100 mmol), and NCy_2Me (0.06 mL, 0.271 mmol) in 1.5 mL of 1,4-dioxane. The solution was stirred at 90 °C overnight. After that, the reaction mixture was filtered through 1 cm Celite, washed with THF and the solvent was removed under vacuum. The residue was dissolved in 1 mL of THF, then 10 mL of CH_3OH was added and the precipitated solid was filtered and washed with CH_3OH giving a white solid. Yield: 19 mg, 75%. A solution of **2** in THF/CH_3OH gave crystals suitable for X-ray analysis. ^{1}H NMR ($CDCl_3$, TMS): δ = 7.56-7.52 (m, 8H, C_6H_4 and C_6H_5), 7.39 (m, 4H, C_6H_5), 7.31 (d, ^{3}J(H,H)=6 Hz, 2H, C_6H_5), 7.24 (d, ^{3}J(H,H)=6 Hz, 2H, C_6H_4), 7.14 (s, 4H, C*H*=C*H*), 3.67 (s, 4H, CH_2); ^{1}H{^{11}B} NMR ($CDCl_3$, TMS): δ = 7.56-7.52 (m, 8H, C_6H_4 and C_6H_5), 7.39 (m, 4H, C_6H_5), 7.31 (d, ^{3}J(H,H)=9 Hz, 2H, C_6H_5), 7.24 (d, ^{3}J(H,H)=9 Hz, 2H, C_6H_4), 7.14 (s, 4H, C*H*=C*H*), 3.67 (s, 4H, CH_2), 2.30 (s, 2H, B-*H*), 2.12 (s, 8H, B-*H*);); ^{11}B NMR ($CDCl_3$): δ = -4.74 (d, ^1J(B,H) = 112 Hz, 2B), -10.36 (d, ^1J(B,H) = 117 Hz, 6B); ^{13}C{^{1}H} NMR ($CDCl_3$): δ = 137.29 (s, CH-C_6H_4), 137.17 (s, CH-C_6H_5), 134.19 (s, CH-C_6H_4), 130.74 (s, C_6H_4), 129.54 (s, C_6H_5), 128.72 (s, C_6H_5), 128.29 (s, *C*H=*C*H), 127.85 (s, C_6H_5), 126.66 (s, C_6H_4), 79.32 (s, C_c), 41.13 (s, -*C*H_2-); ATR-IR (cm^{-1}): $\tilde{\nu}$ = 2592 (i, B-H str); elemental analysis calcd for $C_{32}H_{36}B_{10}$: C 72.69, H 6.86; found: C 71.43, H 7.01.

Compound 3.- A solution of nBuLi 1.6M in hexane (0.52 mL, 0.832 mmol) was added dropwise to a solution of 1,7-closo-$C_2B_{10}H_{12}$ (54 mg, 0.375 mmol) in THF (2 mL) at 0°C. The mixture was stirred for 1 h at room temperature, cooled again at 0°C, and [4-(CH_2=CH)-C_6H_4-CH_2]Cl (0.13 mL, 0.832 mmol) was added. The mixture was stirred 1h at room temperature and reflux overnight. After that, the solvent was removed under vacuum and the mixture was quenched with H_2O (15 mL), transferred to a separating funnel, and extracted with Et_2O (3x10 mL). The organic layer was dried over $MgSO_4$ and the volatiles were reduced under vacuum. The orange oil was purified by preparative layer chromatography (dichloromethane/hexane 1:9) giving a colorless oil. Yield: 0.057 g, 41 %. ^{1}H NMR ($CDCl_3$, TMS): δ = 7.35 (d, ^{3}J(H,H)=9 Hz, 4H, C_6H_4), 7.02 (d, ^{3}J(H,H)=9 Hz, 4H, C_6H_4), 6.73 (dd, ^{3}J(H,H)=18 Hz, ^{3}J(H,H)=12 Hz, 2H, C*H*=CH_2), 5.77 (d, ^{3}J(H,H)=18 Hz, 2H, CH=CH_2), 5.28 (d, ^{3}J(H,H)=12 Hz, 2H, CH=CH_2), 3.15 (s, 4H, C_c– CH_2); ^{1}H{^{11}B}

NMR ($CDCl_3$, TMS): δ = 7.35 (d, ^{3}J(H,H)=9 Hz, 4H, C_6H_4), 7.02 (d, ^{3}J(H,H)=9 Hz, 4H, C_6H_4), 6.73 (dd, ^{3}J(H,H)=18 Hz, ^{3}J(H,H)=12 Hz, 2H, C*H*=CH_2), 5.77 (d, ^{3}J(H,H)=18 Hz, 2H, CH=CH_2), 5.28 (d, ^{3}J(H,H)=12 Hz, 2H, CH=CH_2), 3.15 (s, 4H, C_c– CH_2), 2.52 (s, 2H, B-*H*), 2.23 (s, 2H, B-*H*), 2.17 (s, 4H, B-*H*), 2.06 (s, 2H, B-*H*); ^{11}B NMR ($CDCl_3$): δ = -7.14 (d, ^1J(B,H) = 158 Hz, 2B), -10.11 (d, ^1J(B,H) = 153 Hz, 6B), -13.97 (d, ^1J(B,H) = 174 Hz, 2B); ^{13}C{^{1}H} NMR ($CDCl_3$): δ = 136.83 (s, C_6H_4), 136.53 (s, C_6H_4), 136.39 (s, *C*H=CH_2), 130.02 (s, C_6H_4), 126.18 (s, C_6H_4), 114.01 (s, CH=*C*H_2), 76.24 (s, C_c-CH_2), 42.70 (s, CH_2); ATR-IR (cm^{-1}): $\tilde{\upsilon}$ = 2587 (i, B-H str), 1629 (m, C=C str); elemental analysis calcd for $C_{20}H_{28}B_{10}$: C 63.79, H 7.50; found: C 64.10, H 7.65.

Compound 4.- The procedure was the same as for 2, but using **3** (52 mg, 0.138 mmol), Pd[P(t-Bu_3)]$_2$ (2 mg, 0.004 mmol), Pd_2(dba)$_3$ (2 mg, 0.002 mmol), iodobenzene (33 μL, 0.289 mmol), and NCy_2Me (0.15 mL, 0.679 mmol) in 2 mL of 1,4-dioxane giving a yellowish solid. Yield: 47 mg, 61%. A solution of **4** in THF/CH_3OH gave crystals suitable for X-ray analysis. ^{1}H NMR ($CDCl_3$, TMS): δ = 7.52 (d, ^{3}J(H,H)=6 Hz, 4H, C_6H_4), 7.45 (d, ^{3}J(H,H)=9 Hz, 4H, C_6H_5), 7.37 (m, 4H, C_6H_5), 7.30 (d, ^{3}J(H,H)=6 Hz, 2H, C_6H_5), 7.11 (s, 4H, C*H*=C*H*), 7.05 (d, 2H, ^3J(H,H)=9 Hz, C_6H_4), 3.16 (s, 4H, CH_2); ^{1}H{^{11}B} NMR ($CDCl_3$, TMS): δ = 7.52 (d, ^{3}J(H,H)=6 Hz, 4H, C_6H_4), 7.45 (d, ^{3}J(H,H)=9 Hz, 4H, C_6H_5), 7.37 (m, 4H, C_6H_5), 7.30 (d, ^{3}J(H,H)=6 Hz, 2H, C_6H_5), 7.11 (s, 4H, C*H*=C*H*), 7.05 (d, 2H, ^3J(H,H)=9 Hz, C_6H_4), 3.16 (s, 4H, CH_2), 2.52 (s, 2H, B-*H*), 2.23-2.19 (s, 6H, B-*H*), 2.07 (s, 2H, B-*H*); ^{11}B NMR ($CDCl_3$): δ = -7.05 (d, ^1J(B,H) = 198 Hz, 2B), -11.02 (d, ^1J(B,H) = 146 Hz, 6B), -13.95 (d, ^1J(B,H) = 209 Hz, 2B); ^{13}C{^{1}H} NMR ($CDCl_3$): δ = 137.61 (s, CH_2-C_6H_4), 136.61 (s, CH-C_6H_4), 136.36 (s, CH-C_6H_5), 130.18 (s, C_6H_4), 128.97 (s, C_6H_5), 128.70 (s, C_6H_5), 128.15 (s, CH=*C*H), 127.68 (s, *C*H=CH), 126.53 (s, C_6H_4), 126.43 (s, C_6H_5), 42.73 (s, -*C*H_2-); ATR-IR (cm^{-1}): $\tilde{\upsilon}$ = 2584 (i, B-H str); elemental analysis calcd for $C_{32}H_{36}B_{10}$: C 72.69, H 6.86; found: C 73.20, H 6.99.

Compound 5.- The procedure was the similar as for 3, but using a solution of 9-I-1,7-dicarba-*closo*-dodecaborane (150 mg, 0.555 mmol) in Et_2O/THF (2.5:2) at room temperature, nBuLi 1.6M in hexane (0.8 mL, 1.28 mmol) and [4-(CH_2=CH)-C_6H_4-CH_2]Cl (0.20 mL, 1.28 mmol). After extraction 3x10 mL brine:CH_2Cl_2 the yellowish oil was purified by preparative layer chromatography (Petroleum Ether) giving a colorless oil.

Yield: 0.111 g, 40 %. ^{1}H NMR ($CDCl_3$, TMS): δ = 7.35 (d, ^{3}J(H,H)=9 Hz, 4H, C_6H_4), 7.02 (d, ^{3}J(H,H)=9 Hz, 4H, C_6H_4), 6.74 (dd, ^{3}J(H,H)=18 Hz, ^{3}J(H,H)=12 Hz, 2H, C*H*=CH_2), 5.80 (d, ^{3}J(H,H)=18 Hz, 2H, CH=CH_2), 5.32 (d, ^{3}J(H,H)=12 Hz, 2H, CH=CH_2), 3.17 (s, 4H, C_c– CH_2); ^{1}H{^{11}B} NMR ($CDCl_3$, TMS): δ = 7.35 (d, ^{3}J(H,H)=9 Hz, 4H, C_6H_4), 7.02 (d, ^{3}J(H,H)=9 Hz, 4H, C_6H_4), 6.74 (dd, ^{3}J(H,H)=18 Hz, ^{3}J(H,H)=12 Hz, 2H, C*H*=CH_2), 5.80 (d, ^{3}J(H,H)=18 Hz, 2H, CH=CH_2), 5.32 (d, ^{3}J(H,H)=12 Hz, 2H, CH=CH_2), 3.17 (s, 4H, C_c– CH_2), 2.90-2.55 (10H, B-*H*); ^{11}B NMR ($CDCl_3$): δ = -8.66 (d, 2B, ^{1}J(B,H) = 118 Hz), -11.51 (br, 1B), -12.64 (br, 2B), -13.35 (br, 1B), -15.14 (br, 1B), -16.16 (br, 1B), -18.17 (d, 1B, ^{1}J(B,H) = 184 Hz), -26.37 (s, 1B, *B*-I); ^{13}C{^{1}H} NMR ($CDCl_3$): δ = 136.56 (s, C_6H_4), 133.74 (s, C_6H_4), 133.43 (s, *C*H=CH_2), 127.43 (s, C_6H_4), 123.83 (s, C_6H_4), 111.78 s, CH=*C*H_2), 40.00 (s, CH_2); ATR-IR (cm^{-1}): $\tilde{\upsilon}$ = 2606 (i, B-H str), 1628 (m, C=C str); elemental analysis calcd for $C_{20}H_{27}B_{10}I$: C 47.81, H 5.42; found: C 47.81, H 5.59.

Compound 6.- The procedure was the same as for 2, but using **5** (111 mg, 0.221 mmol), Pd[P(t-Bu_3)]$_2$ (3 mg, 0.006 mmol), Pd_2(dba)$_3$ (3 mg, 0.003 mmol), iodobenzene (53 μL, 0.465 mmol), and NCy_2Me (0.20 mL, 0.905 mmol) in 2 mL of 1,4-dioxane giving a white solid. Yield: 94 mg, 65%. ^{1}H NMR ($CDCl_3$, TMS): δ = 7.52 (d, ^{3}J(H,H)=6 Hz, 4H, C_6H_4), 7.47 (d, ^{3}J(H,H)=9 Hz, 4H, C_6H_5), 7.38 (m, 4H, C_6H_5), 7.30 (d, ^{3}J(H,H)=6 Hz, 2H, C_6H_5), 7.12 (s, 4H, C*H*=C*H*), 7.05 (d, 2H, ^{3}J(H,H)=9 Hz, C_6H_4), 3.18 (s, 4H, CH_2); ^{1}H{^{11}B} NMR ($CDCl_3$, TMS): δ = 7.52 (d, ^{3}J(H,H)=6 Hz, 4H, C_6H_4), 7.47 (d, ^{3}J(H,H)=9 Hz, 4H, C_6H_5), 7.38 (m, 4H, C_6H_5), 7.30 (d, ^{3}J(H,H)=6 Hz, 2H, C_6H_5), 7.12 (s, 4H, C*H*=C*H*), 7.05 (d, 2H, ^{3}J(H,H)=9 Hz, C_6H_4), 3.18 (s, 4H, CH_2), 2.90-2.25 (9H, B-*H*); ^{11}B NMR ($CDCl_3$): δ = -6.08 (br, 2B), -10.10 (br, 5B), -14.15 (br, 1B), -15.23 (br, 1B), -23.83 (s, 1B, *B*-I); ^{13}C{^{1}H} NMR ($CDCl_3$): δ = 137.21 (s, CH_2-C_6H_4), 136.91 (s, CH-C_6H_4), 135.74 (s, CH-C_6H_5), 130.12 (s, C_6H_4), 129.24 (s, C_6H_5), 128.74 (s, C_6H_5), 128.01 (s, CH=*C*H), 127.78 (s, *C*H=CH), 126.60 (s, C_6H_4), 126.60 (s, C_6H_5), 42.73 (s, -*C*H_2-); ATR-IR (cm^{-1}): $\tilde{\upsilon}$ = 2614 (i, B-H str); elemental analysis calcd for $C_{32}H_{35}B_{10}I$: C 58.71, H 5.39; found: C 59.84, H 5.44.

Compound 7.- The procedure was the same as for 5 but using a solution of 9,10-I_2-1,7-dicarba-*closo*-dodecaborane (321 mg, 0.810 mmol) in THF (6 mL), nBuLi 1.6M (1.17 mL, 1.864 mmol) and [4-(CH_2=CH)-C_6H_4-CH_2]Cl (0.30 mL, 1.864 mmol) at 0°C. The yellowish solid was recrystallized in CH_2Cl_2 and slowly washed with Et_2O giving a white

solid. Yield: 0.308 g, 61 %. A solution of **7** in THF/CH_3OH gave crystals suitable for X-ray analysis. ^{1}H NMR ($CDCl_3$, TMS): δ = 7.37 (d, ^{3}J(H,H)=9 Hz, 4H, C_6H_4), 6.99 (d, ^{3}J(H,H)=9 Hz, 4H, C_6H_4), 6.72 (dd, ^{3}J(H,H)=18 Hz, ^{3}J(H,H)=12 Hz, 2H, C*H*=CH_2), 5.77 (d, ^{3}J(H,H)=18 Hz, 2H, CH=CH_2), 5.28 (d, ^{3}J(H,H)=12 Hz, 2H, CH=CH_2), 3.15 (s, 4H, C_c– CH_2); ^{1}H{^{11}B} NMR ($CDCl_3$, TMS): δ = 7.37 (d, ^{3}J(H,H)=9 Hz, 4H, C_6H_4), 6.99 (d, ^{3}J(H,H)=9 Hz, 4H, C_6H_4), 6.72 (dd, ^{3}J(H,H)=18 Hz, ^{3}J(H,H)=12 Hz, 2H, C*H*=CH_2), 5.77 (d, ^{3}J(H,H)=18 Hz, 2H, CH=CH_2), 5.28 (d, ^{3}J(H,H)=12 Hz, 2H, CH=CH_2), 3.15 (s, 4H, C_c– CH_2), 2.95 (s, 2H, B-*H*), 2.86 (s, 2H, B-*H*), 2.71 (s, 4H, B-*H*); ^{11}B NMR ($CDCl_3$): δ = -4.88 (d, ^1J(B,H) = 131 Hz, 2B), -10.07 (d, ^1J(B,H) = 153 Hz, 4B), -15.64 (d, ^1J(B,H) = 165 Hz, 2B), -21.14 (s, 2B, *B*-I); ^{13}C{^{1}H} NMR ($CDCl_3$): δ = 137.33 (s, C_6H_4), 136.15 (s, C_6H_4), 135.34 (s, *C*H=CH_2), 129.87 (s, C_6H_4), 126.49 (s, C_6H_4), 114.50 (s, CH=*C*H_2), 78.26 (s, C_c-CH_2), 42.44 (s, CH_2); ATR-IR (cm^{-1}): $\tilde{\upsilon}$ = 2621 (i, B-H str), 2613 (i, B-H str), 2603 (i, B-H str), 2591 (i, B-H str), 1628 (m, C=C str); elemental analysis calcd for $C_{20}H_{26}B_{10}I_2$: C 38.23, H 4.17; found: C 38.00, H 4.20.

Compound 8.- The procedure was the same as for 2, but **7** (75 mg, 0.119 mmol), Pd[P(t-Bu_3)]$_2$ (3 mg, 0.006 mmol), Pd_2(dba)$_3$ (3 mg, 0.003 mmol), iodobenzene (28 μL, 0.246 mmol), and NCy_2Me (0.15 mL, 0.679 mmol) in 2 mL of 1,4-dioxane giving a white solid. Yield: 54 mg, 58%. A solution of **8** in THF/CH_3OH gave crystals suitable for X-ray analysis. ^{1}H NMR ($CDCl_3$, TMS): δ = 7.53 (d, ^{3}J(H,H)=6 Hz, 4H, C_6H_4), 7.47 (d, ^{3}J(H,H)=9 Hz, 4H, C_6H_5), 7.38 (m, 4H, C_6H_5), 7.31 (d, ^{3}J(H,H)=6 Hz, 2H, C_6H_5), 7.13 (s, 2H, C*H*=CH), 7.11 (s, 2H, CH=C*H*), 7.03 (d, 2H, ^3J(H,H)=9 Hz, C_6H_4), 3.18 (s, 4H, CH_2); ^{1}H{^{11}B} NMR ($CDCl_3$, TMS): δ = 7.52 (d, ^{3}J(H,H)=6 Hz, 4H, C_6H_4), 7.47 (d, ^{3}J(H,H)=9 Hz, 4H, C_6H_5), 7.38 (m, 4H, C_6H_5), 7.30 (d, ^{3}J(H,H)=6 Hz, 2H, C_6H_5), 7.13 (s, 2H, C*H*=CH), 7.11 (s, 2H, CH=C*H*), 7.03 (d, 2H, ^3J(H,H)=9 Hz, C_6H_4), 3.18 (s, 4H, CH_2), 2.97 (s, 2H, B-*H*), 2.90 (s, 2H, B-*H*), 2.74 (s, 2H, B-*H*); ^{11}B NMR ($CDCl_3$): δ = -4.92 (d, ^1J(B,H) = 130 Hz, 2B), -10.15 (d, ^1J(B,H) = 109 Hz, 4B), -15.66 (d, ^1J(B,H) = 133 Hz, 2B), -21.14 (s, 2B, *B*-I); ^{13}C{^{1}H} NMR ($CDCl_3$): δ = 137.14 (s, C_6H_4), 137.14 (s, C_6H_5), 135.15 (s, C_6H_4), 130.03 (s, C_6H_4), 129.42 (s, C_6H_5), 128.73 (s, C_6H_5), 127.84 (s, *C*H=CH), 127.84 (s, CH=*C*H), 126.73 (C_6H_4), 126.58 (s, C_6H_5), 42.47 (s, -*C*H_2-); ATR-IR (cm^{-1}): $\tilde{\upsilon}$ = 2618 (i, B-H str), 2582 (i, B-H str); elemental analysis calcd for $C_{32}H_{34}B_{10}I_2$: C 49.24, H 4.39; found: C 49.24, H 4.42.

Scheme 1. Synthetic route to obtain compounds **2-8**.

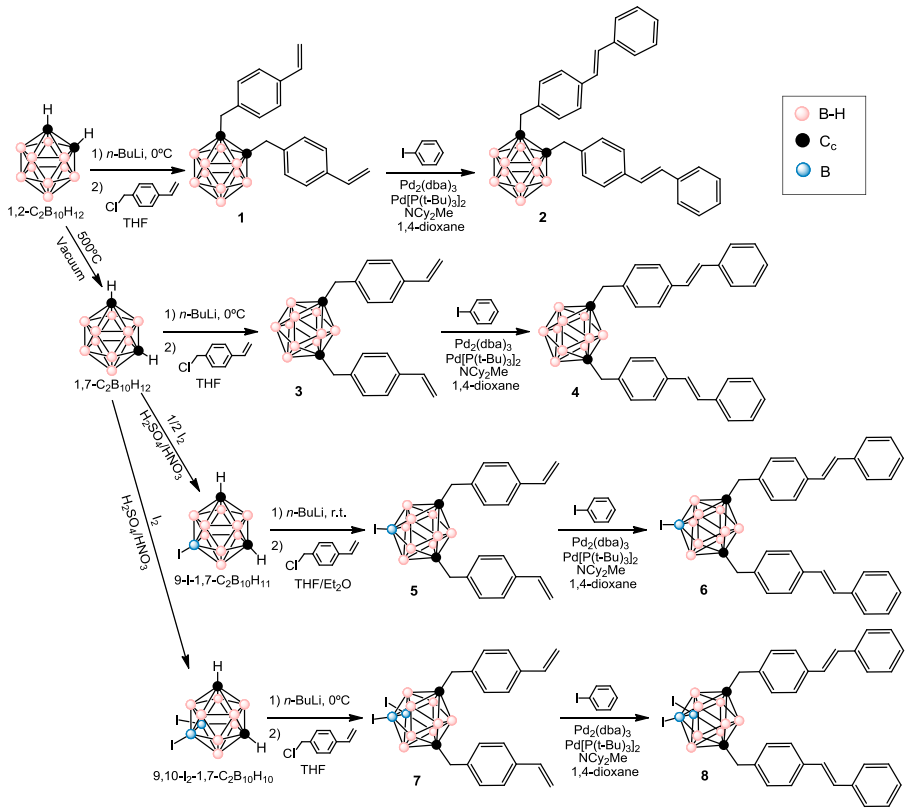

Figure 1. Crystal structure of a) compound **2** and b) compound **4**

(a)

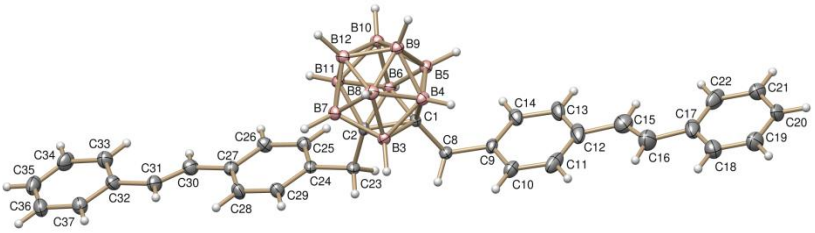

(b)

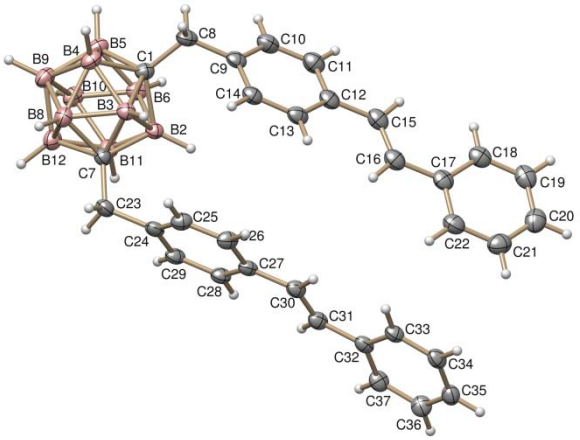

Figure 1. Crystal structure of a) compound **2** and b) compound **4**

a)

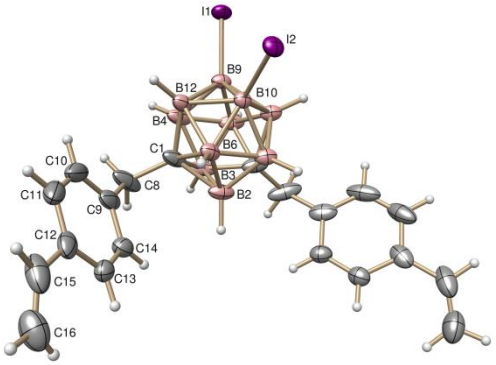

b)

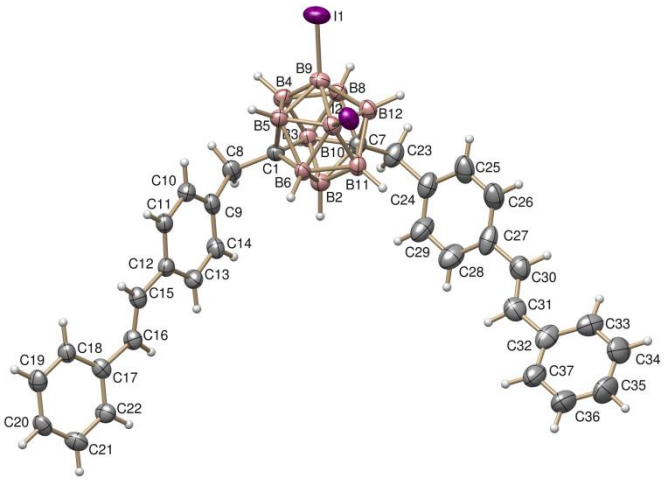

Figure 2. Crystal structure of compounds **7** and **8**.

(a)

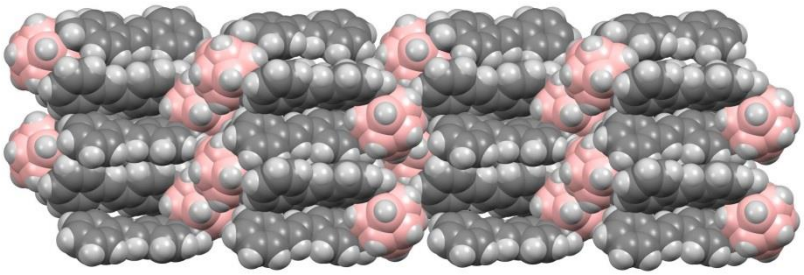

(b)

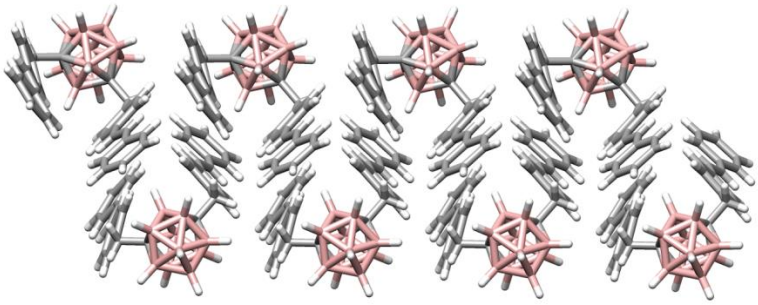

Figure 3. Packing of **4:** (a) viewed along the crystallographic a-axis and (b) showing the nearest and non-nearest neighbor arrangement

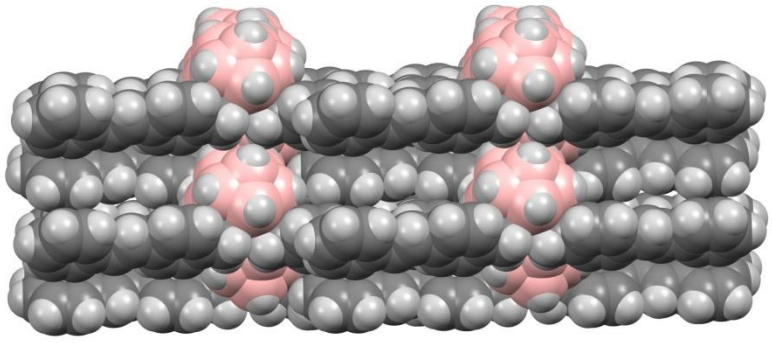

Figure 4. Packing of **2** viewed along the crystallographic a-axis.

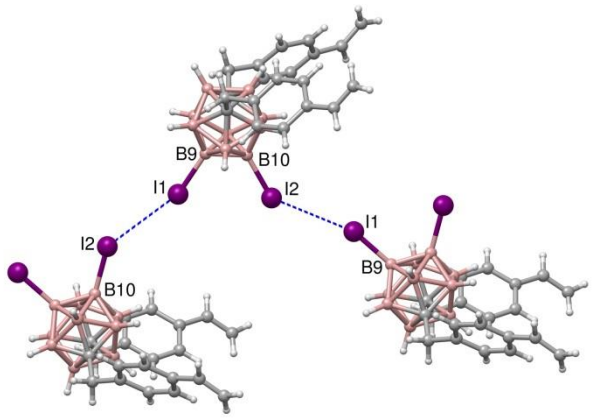

Figure 5. Halogen-halogen interactions in **7**. The I1-I2$^{\#1}$ distance is 3.8379(3) Å, and the angles B9-I1-I2$^{\#2}$ and B10-I2-I1$^{\#3}$ 160.65(8)° and 141.71(8)° respectively (#1: -0.5+X, +Y, 2.5-Z, #2: -0.5+X, +Y, 2.5+Z, #3: 0.5+X, +Y, 2.5-Z).

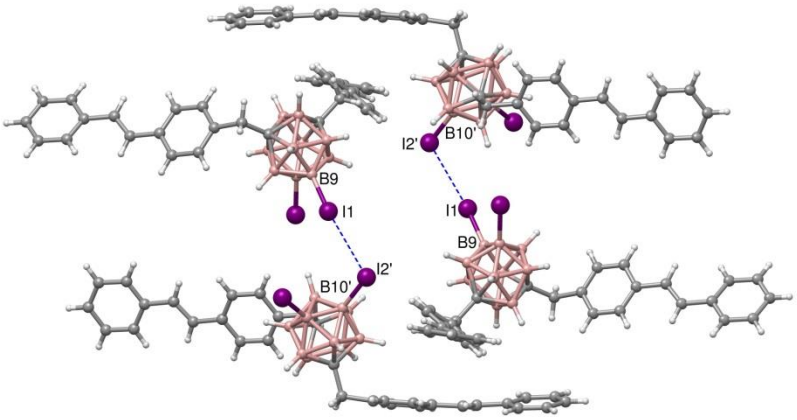

Figure 6. Halogen bonds in **8**. The The I1···I2' distance is 3.8415(6) Å, and the angles: B9-I1-I2'$^{\#1}$ and B10'-I2'-I1$^{\#1}$ 95.6(2)° respectively (#1: 1-X, 1-Y, 1-Z).

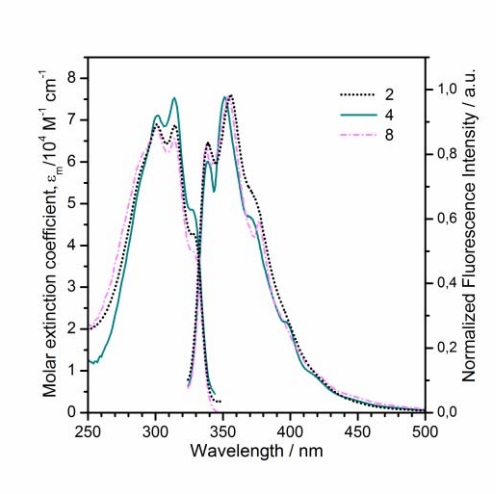

Figure 7: Absorption (left) and PL spectra (right, excitation wavelength 314 nm) of compounds 2 (black-dotted lines), **4** (blue-solid lines) and **8** (pink-dot-dashed lines), recorded in THF.

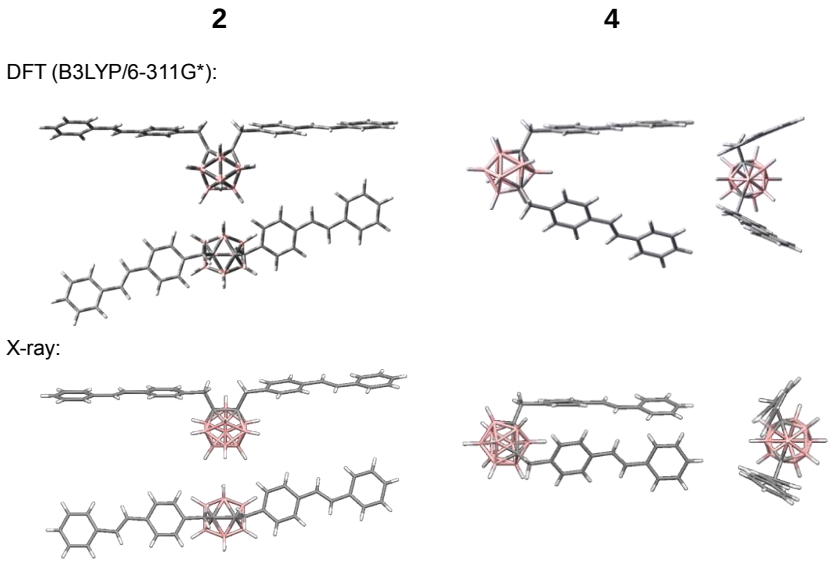

Figure. 8: Geometry of **2** and **4**: DFT calculation vs. x-ray analysis.

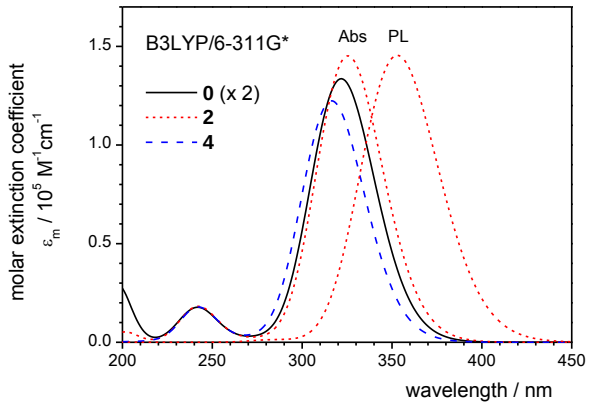

Figure 9: UV/Vis absorption spectra of **2** and **4** and PL spectrum of **2**, as calculated by TD-DFT (pure electronic transitions, broadened by a Gaussian with a half-width of 0.25 eV); the spectrum of the mono-substituted stilbene-carborane (**0**) is shown for comparison (multiplied by a factor of 2).

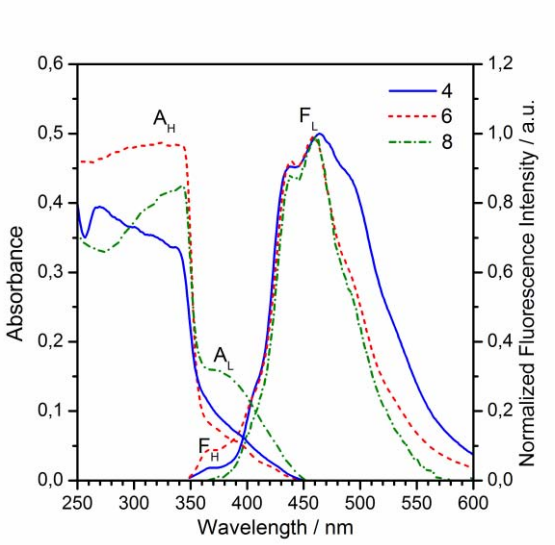

Figure 10: PL spectra (excitation wavelength 314 nm) of compounds **4** (blue-solid line), **6** (red-dashed line), and **8** (green-dot-dashed line) in films.

Table 2: PL lifetimes τ_F and quantum yields Φ_F of the di-stilbene compounds in THF solution; calculated radiative and non-radiative rate constants $k_F = \Phi_F/\tau_F$ and $k_{nr} = (1-\Phi_F)/\tau_F$. (Excitation 337 nm; data recorded at λ_{em} = 360nm)

Compound	ε /10^4 M^{-1} cm^{-1}	τ_F [a] / ns	Φ_F	k_F / ns^{-1}	k_{nr} / ns^{-1}
2	6.86	0.14	0.05	0.36	6.78
4	7.53	0.18	0.07	0.39	5.16
6	8.17	0.21	0.08	0.36	4.04
8	7.28	0.23	0.08	0.33	4.01

[a] intensity-average from bi-exponential fit.

References

[1] a) R. N. Grimes, *Carboranes*, Academic Press, **2011**; b) G. A. Olah, G. K. S. Prakash, K. Wade, Á. Molnár, R. E. Williams, *Hypercarbon Chemistry*, John Wiley & Sons, Inc., **2011**.

[2] R. Núñez, P. Farràs, F. Teixidor, C. Viñas, R. Sillanpää, R. Kivekäs, *Angew. Chem. Int. Ed.* **2006**, *45*, 1270-1272

[3] a) N. Tsuboya, M. Lamrani, R. Hamasaki, M. Ito, M. Mitsuishi, T. Miyashita, Y. Yamamoto, *J. Mater. Chem.* **2002**, *12*, 2701-2705; b) O. Crespo, M. C. Gimeno, A. Laguna, I. Ospino, G. Aullon, J. M. Oliva, *Dalton Trans.* **2009**, 3807-3813; c) L. Weber, J. Kahlert, R. Brockhinke, L. Böhling, A. Brockhinke, H.-G. Stammler, B. Neumann, R. A. Harder, M. A. Fox, *Chem. Eur. J.* **2012**, *18*, 8347-8357

[4] a) A. Ferrer-Ugalde, E. J. Juárez-Pérez, F. Teixidor, C. Viñas, R. Sillanpää, E. Pérez-Inestrosa, R. Núñez, *Chem. Eur. J.* **2012**, *18*, 544-553; b) A. Ferrer-Ugalde, A. González-Campo, C. Viñas, J. Rodríguez-Romero, R. Santillan, N. Farfán, R. Sillanpää, A. Sousa-Pedrares, R. Núñez, F. Teixidor, *Chem. Eur. J.* **2014**, *20*, 9940-9951

[5] a) F. Lerouge, A. Ferrer-Ugalde, C. Viñas, F. Teixidor, R. Sillanpaa, A. Abreu, E. Xochitiotzi, N. Farfan, R. Santillan, R. Nuñez, *Dalton Trans.* **2011**, *40*, 7541-7550; b) A. González-Campo, A. Ferrer-Ugalde, C. Viñas, F. Teixidor, R. Sillanpää, J. Rodríguez-Romero, R. Santillan, N. Farfán, R. Núñez, *Chem. Eur. J.* **2013**, *19*, 6299-6312; c) A. Ferrer-Ugalde, E. J. Juárez-Pérez, F. Teixidor, C. Viñas, R. Núñez, *Chem. Eur. J.* **2013**, *19*, 17021-17030; d) J. Cabrera-González, E. Xochitiotzi-Flores, C. Viñas, F. Teixidor, H. García-Ortega, N. Farfán, R. Santillan, T. Parella, R. Núñez, *Inorg. Chem.* **2015**, *54*, 5021-5031

[6] a) M. Eo, H. J. Bae, M. Hong, Y. Do, S. Cho, M. H. Lee, *Dalton Trans.* **2013**, *42*, 8104-8112; b) J. Marshall, J. Hooton, Y. Han, A. Creamer, R. S. Ashraf, Y. Porte, T. D. Anthopoulos, P. N. Stavrinou, M. A. McLachlan, H. Bronstein, P. Beavis, M. Heeney, *Polym. Chem.* **2014**, *5*, 6190-6199

[7] a) K.-R. Wee, Y.-J. Cho, S. Jeong, S. Kwon, J.-D. Lee, I.-H. Suh, S. O. Kang, *J. Am. Chem. Soc.* **2012**, *134*, 17982-17990; b) A. R. Davis, J. J. Peterson, K. R. Carter, *ACS Macro Lett* **2012**, *1*, 469-472; c) E. G. Cansu-Ergun, A. Cihaner, *Mater. Chem. Phys.* **2013**, *143*, 387-392

[8] a) R. Bernard, D. Cornu, P. L. Baldeck, J. Caslavsky, J. M. Letoffe, J. P. Scharff, P. Miele, *Dalton Trans.* **2005**, 3065-3071; b) R. Bernard, D. Cornu, J.-P. Scharff, R. Chiriac, P. Miele, P. L. Baldeck, J. Čáslavský, *Inorg. Chem.* **2006**, *45*, 8743-8748; c) J.-F. Nicoud, F. Bolze, X.-H. Sun, A. Hayek, P. Baldeck, *Inorg. Chem.* **2011**, *50*, 4272-4278; d) F. Bolze, A. Hayek, X. H. Sun, P. L. Baldeck, C. Bourgogne, J. F. Nicoud, *Opt. Mater.* **2011**, *33*, 1453-1458; e) L. Zhu, W. Lv, S. Liu, H. Yan, Q. Zhao, W. Huang, *Chem. Commun.* **2013**, *49*, 10638-10640

[9] a) A. V. Puga, F. Teixidor, R. Sillanpää, R. Kivekäs, C. Viñas, *Chem. Eur. J.* **2009**, *15*, 9764-9772; b) Z. Zheng, W. Jiang, A. A. Zinn, C. B. Knobler, M. F. Hawthorne, *Inorg. Chem.* **1995**, *34*, 2095-2100; c) A. V. Safronov, K. Z. Kabytaev, S. S. Jalisatgi, M. F. Hawthorne, *Dalton Trans.* **2014**, *43*, 12467-12469

[10] a) A. V. Puga, F. Teixidor, R. Sillanpaa, R. Kivekas, C. Viñas, *Chem. Commun.* **2011**, *47*, 2252-2254; b) Y. Sevryugina, R. L. Julius, M. F. Hawthorne, *Inorg. Chem.* **2010**, *49*, 10627-10634; c) A. Himmelspach, M. Finze, *Eur. J. Inorg. Chem.* **2010**, *2010*, 2012-2024; d) I. P. Beletskaya, V. I. Bregadze, V. A. Ivushkin, G. G. Zhigareva, P. V. Petrovskii, I. B. Sivaev, *Russ. J. Org. Chem.* **2005**, *41*, 1359-1366; e) D. Olid, R. Nuñez, C. Viñas, F. Teixidor, *Chem. Soc. Rev.* **2013**, *42*, 3318-3336

[11] a) S. Janczak, A. Olejniczak, S. Balabańska, M. K. Chmielewski, M. Lupu, C. Viñas, Z. J. Lesnikowski, *Chem. Eur. J.* **2015**, *21*, 15118-15122; b) M. Scholz, E. Hey-Hawkins, *Chem. Rev.* **2011**, *111*, 7035-7062

[12] G. Likhtenshtein, in *Stilbenes: Applications in Chemistry, Life Sciences and Materials Science*, Wiley-VCH Verlag GmbH & Co. KGaA, **2009**, pp. 159-188.

[13] a) Y. Wang, Y. Jiang, X. Fan, H. Tan, H. Zeng, Y. Wang, P. Chen, M. Huang, H. Bi, *Toxicol. Lett.* **2015**, *236*, 82-89; b) I. Chrząścik, *Crit. Rev. Anal. Chem.* **2009**, *39*, 70-80; c) G. Likhtenshtein, in *Stilbenes: Applications in Chemistry, Life Sciences and Materials Science*, Wiley-VCH Verlag GmbH & Co. KGaA, **2009**, pp. 189-223.

[14] a) H. Meier, *Angew. Chem. Int. Ed.* **1992**, *31*, 1399-1420; b) D. G. Whitten, *Acc. Chem. Res.* **1993**, *26*, 502-509; c) A. S. Polo, M. K. Itokazu, K. M. Frin, A. O. de Toledo Patrocínio, N. Y. Murakami Iha, *Coord. Chem. Rev.* **2006**, *250*, 1669-1680; d) A. S. Polo, M. K. Itokazu, K. M. Frin, A. O. de Toledo Patrocínio, N. Y. Murakami Iha, *Coord. Chem. Rev.* **2007**, *251*, 255; e) P. Gütlich, Y. Garcia, T. Woike, *Coord. Chem. Rev.* **2001**, *219–221*, 839-879; f) Z. R. Grabowski, K. Rotkiewicz, W. Rettig, *Chem. Rev.* **2003**, *103*, 3899-4032

[15] a) J. Saltiel, Y. P. Sun, in *Photochromism* (Ed.: H. D. Bouas-Laurent), Elsevier Science, Amsterdam, **2003**, pp. 64-164; b) D. H. Waldeck, *Chem. Rev.* **1991**, *91*, 415-436; c) M. Aguiar, L. Akcelrud, M. Pinto, T. Atvars, F. Karasz, J. Saitiel, *J. Photosci.* **2003**, *10*, 149-156

[16] S. Samori, M. Hara, S. Tojo, M. Fujitsuka, T. Majima, *J. Photochem. Photobiol. A* **2006**, *179*, 115-124

[17] a) J. Gierschner, H.-G. Mack, L. Lüer, D. Oelkrug, *J. Chem. Phys.* **2002**, *116*, 8596-8609; b) G. Srinivasan, J. A. Villanueva-Garibay, K. Muller, D. Oelkrug, B. Milian Medina, D. Beljonne, J. Cornil, M. Wykes, L. Viani, J. Gierschner, R. Martinez-Alvarez, M. Jazdzyk, M. Hanack, H. J. Egelhaaf, *Phys. Chem. Chem. Phys.* **2009**, *11*, 4996-5009

[18] J. Gierschner, L. Lüer, B. Milián-Medina, D. Oelkrug, H.-J. Egelhaaf, *J. Phys. Chem. Lett.* **2013**, *4*, 2686-2697

[19] a) J. Gierschner, H. J. Egelhaaf, D. Oelkrug, K. Müllen, *J Fluoresc.* **1998**, *8*, 37-44; b) D. Oelkrug, A. Tompert, J. Gierschner, H.-J. Egelhaaf, M. Hanack, M. Hohloch, E. Steinhuber, *J. Phys. Chem. B* **1998**, *102*, 1902-1907; c) H. J. Egelhaaf, J. Gierschner, D. Oelkrug, *Synth. Met.* **2002**, *127*, 221-227

[20] F. D. Lewis, J.-S. Yang, C. L. Stern, *J. Am. Chem. Soc.* **1996**, *118*, 2772-2773

[21] J. Gierschner, H.-G. Mack, D. Oelkrug, I. Waldner, H. Rau, *J. Phys. Chem. A* **2004**, *108*, 257-263

[22] M. A. Fox, PhD Thesis thesis, University of Durham **1991**.

[23] CrysAlisPro, *A. T. inc.*, **2013**, Yarnton, Oxfordshire, England

[24] L. Palatinus, G. Chapuis, *J. Appl. Crystallogr.* **2007**, *40*, 786-790

[25] SADABSBruker AXS Inc, *G. Sheldrick*, **2012**, Madison, Wisconsin, USA

[26] G. M. Sheldrick, *Acta Crystallogr., Sect. A* **2008**, *64*, 112-122

[27] A. L. Spek, *Acta Crystallogr. Sect. D. Biol. Crystallogr.* **2009**, *65*, 148-155

[28] Gaussian 09, Revision D.01, *M. J. Frisch, G. W. Trucks, H. B. Schlegel, G. E. Scuseria, M. A. Robb, J. R. Cheeseman, G. Scalmani, V. Barone, B. Mennucci, G. A. Petersson, H. Nakatsuji, M. Caricato, X. Li, H. P. Hratchian, A. F. Izmaylov, J. Bloino, G. Zheng, J. L. Sonnenberg, M. Hada, M. Ehara, K. Toyota, R. Fukuda, J. Hasegawa, M. Ishida, T. Nakajima, Y. Honda, O. Kitao, H. Nakai, T. Vreven, J. A. Montgomery Jr., J. E. Peralta, F. Ogliaro, M. J. Bearpark, J. Heyd, E. N. Brothers, K. N. Kudin, V. N. Staroverov, R. Kobayashi, J. Normand, K. Raghavachari, A. P. Rendell, J. C. Burant, S. S. Iyengar, J. Tomasi, M. Cossi, N. Rega, N. J. Millam, M. Klene, J. E. Knox, J. B. Cross, V. Bakken, C. Adamo, J. Jaramillo, R. Gomperts, R. E. Stratmann, O. Yazyev, A. J. Austin, R. Cammi, C. Pomelli, J. W. Ochterski, R. L. Martin, K. Morokuma, V. G. Zakrzewski, G. A. Voth, P. Salvador, J. J. Dannenberg, S. Dapprich, A. D. Daniels, Ö. Farkas, J. B. Foresman, J. V. Ortiz, J. Cioslowski, D. J. Fox*, **2009**, Wallingford, CT, USA

High fluorescent carborane-substituted vinylstilbenes containing octasilsesquioxanes (POSS)

Justo Cabrera-González,[a]# Albert Ferrer-Ugalde,[a] Johannes Gierschner,[b] Santanu Bhattacharyya,[b] Francesc Teixidor,[a] Clara Viñas,[a] Rosario Núñez*[a]

[a] Institut de Ciència de Materials de Barcelona (ICMAB-CSIC), Campus U.A.B., 08193, Bellaterra, Barcelona, Spain. E-mail: rosario@icmab.es

[b] Madrid Institute for Advanced Studies, IMDEA Nanoscience, Calle Faraday 9, Campus Cantoblanco, 28049 Madrid, Spain.

Corresponding Author: Dr. Rosario Núñez, Institut de Ciència de Materials, CSIC, Campus U.A.B., 08193 Bellaterra, Barcelona, Spain. Tel.: +34 93 580 1853. Fax: +34 93 580 5729. rosario@icmab.es

Introduction.

Icosahedral carborane clusters possess unique properties such as three dimensional structure, σ-aromaticity, chemical and photochemical stability, and special electronic properties that make them exceptional candidates for material science.[1] In addition, the carborane clusters are versatile building blocks thermally very stable, and the incorporation of these systems into π-conjugated structures result in materials with extremely high thermal stability.[2] The recent use of carborane clusters in material science has been focused on the development of polymers, boron-rich dendrimers, liquid crystals, nonlinear optics and more recently luminescent materials. During the last few years, different fluorescent molecular systems, in which the carborane is linked to a fluorescent π-conjugated organic systems, to different type of polymers, to fluorophores, among others, have been recently described, and the influence of the cluster on the emission properties studied.[3]

We have earlier reported a set of fluorescent carboranyl decorated polyhedral oligomeric silsesquioxanes that were synthesized using the cross-metathesis of styrene-containing carboranes with vinyl-POSS catalyzed by Grubbs' first generation catalyst.[4] These compounds have shown a remarkable properties, making them excepcional in material science as additives of polymers and ceramics to increase the thermal stability, resistance to oxidation and flame retardant,[5] as well as interesting photoluminescence properties (PL).[6]

Results and Discussion.

Synthesis and characterization of compounds: In this work we report the decoration of a set of silsesquioxanes with carborane-subtituted vinylstilbenes. Following the procedure reported by Laine et at.,[7] octa(p-bromostyrenyl)silsesquioxane (*p*-BrStyrenylOS) serves as core and is functionalized with appropriated carboranyl derivatives via Heck reaction. The starting carboranyl derivatives 1-3 were prepared from *orto*-carborane, methyl-*orto*-carborane and phenyl-*orto*-carborane, respectively, whereas compound 4 was prepared from Ph-*meta*-carborane, following literature procedures (see Scheme 1).[3d, 8] The Heck reactions were carried out in a 1,4-dioxane solution of 1-4 with *p*-BrStyrenylOS using NCy_2Me as a base and $Pd[P(t\text{-}Bu_3)]_2$ and $Pd_2(dba)_3$ as catalysts at 85ºC, leading to the formation of POSS-H, POSS-Me, POSS-Ph and POSS-mPh, respectively. POSS-derivatives were isolated by precipitation with a mixture of THF/methanol without further purification in a 62, 66, 43 and 65 % yield respectively (Scheme 1). The reaction was monitored by ^1H NMR and the complete conversion was confirmed because of the change in the aromatic proton resonance distributions as well as the chemical shif of the peak corresponding to the Si-CH proton (Figure S1).

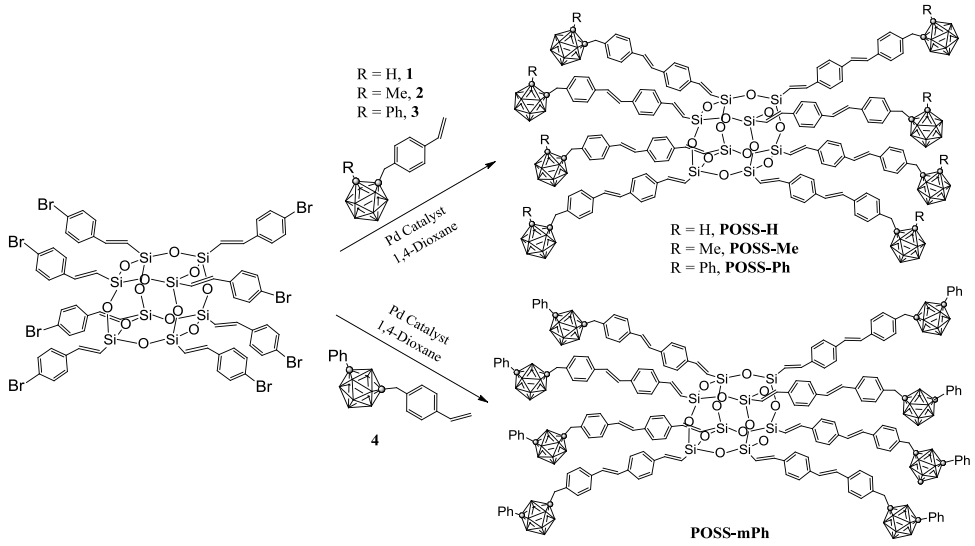

Scheme 1.- Synthesis of carborane-subtituted vinylstilbenes containing POSS.

All the carborane-subtituted vinylstilbenes containing POSS were characterized by ATR-IR, $^{1}H\{^{11}B\}$, $^{13}C\{^{1}H\}$, ^{11}B and $^{11}B\{^{1}H\}$, UV-vis spectroscopy, as well as elemental analysis. The IR spectra for *orto*-derivatives, POSS-H, POSS-Me and POSS-Ph, show the characteristic υ(B-H) strong band around 2580 cm^{-1}, whereas the *meta*-derivative POSS-mPh shows a band at 2594 cm^{-1}. Moreover, for all the compounds a band near 1600 cm^{-1} attributed to the υ(C=C) and the typical broad band between 1000–1200 cm^{-1} due to the Si-O bond were observed. ^{1}H NMR spectra for all the POSS derivatives show aromatic resonances in the region 7.75-6.85 ppm and the C*H*-Si appears as a doublet ($^{2}J_{H-H}$ = 21 Hz) in the region from δ 6.37 to 6.42 ppm, downfield respect to the starting *p*-BrStyrenylOS at 6.27 ppm. In addition, the -CH_2- proton resonances for *orto*-derivatives depend on the second $C_{cluster}$ (C_c) substituent (H, Me or Ph), being shifted to upfield in the case of Ph, which is in agreement with previous results.[3d] Despite the presence of one C_c-Ph group in POSS-mPh, the -CH_2- proton resonance appears shifted to downfield respect to POSS-Ph, since in the former one there is no influence of the ring electronic current on these protons (Figure S1). Aditionally, for POSS-H, the singlet at 3.27 ppm is attributed to the C_c-H proton. The $^{11}B\{^{1}H\}$ NMR spectra of POSS containing Me- or Ph-substituents in the cluster show overlapped boron resonances with a patterns 2:8 or 2:6:2, in the range from δ -3.85 to -12.97 ppm, however for the more asymmetric

unsubstituted *ortho*-carborane containing POSS-H the pattern is 1:1:4:2:2, in the region from δ -2.9 to -13 ppm. The $^{13}C\{^{1}H\}$NMR spectra for all compounds show the aromatic and vinylic resonances between δ 149 and 117 ppm and peaks in the region 40-44 ppm attributed to the -CH_2- methylene C atom. Resonances in the range 74-82 ppm due to the C_c-C, except the resonances attributed to the C_c-H in POSS-H that appear at 59.40 ppm. Elemental analyses have confirmed the structures of POSS compounds (see details in the Experimental Part). Nevertheless, it was not possible to obtain the MALDI-TOF MS spectra for our compounds.

To determine the conformation of the compounds we performed density functional theory (DFT) studies of POSS-H within the D_2 point group, which allows for full conformational freedom for each vinylstilbene-carborane ligand, but at the same time imposes the same conformational environment. Geometry optimization of POSS-H resulted in planar vinylstilbenes with minimized (π–π) interactions between them, see Fig. 1.

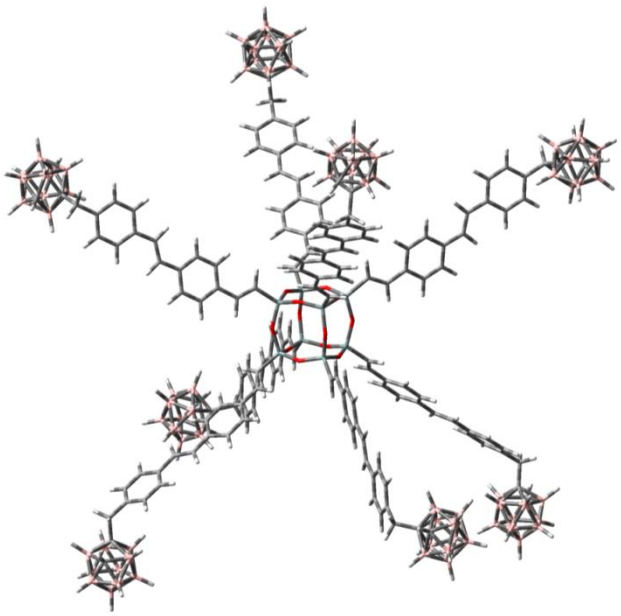

Fig. 1: DFT-optimized structure of POSSH.

UV/Vis Absorption and Fluorescence

All synthesized POSS derivatives show a somewhat vibronically structured UV/Vis absorption spectrum in THF, which peak at 338 nm (3.67 eV; see Fig. 2), very similar to the carborane-free, (p-methyl-stilbene-vinyl)$_8$OVS system in THF reported by Laine.[7] However, while the latter shows an unstructured fluorescence spectrum, the fluorescence of the current compounds is vibronically structured, indicating a rather steep torsional potential hypersurface in the first excited singlet state S_1 compared to the ground state S_0, similar to what was found for the oligomer series of stilbenoid compounds.[9] The fluorescence quantum yield for POSS-H is high with 59% and the (intensity averaged) lifetime of 0.82 ns, from which a radiative rate of 0.65 ns^{-1} is calculated, see Table 1. It is noticeable the increment in the quantum yield in 23 %for POSS-H compared to (p-stilbene-vinyl)$_8$OVS.[10] This is similar to what is expected for vinylstilbene itself,[11] and indicates only small excitonic interactions between the vinylstilbene arms in the complex. According to the TD-DFT calculations, weak H-aggregation is found with a forbidden lowest singlet state (S_1), however separated from the state with highest oscillator strength (3.43 eV, f = 3.45) by only 0.06 eV, so that Herzberg-Teller type coupling should be highly efficient and the emitting state becomes practically allowed in accordance with the experimental results.

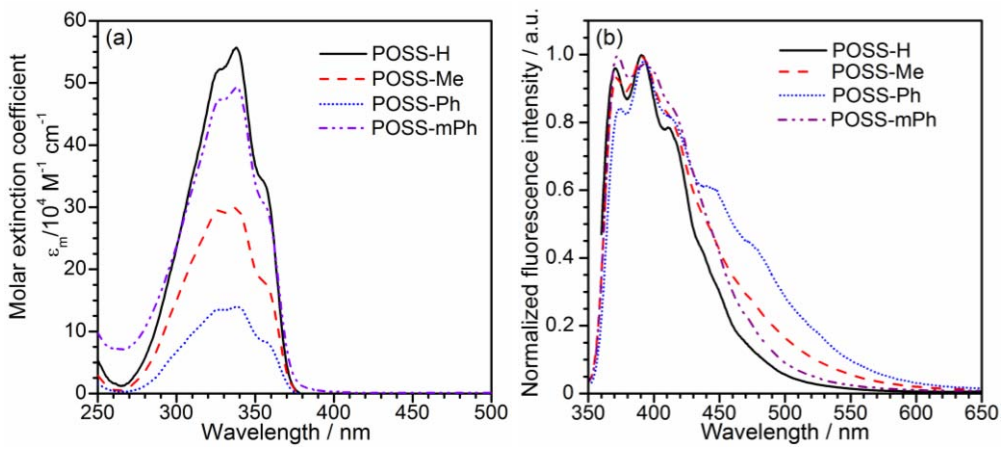

Figure 2: UV/Vis absorption (left) and fluorescence emission (right; excitation wavelength 340 nm) spectra of POSS-H, POSS-Me, POSS-Ph and POSS-mPh in DCM solution

Table 1: PL lifetimes τ_F and quantum yields Φ_F of the compounds in DCM solution; calculated radiative and non-radiative rate constants $k_F = \Phi_F/\tau_F$ and $k_{nr} = (1-\Phi_F)/\tau_F$.

Compound	λ_{abs} (nm)	$\varepsilon_m \cdot 10^{-4}$ ($M^{-1} \cdot cm^{-1}$)	λ_{em} (nm)	Φ_F	τ_F[a] (ns)	k_F (ns^{-1})	k_{nr} (ns^{-1})
POSS-H	338	55.7	391	0.59	0.82	0.65	0.54
POSS-Me	338	29.9	391	0.24	0.80	0.29	0.96
POSS-Ph	338	14.0	392	0.21	0.33	0.64	2.39
POSS-mPh	338	49.3	391	0.36	0.83	0.43	0.77

[a] intensity-average from bi-exponential fit.

Moreover, the UV/Vis absorption and fluorescence were recorded un films for all the compounds (Fig. 3). The UV/Vis spectra exhibit no changes in the maxima peak, at 338 nm, but the maxima of fluorescence emission is redshifted about 54-93 nm compared to DCM solutions with an unstructured fluorescence spectra. In addition, the absolute quantum yields (Φ_{Abs}) were determined in solid state (Table 2) showing an important decreeased, with values in the range 4.3-6.6 %. Although in solid there is an small increase in the τ_F (0.94-1.26 ns) for all POSS, it should be note that the k_F values have decreased dramatically to 0.03-0.06 ns^{-1}. These effects could be attributed to the aggregation in solid and the interactions of aromatics groups between different molecules, responsible of the fluorescence quenching and the redshift of emission as was reported by Laine et *al*. for the equivalent molecule (p-stilbene-vinyl)$_8$OVS without the boron clusters.[10]

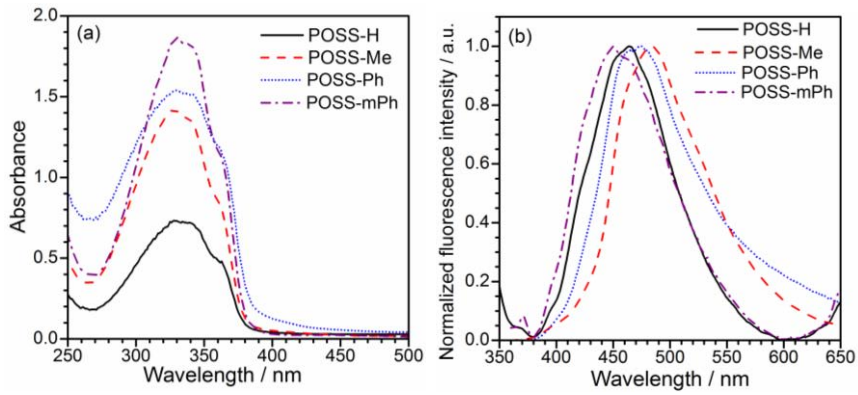

Figure 3: UV/Vis absorption (left) and fluorescence emission (right; excitation wavelength 340 nm) spectra of POSS-H, POSS-Me, POSS-Ph and POSS-mPh in films.

Table 2: PL lifetimes τ_F and quantum yields Φ_F of the compounds in films; calculated radiative and non-radiative rate constants $k_F = \Phi_F/\tau_F$ and $k_{nr} = (1-\Phi_F)/\tau_F$.

Compound	λ_{abs} (nm)	λ_{em} (nm)	Φ_{Abs}	τ_F[a] (ns)	k_F (ns^{-1})	k_{nr} (ns^{-1})
POSS-H	329-339	464	0.066	1.15	0.06	0.81
POSS-Me	329-339	484	0.059	0.94	0.06	1.00
POSS-Ph	329-339	475	0.056	1.15	0.05	0.82
POSS-mPh	329-339	450	0.043	1.26	0.03	0.76

Instrumentation. Elemental analyses were performed using a Carlo Erba EA1108 microanalyzer. ATR-IR spectra were recorded on a high-resolution spectrometer FT-IR PerkinElmer Spectrum One. The ^{1}H NMR (300.13 MHz), $^{11}B\{^{1}H\}$ and ^{11}B NMR (96.29 MHz), $^{13}C\{^{1}H\}$ NMR (75.47 MHz) and $^{29}Si\{^{1}H\}$ NMR (59.62 MHz) spectra were recorded on a Bruker ARX 300 spectrometer. All NMR spectra were recorded in $CDCl_3$ at 25ºC. Chemical shift values for $^{11}B\{^{1}H\}$ NMR spectra were referenced to external $BF_3{\cdot}OEt_2$, and those for ^{1}H and $^{13}C\{^{1}H\}$ NMR were referenced to $SiMe_4$. Chemical shifts are reported in units of parts per million downfield from reference, and all coupling constants are reported in Hertz.

Absorption and photoluminescence (PL) measurements: The UV/Vis absorption spectra were performed in spectroscopic grade THF solution (Sigma-Aldrich) with concentrations ~1.10^{-6} M in normal quartz cuvette having 1 cm path length; giving an absorbance of 0.1-0.2 at the excitation wavelength. Solid state film experiments were performed upon drop casting the THF solutions on quartz surface (thickness having ~100 nm) upon slow solvent evaporation in room temperature. Absorption spectra of both solutions and solid state were measured by a Varian Cary-50 Bio UV/Visible spectrometer after proper base line correction. Fluorescence emission and excitation for both the solution and film were performed by Fluoromax-4 spectrophotometer (Horiba), equipped with a Xenon high pressure lamp source and double monochromators for excitation and emission. The emission and excitation spectra were corrected for the wavelength sensitivity of the PMT, and the excitation source, respectively. For display in the energy scale, the emission spectra were λ^2 corrected for constancy of the integrated area. Fluorescence quantuum yields were determined by relative measurements against quinine sulfate (0.1 M H_2SO_4) with Φ_F = 0.55.

TCSPC measurements: Time resolved fluorescence lifetime measurements for solutions and films were done by the time correlated single photon counting (TCSPC) technique using a using an Acton SP2500 spectrometer, and low dark current photomultiplier (PMA 06, PicoQuant) for detection. A HydraHarp-400

TCSPC event timer with 1 ps time resolution was used to measure the fluorescence decays. The excitation source was a 337 nm NanoLED (PicoQuant, PLS-8-2-651; 0.5 microwatt power; Trigger level 10 MHz at 90 % intensity) with FWHM ~250 ps. The decay time data was fitted after de-convolution with the IRF data by Fluofit software (PicoQuant).

Calculations. Geometries of the ground and relevant electronic excited states of POSS-H were calculated at the (TD)DFT level of theory, imposing the highest non-planar symmetry (D_2), and using the B3LYP functional and 6-311G** basis set as described in the Gaussian 09 program package.[12]

Materials. All reactions were performed under an atmosphere of dinitrogen employing standard Schlenk techniques and 1,4-dioxane was purchased from Merck and distilled from sodium benzophenone previously to use. Commercial grade tetrahydrofurane, methanol were used without further purification. Compounds 1,2-closo-$C_2B_{10}H_{12}$ and 1-CH_3-1,2-closo-$C_2B_{10}H_{11}$ were supplied by Katchem Ltd. (Prague) and used as received. 1-C_6H_5-1,2-closo-$C_2B_{10}H_{11}$, 1-C_6H_5-1,7-closo-$C_2B_{10}H_{11}$, Octa(p-bromostyrenyl)silsesquioxane, compounds 1, 2, 3 and 4 were obtained following the literature procedure.[3d, 7-8, 13] The 4-vinylbenzyl chloride, n-BuLi solution (1.6 M in hexane), 4-Bromostyrene, $Pd_2(dba)_3$ and Pd(t-$Bu_3P)_2$ were purchased from Aldrich and NCy_2Me from Acros.

Synthesis of POSS-H: A 5 mL round-bottomed flask under nitrogen was charged with Octa(*p*-bromostyrenyl)silsesquioxane (50 mg, 0.027 mmol), Pd[P(*t*-Bu_3)]$_2$ (2 mg, 0.004 mmol), $Pd_2(dba)_3$ (2 mg, 0.002 mmol) and 1-[$CH_2C_6H_4$-4'-(CH=CH_2)]-1,2-*closo*-$C_2B_{10}H_{10}$ (1) (83 mg, 0.319 mmol). The solids were dissolved in 2 mL of dry 1,4-Dioxane, followed by the addition of NCy_2Me (0.15 mL, 0.679 mmol) and stirred at 85°C overnight. The reaction mixture was filtered through 1 cm Celite, washed with 10 mL of THF and the solvent was removed under vacuum. The oily residue was dissolved in 1 mL of THF, then 15 mL of CH_3OH was added and the precipitated solid was filtered and washed with 10 mL of CH_3OH giving a yellowish solid identified as POSS-H. Yield: 55 mg, 62%. ^{1}H NMR ($CDCl_3$): δ = 7.53-7.50 (m, 48H, C_6H_4), 7.42 (d, 8H, ^3J(H,H) = 21 Hz, C*H*=CH-Si), 7.15 (d, 16H, ^3J(H,H) = 9 Hz, C_6H_4), 7.13 (s, 16H, Ph-C*H*=C*H*-Ph), 6.38 (d, 8H, ^3J(H,H) = 21 Hz, CH=C*H*-Si), 3.54 (s, CH_2), 3.27 (s, C_c-*H*); ^{1}H{^{11}B} NMR ($CDCl_3$): δ = 7.53-7.50 (m, 48H, C_6H_4), 7.42 (d, 8H, ^3J(H,H) = 21 Hz, C*H*=CH-Si), 7.15 (d, 16H, ^3J(H,H) = 9 Hz, C_6H_4), 7.13 (s, 16H, Ph-C*H*=C*H*-Ph), 6.38 (d, 8H, ^3J(H,H) = 21 Hz, C*H*=CH-Si), 3.54 (s, 16H, CH_2), 3.27 (s, 8H, C_c-*H*), 2.33 (s, 21H, B-*H*), 2.24 (s, 40H, B-*H*), 2.08 (s, 19H, B-*H*); ^{11}B NMR ($CDCl_3$): δ = -2.85 (br, 8B), -5.71 (br, 8B), -9.14 (d, 32B, ^1J(B,H) = 149 Hz), -10.98 (d, 16H, , ^1J(B,H) = 175 Hz), -12.80 (d, 16H, , ^1J(B,H) = 204 Hz); ^{13}C{^{1}H} NMR ($CDCl_3$): δ = 148.75 (s, *C*H=CH-Si), 137.77 (s, =CH-*C*$_6$H$_4$), 137.45 (s, =CH-*C*$_6$H$_4$), 136.94 (s, =CH-*C*$_6$H$_4$), 133.70 (s, -CH_2-*C*$_6$H$_4$), 130.23 (s, *C*$_6$H$_4$), 129.18 (s, *C*H=CH), 128.20 (s, CH=*C*H),

127.45 (s, C_6H_4), 127.09 (s, C_6H_4), 126.93 (s, C_6H_4), 117.43 (s, CH=*C*H-Si), 74.48 (s, C_c-CH_2), 59.40 (s, C_c-H), 43.28 (s, *C*H_2); ATR-IR (cm^{-1}): $\tilde{\upsilon}$ = 2578 (s, B-H st), 1599 (m, C=C st), 1090 (br s, Si-O st); elemental analysis calcd for $C_{152}H_{200}B_{80}O_{12}Si_8$: C 55.18, H 6.09; found: C 55.53, H 6.11.

Synthesis of POSS-Me: The procedure was the same as that for POSS-H; Octa(*p*-bromostyrenyl)silsesquioxane (51 mg, 0.027 mmol), Pd[P(*t*-Bu_3)]$_2$ (2 mg, 0.004 mmol), $Pd_2(dba)_3$ (2 mg, 0.002 mmol), 1-[$CH_2C_6H_4$-4'-($CH=CH_2$)]-2-CH_3-1,2-*closo*-$C_2B_{10}H_{10}$ (2) (90 mg, 0.328 mmol), NCy_2Me (0.1 mL, 0.453 mmol) in 2 mL of 1,4-Dioxane; After workup, POSS-Me was obtained as a yellowish solid. Yield: 62 mg, 66%. ^{1}H NMR ($CDCl_3$): δ = 7.53-7.37 (m, 56H, C_6H_4 and C*H*=CH-Si), 7.20 (d, 16H, ^3J(H,H) = 6 Hz, C_6H_4), 7.14 (s, 16H, Ph-C*H*=C*H*-Ph), 6.37 (d, 8H, ^3J(H,H) = 18 Hz, CH=C*H*-Si), 3.49 (s, 16H, CH_2), 2.19 (s, C_c-CH_3); ^{1}H{^{11}B} NMR ($CDCl_3$): δ = 7.53-7.37 (m, 56H, C_6H_4 and C*H*=CH-Si), 7.20 (d, 16H, ^3J(H,H) = 6 Hz, C_6H_4), 7.14 (s, 16H, Ph-C*H*=C*H*-Ph), 6.37 (d, 8H, ^3J(H,H) = 18 Hz, CH=C*H*-Si), 3.49 (s, 16H, CH_2), 2.30 (s, 20H, B-*H*), 2.23 (s, 20H, B-*H*), 2.19 (s, 24H, C_c-CH_3), 2.11 (s, 40H, B-*H*); ^{11}B NMR ($CDCl_3$): δ = -5.85 (d, 16B, ^1J(B,H) = 155 Hz), -10.48 (d, 64B, ^1J(B,H) = 133 Hz); ^{13}C{^{1}H} NMR ($CDCl_3$): δ = 148.73 (s, *C*H=CH-Si), 137.97 (s, =CH-C_6H_4), 137.04 (s, =CH-C_6H_4), 136.84 (s, =CH-C_6H_4), 134.43 (s, -CH_2-C_6H_4), 130.70 (s, C_6H_4), 128.83 (s, *C*H=CH), 128.44 (s, CH=*C*H), 127.39 (s, C_6H_4), 126.83 (s, C_6H_4), 126.69 (s, C_6H_4), 117.35 (s, CH=*C*H-Si), 74.97 (s, C_c), 41.00 (s, *C*H_2), 23.67 (s, *C*H_3); ATR-IR (cm^{-1}): $\tilde{\upsilon}$ = 2580 (s, B-H st), 1600 (m, C=C st), 1088 (br s, Si-O st); elemental analysis calcd for $C_{160}H_{216}B_{80}O_{12}Si_8 \cdot 1\ H_2O \cdot 0.5\ CHCl_3$: C 55.10, H 6.25; found: C 55.05, H 6.26.

Synthesis of POSS-Ph: The procedure was the same as that for POSS-H; Octa(*p*-bromostyrenyl)silsesquioxane (50 mg, 0.027 mmol), Pd[P(*t*-Bu_3)]$_2$ (2 mg, 0.004 mmol), $Pd_2(dba)_3$ (2 mg, 0.002 mmol), 1-[$CH_2C_6H_4$-4'-($CH=CH_2$)]-2-C_6H_5-1,2-*closo*-$C_2B_{10}H_{10}$ (3) (108 mg, 0.321 mmol), NCy_2Me (0.1 mL, 0.453 mmol) in 2 mL of 1,4-Dioxane; After workup, POSS-Ph was obtained as a yellowish solid. Yield: 45 mg, 43%. ^{1}H NMR ($CDCl_3$): δ = 7.75 (d, 16H, ^3J(H,H) = 6 Hz, C_6H_5), 7.54-7.46 (m, 56H, C_6H_4 and C*H*=CH-Si), 7.43 (t, 24H, ^3J(H,H) = 9 Hz, C_6H_5), 7.12 (s, 16H, Ph-C*H*=C*H*-Ph), 6.85 (d, 16H, ^3J(H,H) = 6 Hz, C_6H_4), 6.42 (d, 8H, ^3J(H,H) = 18 Hz, CH=C*H*-Si), 3.13 (s, CH_2); ^{1}H{^{11}B} NMR ($CDCl_3$): δ = 7.76 (d, 16H, ^3J(H,H) = 9 Hz, C_6H_5), 7.54-7.46 (m, 56H, C_6H_4 and C*H*=CH-Si), 7.43 (t, 24H, ^3J(H,H) = 9 Hz, C_6H_5), 7.12 (s, 16H, Ph-C*H*=C*H*-Ph), 6.85 (d, 16H, ^3J(H,H) = 6 Hz, C_6H_4), 6.42 (d, 8H, ^3J(H,H) = 18 Hz, CH=C*H*-Si), 3.13 (s, 16H, CH_2), 2.78 (s, 20H, B-*H*), 2.46 (s, 25H, B-*H*), 2.29 (s, 35H, B-*H*); ^{11}B NMR ($CDCl_3$): δ = -3.87 (d, 16B, ^1J(B,H) = 136 Hz), -10.16 (d, 64B, ^1J(B,H) = 81 Hz); ^{13}C{^{1}H} NMR ($CDCl_3$): δ = 148.84 (s, *C*H=CH-Si), 137.94 (s, C_c-C_6H_5), 136.79 (s, =CH-C_6H_4), 136.79 (s, =CH-C_6H_4), 136.79 (s, =CH-C_6H_4), 134.72 (s, -CH_2-C_6H_4), 131.53 (s, C_c-C_6H_5), 130.94 (s, CH=*C*H), 130.85 (s, C_c-C_6H_5), 130.47 (s, C_6H_4), 129.12 (s, C_c-C_6H_5), 128.65 (s, *C*H=CH), 127.44 (s, C_6H_4), 126.86 (s, C_6H_4), 126.51 (s, C_6H_4), 117.28 (s, CH=*C*H-Si), 83.79 (s, C_c-C_6H_5), 82.06 (s, C_c-CH_2), 40.74 (s, *C*H_2); ATR-IR (cm^{-1}): $\tilde{\upsilon}$ =

2579 (s, B-H st), 1599 (m, C=C st), 1087 (br s, Si-O st); elemental analysis calcd for $C_{160}H_{216}B_{80}O_{12}Si_8 \cdot 1\ H_2O \cdot 0.5\ CHCl_3$: C 59.67, H 5.83; found: C 59.69, H 5.82.

Synthesis of POSS-mPh: The procedure was the same as that for POSS-H; Octa(*p*-bromostyrenyl)silsesquioxane (33 mg, 0.018 mmol), $Pd[P(t\text{-}Bu_3)]_2$ (2 mg, 0.004 mmol), $Pd_2(dba)_3$ (2 mg, 0.002 mmol), 1-$[CH_2C_6H_4$-4'-$(CH{=}CH_2)]$-7-C_6H_5-1,2-*closo*-$C_2B_{10}H_{10}$ (4) (57 mg, 0.170 mmol), NCy_2Me (0.1 mL, 0.453 mmol) in 2 mL of 1,4-Dioxane; After workup, POSS-mPh was obtained as a yellowish solid. Yield: 45 mg, 65%. ^{1}H NMR ($CDCl_3$): δ = 7.53-7.45 (m, 48H, C_6H_4), 7.39-7.36 (d, 32H, ^3J(H,H) = 9 Hz, C_6H_4 and C_6H_5), 7.26-7.21 (m, 32H, and C*H*=CH-Si and C_6H_5), 7.13 (s, 16H, Ph-C*H*=C*H*-Ph), 6.37 (d, 8H, ^3J(H,H) = 18 Hz, C*H*=CH-Si), 3.29 (s, CH_2); ^{1}H{^{11}B} NMR ($CDCl_3$): δ =7.53-7.45 (m, 48H, C_6H_4), 7.39-7.36 (d, 32H, ^3J(H,H) = 9 Hz, C_6H_4 and C_6H_5), 7.26-7.21 (m, 32H, and C*H*=CH-Si and C_6H_5), 7.13 (s, 16H, Ph-C*H*=C*H*-Ph), 6.37 (d, 8H, ^3J(H,H) = 18 Hz, C*H*=CH-Si), 3.29 (s, 16H, CH_2), 2.92 (s, 16H, B-*H*), 2.51 (s, 24H, B-*H*), 2.33 (s, 24H, B-*H*), 2.20 (s, 16H, B-*H*); ^{11}B NMR ($CDCl_3$): δ = -6.11 (br, 16B), -10.76 (d, 48B, ^1J(B,H) = 141 Hz), -12.97 (br, 16B); ^{13}C{^{1}H} NMR ($CDCl_3$): δ = 148.71 (s, *C*H=CH-Si), 136.74 (s, C_c-C_6H_5), 136.53 (s, =CH-C_6H_4), 136.47 (s, =CH-C_6H_4), 136.47 (s, =CH-C_6H_4), 135.26 (s, -CH_2-C_6H_4), 130.28 (s, C_c-C_6H_5), 128.57 (s, C_c-C_6H_5), 128.44 (s, C_c-C_6H_5), 128.27 (s, C_6H_4), 127.78 (s, C_c-C_6H_5), 127.39 (s, *C*H=CH), 127.39 (s, *C*H=CH), 126.78 (s, C_6H_4), 126.63 (s, C_6H_4), 117.28 (s, CH=*C*H-Si), 42.94 (s, *C*H_2); ATR-IR (cm^{-1}): $\tilde{\nu}$ = 2594 (s, B-H st), 1599 (m, C=C st), 1091 (br s, Si-O st); elemental analysis calcd for $C_{160}H_{216}B_{80}O_{12}Si_8$: C 61.32, H 5.97; found: C 61.31, H 5.94.

References

[1] a) R. N. Grimes, *Dalton Trans.* **2015**, *44*, 5939-5956; b) F. Teixidor, C. Viñas, A. Demonceau, R. Nunez, *Pure Appl. Chem.* **2003**, *75*, 1305-1314; c) R. N. Grimes, *Carboranes (Second Edition)*, Academic Press, Oxford, **2011**.

[2] A. González-Campo, B. Boury, F. Teixidor, R. Núñez, *Chem. Mater.* **2006**, *18*, 4344-4353

[3] a) P. A. Jelliss, in *Boron Science: New Technologies and Applications* (Ed.: N. S. Hosmane), Taylor & Francis, **2012**, p. 355; b) F. Lerouge, C. Viñas, F. Teixidor, R. Núñez, A. Abreu, E. Xochitiotzi, R. Santillan, N. Farfán, *Dalton Trans.* **2007**, 1898-1903; c) F. Lerouge, A. Ferrer-Ugalde, C. Viñas, F. Teixidor, R. Sillanpaa, A. Abreu, E. Xochitiotzi, N. Farfan, R. Santillan, R. Nuñez, *Dalton Trans.* **2011**, *40*, 7541-7550; d) A. Ferrer-Ugalde, E. J. Juárez-Pérez, F. Teixidor, C. Viñas, R. Sillanpää, E. Pérez-Inestrosa, R. Núñez, *Chem. Eur. J.* **2012**, *18*, 544-553; e) L. Weber, J. Kahlert, R. Brockhinke, L. Böhling, A. Brockhinke, H.-G. Stammler, B. Neumann, R. A. Harder, M. A. Fox, *Chem. Eur. J.* **2012**, *18*, 8347-8357; f) S.-Y. Kim, Y.-J. Cho, G. F. Jin, W.-S. Han, H.-J. Son, D. W. Cho, S. O. Kang, *Phys. Chem. Chem. Phys.* **2015**, *17*, 15679-15682

[4] A. Ferrer-Ugalde, E. J. Juárez-Pérez, F. Teixidor, C. Viñas, R. Núñez, *Chem. Eur. J.* **2013**, *19*, 17021-17030

[5] a) S. Huang, Z. Qiu, *Ind. Eng. Chem. Res.* **2014**, *53*, 15296-15300; b) Y. R. Liu, Y. D. Huang, L. Liu, *Polym. Degrad. Stab.* **2006**, *91*, 2731-2738; c) W.-C. Liu, Y.-Y. Yu, W.-C. Chen, *J. Appl. Polym. Sci.*

2004, *91*, 2653-2660; d) L. Matějka, A. Strachota, J. Pleštil, P. Whelan, M. Steinhart, M. Šlouf, *Macromolecules* **2004**, *37*, 9449-9456; e) S. A. Pellice, D. P. Fasce, R. J. J. Williams, *J. Polym. Sci., Part B: Polym. Phys.* **2003**, *41*, 1451-1461; f) Z. Zhou, L. Cui, Y. Zhang, Y. Zhang, N. Yin, *Eur. Polym. J.* **2008**, *44*, 3057-3066; g) P. D. Aids, p. www.youtube.com/watch?v=kIHgrLFNmGQ.

[6] a) M. Bahrami, J. C. Furgal, H. Hashemi, M. Ehsani, Y. Jahani, T. Goodson, J. Kieffer, R. M. Laine, *J. Phys. Chem. C* **2015**, *119*, 15846-15858; b) T. Maegawa, O. Miyashita, Y. Irie, H. Imoto, K. Naka, *RSC Advances* **2016**, *6*, 31751-31757

[7] S. Sulaiman, A. Bhaskar, J. Zhang, R. Guda, T. Goodson, R. M. Laine, *Chem. Mater.* **2008**, *20*, 5563-5573

[8] A. d. H. c. l. d. Málaga,

[9] J. Gierschner, H.-G. Mack, L. Lüer, D. Oelkrug, *J. Chem. Phys.* **2002**, *116*, 8596-8609

[10] J. C. Furgal, J. H. Jung, T. Goodson, R. M. Laine, *J. Am. Chem. Soc.* **2013**, *135*, 12259-12269

[11] H. J. Egelhaaf, J. Gierschner, D. Oelkrug, *Synth. Met.* **1996**, *83*, 221-226

[12] Gaussian 09, Revision D.01, *M. J. Frisch, G. W. Trucks, H. B. Schlegel, G. E. Scuseria, M. A. Robb, J. R. Cheeseman, G. Scalmani, V. Barone, B. Mennucci, G. A. Petersson, H. Nakatsuji, M. Caricato, X. Li, H. P. Hratchian, A. F. Izmaylov, J. Bloino, G. Zheng, J. L. Sonnenberg, M. Hada, M. Ehara, K. Toyota, R. Fukuda, J. Hasegawa, M. Ishida, T. Nakajima, Y. Honda, O. Kitao, H. Nakai, T. Vreven, J. A. Montgomery Jr., J. E. Peralta, F. Ogliaro, M. J. Bearpark, J. Heyd, E. N. Brothers, K. N. Kudin, V. N. Staroverov, R. Kobayashi, J. Normand, K. Raghavachari, A. P. Rendell, J. C. Burant, S. S. Iyengar, J. Tomasi, M. Cossi, N. Rega, N. J. Millam, M. Klene, J. E. Knox, J. B. Cross, V. Bakken, C. Adamo, J. Jaramillo, R. Gomperts, R. E. Stratmann, O. Yazyev, A. J. Austin, R. Cammi, C. Pomelli, J. W. Ochterski, R. L. Martin, K. Morokuma, V. G. Zakrzewski, G. A. Voth, P. Salvador, J. J. Dannenberg, S. Dapprich, A. D. Daniels, Ö. Farkas, J. B. Foresman, J. V. Ortiz, J. Cioslowski, D. J. Fox*, **2009**, Wallingford, CT, USA

[13] a) P. T. Brain, J. Cowie, D. J. Donohoe, D. Hnyk, D. W. H. Rankin, D. Reed, B. D. Reid, H. E. Robertson, A. J. Welch, M. Hofmann, P. v. R. Schleyer, *Inorg. Chem.* **1996**, *35*, 1701-1708; b) M. F. Hawthorne, D. C. Young, P. M. Garrett, D. A. Owen, S. G. Schwerin, F. N. Tebbe, P. A. Wegner, *J. Am. Chem. Soc.* **1968**, *90*, 862-868

Redox active metallacarborane-decorated octasilsesquioxanes. Electrochemical and thermal properties.

Justo Cabrera-González,[1] Victor Sánchez-Arderiu,[1] Clara Viñas,[1] Teodor Parella,[2] Francesc Teixidor,[1] and Rosario Núñez[1]*

1. Institut de Ciència de Materials de Barcelona (ICMAB-CSIC), Campus de la UAB, 08193, Bellaterra (Barcelona), Spain, Fax:+34-93-5805729. E-mail:rosario@icmab.es

2. Servei de Ressonància Magnètica Nuclear, Universitat Autònoma de Barcelona, E-08193 Bellaterra, Barcelona, Spain

Corresponding Author: Dr. Rosario Núñez, Institut de Ciència de Materials, CSIC, Campus U.A.B., 08193 Bellaterra, Barcelona, Spain. Tel.: +34 93 580 1853. Fax: +34 93 580 5729. rosario@icmab.es

Introduction.

Polyhedral octasilsesquioxanes (POSS) are well-known molecules that consist of a cubic array with eight Si atoms at the vertices bridging oxygen atoms at the edges. The inorganic core of these POSS cages provides mechanical stiffness and thermal stability, whereas the organic pendants provide solubility in organic solvents and an enhancement in thermal stability, mechanical, optical, electrical or electronic properties.[1] All these properties make these molecules promising building blocks for a broad range of hybrid nanomaterials for technological applications.[2] Octasilsesquioxanes have been used as scaffolds for the development of catalysts, dendrimers, OLED diveces, hydrogen storage materials, biocompatible materials, encapsulants for drug delivery, among others.[1,3] As a particular case, the cubic octasilsesquioxane have been used as a core molecule to hold electroactive ferrocenyl units.[4]

Metallacarboranes $[M(C_2B_9H_{11})_2]^-$ are sandwich type compounds in which a central metal ion, commonly Co or Fe, are bonded η^5 to two dicarbollide anions $[C_2B_9H_{11}]^{2-}$.[5] These compounds present high thermal and chemical stability,[6] as well as a peculiar electrochemical behavior. Cobaltabisdicarbollide present three reversible waves under cyclic voltammetry conditions, at -2.64 V for the $Co^{2+/+}$ redox couple, at -1.74 V for $Co^{3+/2+}$ and 1.22 V for $Co^{4+/3+}$ (all values are given vs Fc). The most studied and easy to observe is the $Co^{3+/2+}$ redox couple.[7] Moreover, for the Ferrabisdicarbollide, only one redox wave is observed at -0.78 V vs Fc and corresponds to the transition $Fe^{3+/2+}$. The study on the redox properties of these compounds has been focused on the possible stepwise tuning of the redox value upon dehydrohalogenation of the metallacarboranes.[8] It has been shown that the redox potential of cobaltabisdicarbollide shifts to more anodic potentials with the octaiododerivative from the initial -1.74 V to -0.74 V vs. Fc.[9] The same behavior has been observed for its Fe analog.[10]

Nevertheless, to the best of our knowledge, the investigation of the behavior of octasilsesquioxanes functionalized with redox-active metallacarborane clusters has not been yet explored. Due to their unique photo-physical, thermal and redox properties of metallacarborane and pursuing our work dealing with the development of new materials containing metallacarborane moieties, we report herein the synthesis and complete characterization of two metallacarborane-terminated octasilsesquioxane cages. Molecular sizes for this kind of dendrimers were estimated before and after incorporation of carborane clusters from their hydrodynamic radii (R_H) that were determined using translational diffusion coefficients (D) from DOSY NMR experiments. We study the influence of these boron cluster anions on the thermal properties of POSS systems, as well as the redox behavior and electronic interactions between metallacarborane units attached to the corners of the silsesquioxane core.

Results and Discussion.

Synthesis and characterization: Here we report the decoration of octavinylsilsesquioxane (OVS) with metallacarborane derivatives via cross-metathesis reaction. For this purpose we have synthesized new cosane and fesane derivatives

bearing a terminal styrene group, which is an appropriate group to react by cross-metathesis with the vinyl functions from OVS. Starting from the zwitterionic boron clusters [3,3'-Co(8-$C_4H_8O_2$-1,2-$C_2B_9H_{10}$)(1',2'-$C_2B_9H_{11}$)] and [3,3'-Fe(8-$C_4H_8O_2$-1,2-$C_2B_9H_{10}$)(1',2'-$C_2B_9H_{11}$)], the nucleophilic oxonium ring-opening reaction was conducted[11] using 4-vinylphenol as a nucleophilic precursor. The presence of K_2CO_3 in refluxing acetonitrile causes the 4-vinylphenol deprotonation and the corresponding alkoxide reacts *in situ* with oxonium derivatives under inert conditions. The ring-opening reaction was monitored by ^{11}B NMR spectroscopy by comparison with their parent species.[12] After the completion, the solvent was removed and the final compounds were precipitated as tetramethylammonium salts to isolate **1** in 98.5 % yield; however further purification by a preparative silica plate with dichlorometane was necessary to obtain **2** in 32 % yield (Scheme 1.A).

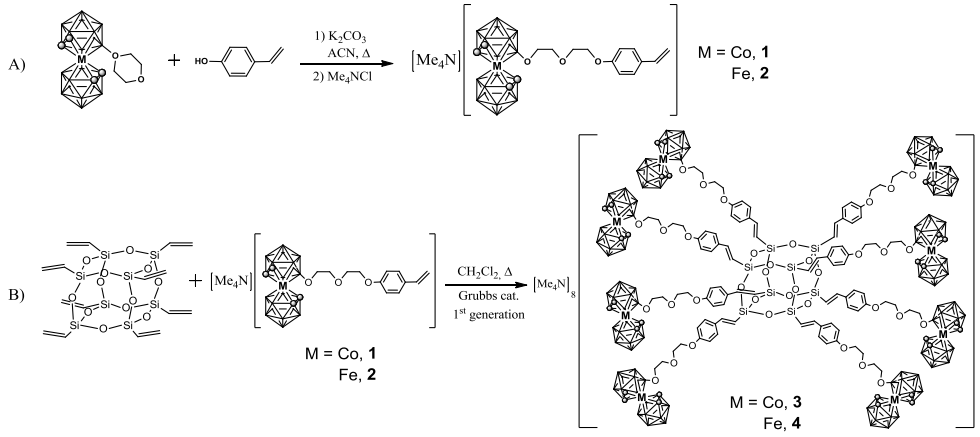

Scheme 1. A) Synthesis of metallacarborane derivatives 1 and 2. B) Cross- metathesis reactions to obtain 3 and 4.

Cross-metathesis reactions of 1 and 2 with OVS were carried out using a first generation Grubbs catalyst,[13] in CH_2Cl_2 at reflux for 60 h and around 15 % of excess of 1 and 2 to ensure the complete functionalization. The regio- and stereoselectivity *E*-isomers of metallacarborane-containing POSS 3 and 4 were obtained in 83 % and 45 % yield, respectively (Scheme 1.B). These results are in agreement with previous reported

works.[14] The cross-metathesis reactions were monitored by ^{1}H NMR to determine the total functionalization of OVS upon the disappearance of the vinyl proton resonance from Si-CH=CH_2 (Figure S1 in the SI).

The structures of compounds 1-4 were established by IR, NMR (1D ^{1}H, 1D $^{13}C\{^{1}H\}$ and 1D $^{11}B\{^{1}H\}$) and elemental analysis, whereas MALDI-TOF was possible only for the compounds 1 and 2 (see SI). The IR spectra for all compounds show the typical υ(B-H) strong bands around 2530 cm^{-1} as well as υ(C=C) stretching bands near 1605 cm^{-1}. Additionally, for metallacarborane-containing POSS 3 and 4 characteristic broad bands between 1090 and 1100 cm^{-1} due to the vibration frequency of the Si-O bond are presented. The ^{1}H NMR spectra of cosane derivatives 1 and 3 show resonances in the region 7.0.-7.5 ppm attributed to the aromatic protons, whereas the CH_2-O resonances appear in the range from δ 3.5 to 4.5 ppm. For 1 the C*H*=CH_2 protons are observed in the range 6.70-5.10 ppm as set of three resonances, two doublets and one doublet of doublets, whereas for 3 the C*H*=C*H* resonances appear as two doublets at 7.41 and 6.29 ppm with a 18 Hz *trans* coupling constant. Compounds 2 and 4 exhibit appreciable paramagnetic shifts of signals, especially for those protons closer to the Fe(III) that appear as a very broad signal in the range between -15 and +80 ppm. Aromatic and olefinic resonances appear in the region 5.3-7.0 ppm and the CH_2-O protons between δ +2.40 and -10.40 ppm. Despite a difficult assignment for 2 it is possible to identify the set of three resonances attributed to C*H*=CH_2 protons in the range 6.45-4.98 ppm, whereas for 4 one the C*H*=CH proton is overlapped with the aromatic resonances. The $^{11}B\{^{1}H\}$ NMR for cosane derivatives 1 and 3 show identical 1:1:1:1:2:2:4:2:2:1:1 patterns, from +25- to -28 ppm, including the resonance at lowest field from B(8) substituted boron atom (B-O) that remains as a singlet in the ^{11}B NMR. [15] Although ^{11}B NMR resonance assignment is difficult because of the paramagnetic effect of Fe(III), compounds 2 and 4 show similar patterns in the region between +118 and -468 ppm, which is in agreement with reported studies of oxonium fesane derivatives.[16] The $^{13}C\{^{1}H\}$NMR spectra show resonances in the aromatic and vinylic region from 160 to 110 ppm for all compounds, albeit the ether groups resonances (-O*C*H_2-) for 1 and 3 appear in the range 72-63 ppm and for 2 and 4 are observed between 63 and -0.22 ppm

because of their nearness to Fe(III). The MALDI-TOF mass spectra were recorded in the negative-ion mode for monomers 1 and 3.

Experimental diffusion coefficients and estimated hydrodynamic radius. Additionally, self-translation Diffusion coefficient and the corresponding hydrodynamic radii of starting compounds and dendrimers **3-4** were determined by pulsed field gradient spin-echo NMR in dilute CD_3CN solutions (concentration ca 10^{-2}M-10^{-3}M) at 298K (Table 1). As a reference, we have measured D for the starting OVS and cosane. Unfortunately, the large broad signals observed in the ^{1}H NMR spectrum of the fesane derivative prevents the measurement of D, but it is expected to be of the same order than cosane (hydrodynamic ratio about 4.1 Å) because it is expected that the different nature of the metal would not change the overall molecular size. The R_H determined for OVS (5.49 Å) is in good agreement with the previously reported for the crystal structure (5.66 Å).[17] The intermediate compounds **1** and **2** show similar sizes than OVS about 5-5.5Å, as predicted by their similar molecular weights. Expectedly, compound **3** and **4** show a considerable increase of its molecular size in the same range up to 16.2-17.0 Å. This result also confirms that compounds **1** and **2** have been coupled to OVS, to give the respective 3 and 4 with a similar level of functionalization.

Table 1: Experimental Diffusion coefficients and estimated hydrodynamic radius of dendrimers 1-4.

Compound	Molecular Weight	Diffusion Coefficient (D, m^2/s)	Hydrodynamic Radii (Å)
OVS	632.8	$1.148 \cdot 10^{-9}$	5,49
cosane	456.67	$1.549 \cdot 10^{-9}$	4,07
fesane	453.58	-	-
compound 1	604.13	$1.175 \cdot 10^{-9}$	5,37
compound 2	601	$1.259 \cdot 10^{-9}$	5,01
compound 3	5241.7	$3.89 \cdot 10^{-10}$	16,2
compound 4	5217	$3.72 \cdot 10^{-10}$	17,0

UV-Vis Spectroscopic: Figure 1 shows the UV-Vis spectra in acetonitrile for **1-4**. In order to perform an adequate comparison of the parameters of the different UV-Vis spectra, a line-fitting analysis with gausssians was performed in a similar manner to that reported earlier by our group.[18] The results obtained are shown in Table 2. All the UV-Vis spectra show three absorption bands, the first one in the region 260-275 nm, a second band between 304 and 314 nm, and the third one of lower intensity between 357 and 369 nm (Figure 1). The first maximum at 260 nm for monomers **1-3** is red-shifted 15 nm in functionalized cages **3-4** that appears to around 275 nm, which is mainly attributed to the presence of the styrene group but also with contribution of the metallacarborane cluster. The second and third maxima around 304-314 nm and 369-372 nm, are attributed to metallacarborane units substituted with -O-$(CH_2)_2$-O-$(CH_2)_2$-B(8) chain, such as have been previously described for cobaltabisdicarbollide derivatives reported by our group.[15] **¡Error! Marcador no definido.**To estimate the number of metallacarborane moieties in our molecules, and confirm the total functionalization of the OVS, we have used the method developed by Kim *et al*.[19] and previously used for us.[20] To this purpose, we have used absorption bands exhibited in the range 304-314 nm, which follow the Lambert-Beer low. The number of metallacarborane fragments for **2** and **4** have been estimated by comparing the molar extinction coefficients (ε) of them with those obtained for the respective monomers **1** and **3** (ε_0). Table 1 collects the molar extinction coefficients (ε) obtained for **1-4** at 304-314 and the calculated number of metallacarborane units using the Lambert-Beer law at 312 nm. As it was expected the number of metallacarborane units (cosane and fesane) fits very well with the theoretical ones, corroborating the complete functionalization of starting OVS (Table 2). The graphic in Figure S3-S6 shows the correlation between the number of metallacarboranes and the absorbance at the same concentration for the reported compounds.

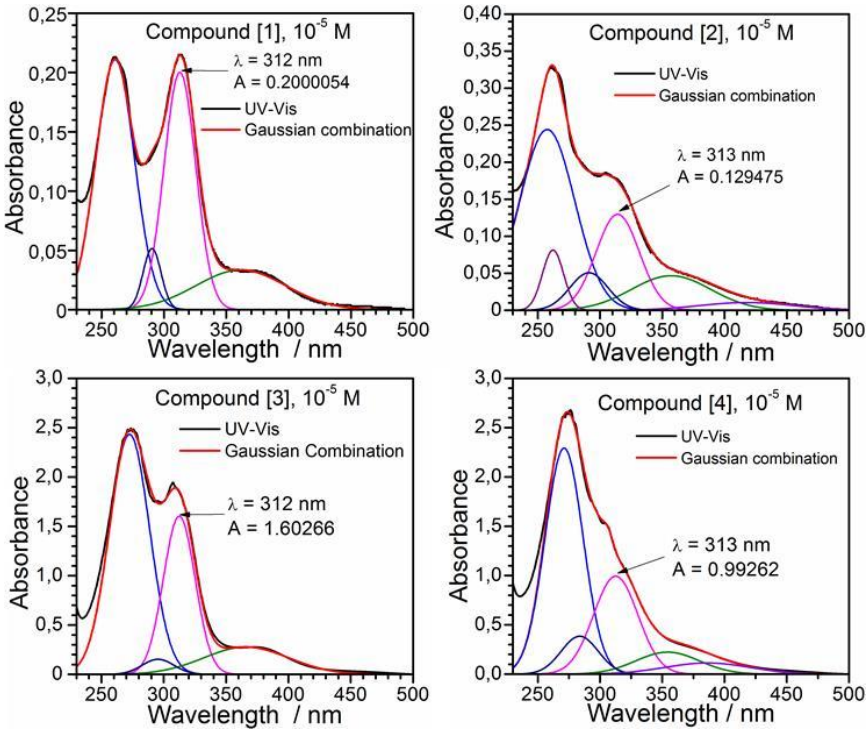

Figure 1. UV-vis spectra of compounds **1**-**4** at 10^{-5} M in acetonitrile and the results of line fitting with gaussians.

Table 2. UV-Vis Spectroscopic Data and Number of Metallacarborane Units Calculated Using the Lambert-Beer Law.

Compound	λ (ε)[a]	theoretical no. of metallacarboranes	λ (ε)[b]	Calculated number metallacarboranes
1	260 (21.6) 314 (21.4)	1	312 (ε_0 = 20.0)	-
2	260 (30.1) 306 (17.6)	1	313 (ε_0 = 12.9)	-
3	273 (25.1) 307 (19.4)	8	312 (160.3)	$\varepsilon/\varepsilon_0$ = 8.02
4	275 (26.4) 304 (15.2)	8	313 (99.3)	$\varepsilon/\varepsilon_0$ = 7.69

[a] λ [nm] and ε [10^{-3} dm^3 mol^{-1} cm^{-1}] experimental values.

[b] λ [nm] and ε [10^{-3} dm^3 mol^{-1} cm^{-1}] calculated values.

Electrochemical study. Cyclic Voltammetries were measured for compounds **1-4** (Figure 2) in previously dried and degassed acetonitrile using a three electrode set up. As it can be observed, compounds **1** and **3** appear at the same redox potential, near -1.74 V *vs*. Fc, that is the redox potential of the pair $Co^{2+/3+}$ in the cobaltabisdicarbollide.[7] The same behavior is observed for compounds **2** and **4** that show a redox potential around -0.74 V *vs*. Fc, similar to the one determined for $Fe^{2+/3+}$ couple in the ferrabisdicarbollide.

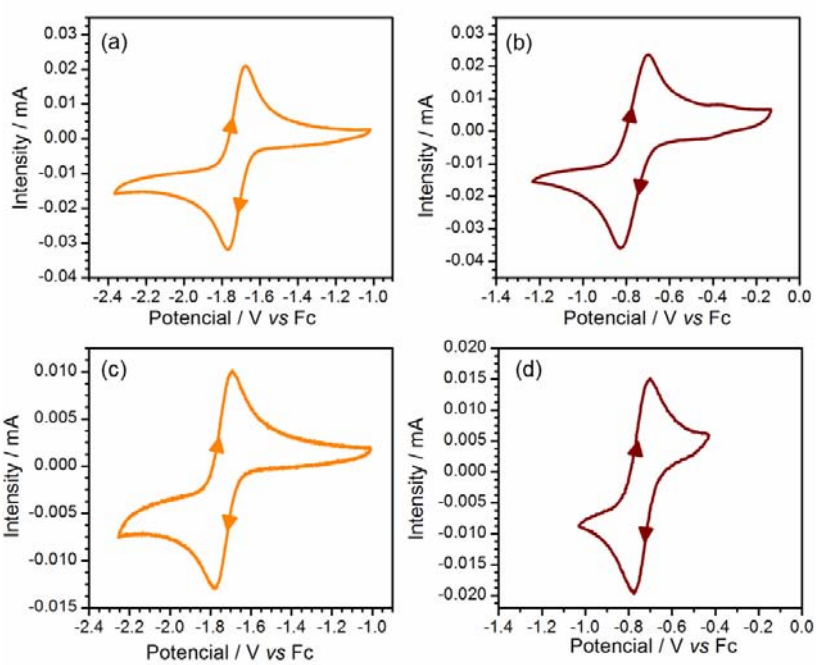

Figure 2. CVs of compounds **1-4**, on the left the CVs of the cobalt derivatives, a) CV of **1** and c) CV of **3**, on the right, CVs of the iron derivatives, b) CV of **2** and d) CV of **4**. All compounds were measured in acetonitrile at 300 mV/s and referenced internally to Fc.

For compounds **3** and **4**, that contain eight metallacarborane units, only one redox wave was observed in the CV, indicating that all units acts independently and there is no connection between them through the octasilsesquioxane cage. A similar behaviour was already observed for octasilsesquioxanes functionalized with eight ferrocenes.[21]

After analyzing the CVs, we wondered if the CV technique is adequate to corroborate the degree of functionalization of dendrimers, such as it is the UV-vis spectroscopy. For

this purpose, the diffusion coefficient of **1-4** were determined by the Randles-Sevcik equation (1) that relates the maximum peak current with the square root of the diffusion coefficient (Table 3). Thus, CVs at different scan rate were performed and the maximum peak current were plotted vs. the square root of the scan rate (Figure SI-**X**), from the slope, the diffusion coefficient can be calculated assuming that n = 1 for compounds **1** and **2** whilst n = 8 for compounds **3** and **4** that have eight metallacarborane units in the periphery, being n the number of electrons involved in the redox reaction.

$$i_p = 0.4463\, n\, F\, A\, C \left(\frac{n\, F\, v\, D}{RT}\right)^{\frac{1}{2}} \qquad (1)$$

The results for the diffusion coefficients obtained by DOSY-NMR and by CV are summarized in table 3.

Compound	D_{NMR} (cm^2/s)	D_{CV} (cm^2/s)
1	$1.175 \cdot 10^{-5}$	$4.75 \cdot 10^{-6}$
2	$1.259 \cdot 10^{-5}$	$4.29 \cdot 10^{-6}$
3	$3.89 \cdot 10^{-6}$	$1.04 \cdot 10^{-7}$
4	$3.72 \cdot 10^{-6}$	$9.64 \cdot 10^{-8}$

From Table 3 it is notice that the diffusion coefficients measured by CV are smaller compared with those determined by NMR. For compound **1** and **2** this difference in the diffusion coefficient is between 2.5 and 3 times smaller in CV, whereas for compounds **3** and **4**, the difference is between 37 and 39 times smaller in CV. This difference could be due to the presence of the inert electrolyte that modifies the viscosity of the medium in CV, making it more viscous and thus making more difficult the diffusion of the analyte from the bulk of the solution to the surface of the electrode. Kaifer *et al* described a methodology to relate the D_{NMR} and D_{CV} in dendrimers functionalized with Fc.[22] However the molecules presented here larger than those used in that method.

Moreover, in our case the dendrimers are anionic and another important different between Fc and metallacarboranes is their special interactions with other molecules.[23] For these reasons, the presence of electrolyte in CV experiments and its interaction with metallacarboranes have altered the D_{CV} value more than the theoretically expected by Kaifer's method. Regarding the good determination of the R_H by DOSY-NMR, we assume the D_{NMR} value as the correct one, since there is no electrolyte effect.

Regarding the single reversible redox wave for each dendrimer at the same potential as that of the corresponding metallacarborane, and considering that **3** (16.2 Å) and **4** (17.0 Å) are small enough to succeed a redox process in the 8 peripheral units,[24] we conclude that for 1 molecule of **3** or **4**, 8 electrons are involve in the electrochemical mechanism (n = 8).

To confirm that is possible to reduce the 8 metallacarboranes in these compounds, we performed a chemical reduction by adding 8 equivalents of sodium naphthalenide to a 3 mg solution of **4** in THF, appearing a pinky solid in a few seconds (inset Figure 3). The ^{11}B NMR of the reduced compound **4**, confirm that all ferrabisdicarbollide units have become diamagnetic (Figure 3), appearing all the new resonances from 19 to -38 ppm. In addition, the signal at δ 18.30 ppm is identified in the typical region for *B*-O in diamagnetic boron clusters.

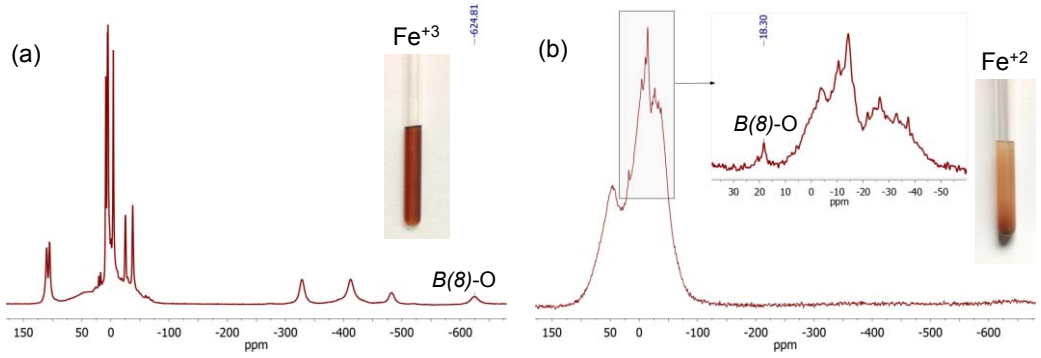

Figure 3. ^{11}B NMR spectra of (a) compound **4** as Fe^{+3} and (b) compound **4** as Fe^{+2}.

We conclude that the complete functionalization of OVS can be confirmed by ^{1}H-NMR, in which the vinyl protons resonances have disappeared, as well as by UV-Vis that

has allowed us to establish a correlation between the absorptions of compound **1** and **2** with the respective **3** and **4**

Thermal behavior of metallacarborane containing POSS. Thermogravimetric analysis **(**TGAs) were run under argon for compounds **1-4** and also in air for **3** at heating rates of 10 ºC/min. For comparison, TGA was also performed for starting octavinylsilsesquioxane. Figure 4 shows TGA data for octavinylsilsesquioxane, **3** and **4**, indicating that later are stable in argon up to around 350 ºC above it a very low weight loss occurs (Table 1). It can be clearly observed that the incorporation of metallacarborane clusters in the POSS structure produces a dramatic increase in the thermal stability of the material, when are compared with unmodified octavinylsilsesquixane. Heating up to 1000 ºC leaves residues with more than 100 % of the initial weight, compared with organic styrene-containing POSS, from which only 40% of residue is recovered. The elimination of the organic part in our materials would lead to a theoretical weight loss of 49.87% for **POSS-4**, 40.37% for **POSS-5** and 37.59 % for **POSS-6** (Table 1), so that the high conservation of the initial mass quantity in the material is obvious. We interpret that only the hydrogen atoms have been removed from our materials. This behavior undoubtedly corroborates that the incorporation of metallcarborane moieties to a compound induces an extraordinary thermal stability.

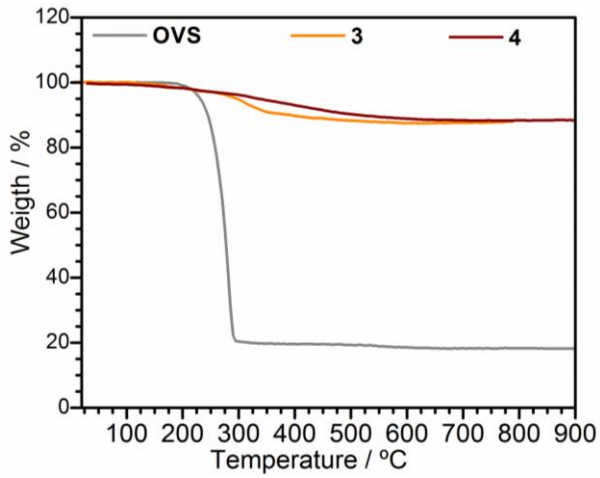

Figure 4. Thermogravimetric analysis (TGA) data under argon (10 ºC/min) for octavinylsilsesquioxane (OVS), compound **3** and compound **4**.

Experimental.

Instrumentation. Elemental analyses were performed using a Carlo Erba EA1108 microanalyzer. ATR-IR spectra were recorded on a high resolution spectrometer FT-IR Perkin Elmer Spectrum One. The ^{1}H and $^{1}H\{^{11}B\}$ NMR (300.13 MHz), $^{11}B\{^{1}H\}$ and ^{11}B NMR (96.29 MHz), $^{13}C\{^{1}H\}$ NMR (75.47 MHz) spectra were recorded on a Bruker ARX 300 spectrometer. All NMR spectra were recorded in $CDCl_3$ or CD_3COCD_3 solutions at 25ºC. Chemical shift values for $^{11}B\{^{1}H\}$ NMR spectra were referenced to external $BF_3{\cdot}OEt_2$, and those for ^{1}H, $^{13}C\{^{1}H\}$ and $^{29}Si\{^{1}H\}$ NMR were referenced to $SiMe_4$ (TMS). Chemical shifts are reported in units of parts per million downfield from reference, and all coupling constants are reported in Hertz.

Diffusion-ordered NMR spectroscopy (DOSY) experiments were performed as described previously (ref) at 298 K on a Bruker AVANCE 500 NMR spectrometer operating at 500.13 MHz and equipped with a cryoprobe *z*-gradient inverse probehead capable of producing gradients in the *z* direction with a maximum strength of 53.5 G cm-1. The double stimulated echo sequence incorporating bipolar gradient pulses and a longitudinal eddy current delay (dstegp3s in the BRUKER library) was used. The gradient strength was linearly incremented in 16 steps from 2% up to 95% of the maximum gradient strength. Diffusion times and gradient pulse durations were optimized for each experiment in order to achieve a 95% decrease in the resonance intensity at the largest gradient amplitude; typically, diffusion times between 100 and 150 ms and bipolar rectangular gradient pulses between 1.0 and 2.0 ms were employed. The longitudinal eddy current delay was held constant to 5 ms, whereas the gradient pulse recovery time was set to 100 □s. After Fourier transformation followed by the same phase and baseline correction of each 1D dataset, the diffusion dimension of the 2D DOSY spectra was obtained by using the dosy protocol included into the of the Bruker TOPSPIN software package (version 1.3).

For a reliable comparison, all DOSY experiments have been carried out on dilute CD_3CN solutions. Similar concentrations have been used to minimize the effect of different solution viscosities for different samples, which were confirmed from the diffusion coefficient of the residual CHD_2CN signal taken as an internal reference. The

translational diffusion coefficient of a particle is related to its hydrodynamic radius according to the Stokes-Einstein equation. The diffusion coefficients obtained from the DOSY experiments were used to evaluate the hydrodynamic radius of the particles for all samples (see Table 2).

UV-Vis spectra were recorded on Shimadzu UV-1700 Pharmaspec spectrophotometer, using 1 cm cuvettes. Different concentrations of the compounds were used to calculate the molar extinction coefficients: 10^{-4}, $5 \cdot 10^{-5}$, 10^{-5}, $5 \cdot 10^{-6}$, $2.5 \cdot 10^{-6}$ and 10^{-6} mol·L^{-1}. The Thermal Analysis were performed on a simultaneous thermogravimetric analysis (TGA) - differential scanning calorimetry/differential thermal analysis (heat flow DSC/DTA) system NETZSCH -STA 449 F1 Jupiter, and a differential scanning calorimeter (power compensation DSC) Perkin Elmer DSC8500 LAB SYS (N5340501) equipped with a Liquid N_2 controller CRYOFILL (N534004). Samples for thermogravimetric characterization were placed in open alumina crucibles. A heating rate of 10 ºC/min was used and all samples were studied between 40 and 1000 ºC.

Acetonitrile was dried for 2 days over molecular sieves (3Å; Merck; activated for 16h at 300 ºC under vacuum). After drying, acetonitrile was degassed using the stablished freeze-pump-thaw protocol. Cyclic Voltammetries (CV) were performed at room temperature and under nitrogen atmosphere. A three electrode set-up was employed, using glassy carbon as working electrode (A = 0.0707 cm^2), a platinum wound as counter electrode and Ag/AgCl 0.1 M TBACl as reference electrode. The glassy carbon electrode was polished prior to measurement with 0.3, 0.1 and 0.05 μm α-Al_2O_3. $TBAPF_6$ was dried overnight at 80 ºC under vacuum and used as supporting electrolyte in a 0.1 M concentration. All potentials were referenced internally to Fc/Fc^+.

Cyclic Voltammetries were obtained with a Radiometer Analytical VoltaLab PGZ402, Universal Pulse Dynamics – EIS Voltammetry, at scan rates from 500 to 10 mV/s and evaluated with the respective instrument software.

Materials. All reactions were performed under an atmosphere of dinitrogen employing standard Schlenk techniques. MeOH, EtOH and hexane were purchased from Merck and used as received; CH_2Cl_2 and toluene were distilled from sodium benzophenone previously to use. Octavinylsilsesquioxane (OVS) was prepared by following the literature procedure[25] as well as 3,3'-Co(8-$C_4H_8O_2$-1,2-$C_2B_9H_{10}$)(1',2'-$C_2B_9H_{11}$)] and 3,3'-Fe(8-$C_4H_8O_2$-1,2-$C_2B_9H_{10}$)(1',2'-$C_2B_9H_{11}$)].[12b, 16] Vinylphenol solution 10 wt. % in propylene glycol was pursached from Aldrich.

Synthesis of [Me_4N][8-(4''-(CH_2=CH)-C_6H_4O-$C_4H_8O_2$)-3,3'-Co(1,2-$C_2B_9H_{10}$)(1',2'-$C_2B_9H_{11}$)] (1): A mixture of [3,3'-Co(8-$C_4H_8O_2$-1,2-$C_2B_9H_{10}$)(1',2'-$C_2B_9H_{11}$)] (250 mg, 0.609 mmol), K_2CO_3 (347 mg, 2.51 mmol), 4-vinylphenol solution (0.71 mL, 0.612 mmol) and 10 mL of dry acetonitrile under nitrogen was refluxed overnight in a 25 mL round-bottomed flask. The reaction mixture was filtered off and the solvent was removed under vacuum. The orange oil was dissolved in 1 mL of EtOH and precipitated as tetramethylammonium salt by adding an aqueous saturated solution of (NMe_4)Cl. The suspension was centrifuged and the orange solid was filtered, rinsed with water and petroleum ether giving an orange solid identified as compound **1**. Yield: 363 mg, 98.5%. ^{1}H NMR (CD_3OCD_3): δ = 7.40 (d, ^3J(H,H) = 6 Hz, 2H, C_6H_4), 6.94 (d, ^3J(H,H) = 6 Hz, 2H, C_6H_4), 6.70 (dd, ^3J(H,H) = 18 Hz, ^3J(H,H) = 12 Hz, 1H, C*H*=CH_2), 5.66 (d, ^3J(H,H) = 18 Hz, 1H, CH=C*H*$_2$), 5.10 (d, ^3J(H,H) = 12 Hz, 1H, CH=C*H*$_2$), 4.30 (br s, 4H, C_c-*H*), 4.15 (t, ^3J(H,H) = 6 Hz, 2H, C*H*$_2$-O), 3.82 (t, ^3J(H,H) = 6 Hz, 2H, C*H*$_2$-O), 3.61 (br, 4H, C*H*$_2$-O), 3.45 (s, 12H, N-C*H*$_3$); ^{1}H{^{11}B} NMR (CD_3OCD_3): δ = 7.40 (d, ^3J(H,H) = 6 Hz, 2H, C_6H_4), 6.94 (d, ^3J(H,H) = 6 Hz, 2H, C_6H_4), 6.70 (dd, ^3J(H,H) = 18 Hz, ^3J(H,H) = 12 Hz, 1H, C*H*=CH_2), 5.66 (d, ^3J(H,H) = 18 Hz, 1H, CH=C*H*$_2$), 5.10 (d, ^3J(H,H) = 2 Hz, 1H, CH=C*H*$_2$), 4.30 (br s, 4H, C_c-*H*), 4.15 (t, ^3J(H,H) = 6 Hz, 2H, C*H*$_2$-O), 3.82 (t, ^3J(H,H) = 6 Hz, 2H, C*H*$_2$-O), 3.61 (br, 4H, C*H*$_2$-O), 3.46 (s, 12H, N-C*H*$_3$), 2.94 (s, B-*H*), 2.97 (s, B-*H*), 2.71 (s, B-*H*), 2.46 (s, B-*H*), 2.01 (s, B-*H*), 1.80 (s, B-*H*), 1.68 (s, B-*H*), 1.58 (s, B-*H*), 1.49 (s, B-*H*); ^{11}B NMR (CD_3OCD_3): δ = 24.21 (s, 1B, *B*-O), 5.18 (d, ^1J(B,H) = 135 Hz, 1B, *B*-H), 1.71 (d, ^1J(B,H) = 143 Hz, 1B, *B*-H), -1.11 (d, ^1J(B,H) = 153 Hz, 1B, *B*-H), -2.86 (d, ^1J(B,H) = 160 Hz, 2B, *B*-H), -6.12 (d, ^1J(B,H) = 83 Hz, 2B, *B*-H), -6.90 (d, ^1J(B,H) = 126 Hz, 4B, *B*-H), -15.93 (d, ^1J(B,H) = 153 Hz, 2B, *B*-H), -19.06 (d, ^1J(B,H) = 153 Hz, 2B, *B*-H), -20.52 (d, ^1J(B,H) = 144 Hz, 1B, *B*-H), -27.16 (d,

^1J(B,H) = 163 Hz, 1B, *B*-H); $^{13}C\{^1H\}$ NMR (CD_3OCD_3): δ = 159.04 (s, *C*-O), 136.62 (s, *C*H-C_6H_4), 130.35 (s, CH-*C*$_6H_4$), 127.32 (s, *C*$_6H_4$), 114.62 (s, *C*$_6H_4$), 110.70 (s, CH=*C*H_2), 72.04 (s, *C*H_2-O), 69.36 (s, *C*H_2-O), 68.41 (s, *C*H_2-O), 67.59 (s, *C*H_2-O), 55.23 (s, N-*C*H_3), 54.58 (s, *C*$_c$-H), 46.39 (s, *C*$_c$-H); MALDI-TOF-MS: m/z calcd for $[M\text{-}N(CH_3)_4]^-$: 530.0; found: 530.5; ATR-IR (cm^{-1}): $\tilde{\upsilon}$ = 2527 (s, B-H st), 1605 (m, C=C st), 1090 (br s, Si-O st); elemental analysis calcd for $C_{20}H_{48}B_{18}CoNO_3 \cdot H_2O$: C 38.61, H 8.10, N 2.25; found: C 38.35, H 7.78, N 2.04.

Synthesis of [Me$_4$N][8-(4''-(CH$_2$=CH)-C$_6$H$_4$O-C$_4$H$_8$O$_2$)-3,3'-Fe(1,2-C$_2$B$_9$H$_{10}$)(1',2'-C$_2$B$_9$H$_{11}$)] (2): The procedure was the same as for **1**, but using [3,3'-Fe(8-$C_4H_8O_2$-1,2-$C_2B_9H_{10}$)(1',2'-$C_2B_9H_{11}$)] (213 mg, 0.523 mmol), K_2CO_3 (720 mg, 5.22 mmol), 4-vinylphenol solution (0.61 mL, 0.526 mmol) and 8 mL of dry acetonitrile.. The suspension was filtered, rinsed with water and the solid was purified by TLC (dichloromethane). The oily compound was dissolved in 0.5 mL dichloromethane and dry in vacuum at 45°C to obtain compound **2** as a brown solid. Yield: 101 mg, 32.2%. ^1H NMR (CD_3OCD_3): δ = 84.40 (br, B-*H*), 76.81 (br, B-*H*), 59.90 (br, B-*H*), 44.83 (br, C_c-H), 42.84 (br, C_c -*H*), 28.78 (br, B-*H*), 6.85 (br, 2H, C$_6H_4$), 6.45 (m, 1H, C*H*=CH$_2$), 5.45 (d, ^3J(H,H) = 18 Hz, 1H, CH=C*H*$_2$), 5.28 (br, 2H, C$_6H_4$), 4.98 (br, 1H, CH=C*H*$_2$), 3.10 (s, 12H, N-C*H*$_3$), 2.62 (s, 2H, C*H*$_2$-O), 0.39 (s, 2H, C*H*$_2$-O), -4.00 (s, 2H, C*H*$_2$-O), -10.40 (s, 2H, C*H*$_2$-O), -10.69 (s, B-*H*); $^1H\{^{11}B\}$ NMR (CD_3OCD_3): δ = 83.97 (br, B-*H*), 76.03 (br, B-*H*), 59.64 (br, B-*H*), 44.92 (br, C_c-H), 43.91 (br, C_c -*H*), 28.66 (br, B-*H*), 6.84 (d, ^3J(H,H) = 6 Hz, 2H, C$_6H_4$), 6.43 (dd, ^3J(H,H) = 18 Hz, ^3J(H,H) = 12 Hz, 1H, C*H*=CH$_2$), 5.44 (d, ^3J(H,H) = 18 Hz, 1H, CH=C*H*$_2$), 5.26 (d, ^3J(H,H) = 6 Hz, 2H, C$_6H_4$), 4.96 (d, ^3J(H,H) = 12 Hz, 1H, CH=C*H*$_2$), 3.06 (s, 12H, N-C*H*$_3$), 2.52 (s, 2H, C*H*$_2$-O), 0.39 (s, 2H, C*H*$_2$-O), -1.96 (s, B-*H*), -2.36 (s, B-*H*), -4.00 (s, 2H, C*H*$_2$-O), -10.45 (s, 2H, C*H*$_2$-O), -10.84 (s, B-*H*); ^{11}B NMR (CD_3OCD_3): δ = 118.07, 101.57 (s, 2B, *B*-H)), 40.51, 30.76, -0.47, -4.91, -39.79, -362.65, -431.81 (s, 5B, *B*-H), -468.10 (s, 1B, *B*-H); $^{13}C\{^1H\}$ NMR (CD_3OCD_3): δ = 156.80 (s, *C*-O), 136.06 (s, *C*H-C_6H_4), 129.75 (s, CH-*C*$_6H_4$), 126.50 (s, *C*$_6H_4$), 113.13 (s, *C*$_6H_4$), 110.62 (s, CH=*C*H_2), 63.01 (s, *C*H_2-O), 61.13 (s, *C*H_2-O), 54.95 (s, N-*C*H_3), 13.42 (s, *C*H_2-O), -0.22 (s, *C*H_2-O), -486.92 (s, *C*$_c$-H), -532.51 (s, *C*$_c$-H); MALDI-TOF-MS: m/z calcd for $[M\text{-}N(CH_3)_4]^-$: 527.4; found:

527.5; ATR-IR (cm^{-1}): $\tilde{\upsilon}$ = 2530 (s, B-H st), 1605 (m, C=C st); elemental analysis calcd for $C_{20}H_{48}B_{18}FeNO_3$: C 39.97, H 8.05, N 2.33; found: C 39.15, H 7.89, N 1.92.

Synthesis of T_8-Cosane (3): A 25 mL round-bottomed flask was charged under nitrogen with OVS (15 mg, 0.024 mmol), compound **1** (137 mg, 0.227 mmol), and first generation Grubbs catalyst (12 mg, 0.014 mmol) in 5 mL of CH_2Cl_2. The solution was stirred and refluxed for 60 h. The solvent was removed under vacuum giving a brown oil. Then 0.5 mL of THF, 5 mL of methanol and a few drops of water were added. The solvents were removed under vacuum giving a solid. The solid was washed with methanol, filtrated and rinsed with petroleum ether to give a brownish-orange solid. Further purification was performed by TLC (acetone/hexane, 7:3) to obtain compound **3** as an orange solid. Yield: 103 mg, 83 %. ^{1}H NMR (CD_3OCD_3): δ = 7.56 (d, ^3J(H,H) = 9 Hz, 16H, C_6H_4), 7.41 (d, ^3J(H,H) = 18 Hz, 8H, CH=C*H*-Si), 7.00 (d, ^3J(H,H) = 9 Hz, 2H, C_6H_4), 6.29 (d, ^3J(H,H) = 18 Hz, 8H, C*H*=CH-Si), 4.29 (br s, 32H, C_c-*H*), 4.17 (t, ^3J(H,H) = 4.5 Hz, 16H, CH_2-O), 3.83 (t, ^3J(H,H) = 4.5 Hz, 16H, CH_2-O), 3.61 (br, 32H, CH_2-O), 3.42 (s, 96H, N-CH_3); ^{1}H{^{11}B} NMR (CD_3OCD_3): δ = 7.56 (d, ^3J(H,H) = 9 Hz, 16H, C_6H_4), 7.41 (d, ^3J(H,H) = 18 Hz, 8H,CH=C*H*-Si), 7.00 (d, ^3J(H,H) = 16 Hz, 2H, C_6H_4), 6.29 (d, ^3J(H,H) = 18 Hz, 8H, C*H*=CH-Si), 4.28 (br s, 32H, C_c-*H*), 4.17 (t, ^3J(H,H) = 4.5 Hz, 16H, CH_2-O), 3.83 (t, ^3J(H,H) = 4.5 Hz, 16H, CH_2-O), 3.61 (br, 32H, CH_2-O), 3.42 (s, 96H, N-CH_3), 2.93 (s, B-*H*), 2.77 (s, B-*H*), 2.47 (s, B-*H*), 2.01 (s, B-*H*), 1.81 (s, B-*H*), 1.68 (s, B-*H*), 1.58 (s, B-*H*), 1.50 (s, B-*H*); ^{11}B NMR (CD_3OCD_3): δ =24.30 (s, 8B, *B*-O), 5.28 (d, ^1J(B,H) = 134 Hz, 8B, *B*-H), 1.76 (d, ^1J(B,H) = 141 Hz, 8B, *B*-H), -1.12 (d, ^1J(B,H) = 150 Hz, 8B, *B*-H), -2.85 (d, ^1J(B,H) = 162 Hz,16B, *B*-H), -6.10 (d, ^1J(B,H) = 84 Hz, 16B, *B*-H), -6.82 (d, ^1J(B,H) = 112 Hz, 32B, *B*-H), -15.88 (d, ^1J(B,H) = 151 Hz, 16B, *B*-H), -19.00 (d, ^1J(B,H) = 149Hz, 16B, *B*-H), -20.62 (d, ^1J(B,H) = 131 Hz, 8B, *B*-H), -26.81 (d, ^1J(B,H) = 98 Hz, 8B, *B*-H); ^{13}C{^{1}H} NMR (CD_3OCD_3): δ = 160.08 (s, *C*-O), 148.87 (s, CH=*C*H-C_6H_4), 130.13 (s, CH-C_6H_4), 128.42 (s, C_6H_4), 114.76 (s, C_6H_4), 114.21 (s, Si-*C*H=CH), 72.05 (s, *C*H_2-O), 69.34 (s, *C*H_2-O), 68.42 (s, *C*H_2-O), 67.68 (s, *C*H_2-O), 55.26 (s, N-*C*H_3), 54.39 (s, C_c-H), 45.86 (s, C_c-H); ATR-IR (cm^{-1}): $\tilde{\upsilon}$ = 2535 (s, B-H st), 1603 (m, C=C st), 1093 (br s, Si-O st); elemental analysis calcd for $C_{160}H_{376}B_{144}Co_8N_8O_{36}Si_8$: C 36.66, H 7.23, N 2.14; found: C 37.62, H 7.97, N 1.92.

Synthesis of T_8-Fesane (4): The procedure was the same as for **1**, but using OVS (12 mg, 0.019 mmol), compound **2** (105 mg, 0.175 mmol), and first generation Grubbs catalyst (7 mg, 0.008 mmol) in 5 mL of CH_2Cl_2 at reflux for 72 h. Further purification was performed by TLC (acetone/hexane, 7:3) to obtain compound **4** as brown solid. Yield: 45 mg, 45.5 %. ^{1}H NMR (CD_3OCD_3): δ = 59.61 (br, B-*H*), 44.36 (br, C_c-H), 42.30 (br, C_c -*H*), 28.54 (br, B-*H*), 7.03 (br, 24H, C_6H_4 and C*H*=CH), 5.98 (br, 8H, CH=C*H*), 5.55 (br, 16H, C_6H_4), 2.94 (s, 96H, N-CH_3), 2.72 (s, CH_2-O), 0.51 (s, 16H, CH_2-O), -3.88 (s, CH_2-O), -10.26 (s, CH_2-O), -10.41 (s, B-*H*), -13.75 (s, B-*H*); ^{1}H{^{11}B} NMR (CD_3OCD_3): δ = 74.86 (s, B-*H*), 59.58 (s, B-*H*), 44.57 (s, C_c-H), 42.85 (s, C_c -*H*), 28.87 (s, B-*H*), 7.17 (br, 24H, C_6H_4 and C*H*=CH), 6.16 (d, ^3J(H,H) = 18 Hz, 8H, C*H*=CH), 5.44 (br, 16H, C_6H_4), 2.95 (s, 96H, N-CH_3), 2.76 (br, CH_2-O), 0.58 (br, 16H, CH_2-O), -1.91 (s, B-*H*), -2.19 (s, B-*H*), -3.88 (br, CH_2-O), -10.32 (br, CH_2-O), -10.71 (s, B-*H*), -13.83 (s, B-*H*); ^{11}B NMR (CD_3OCD_3): δ = 114.51, 98.75 (s, 2B, *B*-H), 39.52, 29.85, -0.76, -5.48, -38.70, -353.42, -420.72 (s, 5B, *B*-H), -454.63 (s, 1B, *B*-H); ^{13}C{^{1}H} NMR (CD_3OCD_3): δ = 158.01 (s, *C*-O), 148.48 (s, *C*H-C_6H_4), 129.28 (s, CH-C_6H_4), 127.63 (s, C_6H_4), 113.94 (s, CH=*C*H_2), 113.32 (s, C_6H_4), 63.11 (s, *C*H_2-O), 61.07 (s, *C*H_2-O), 54.81 (s, N-*C*H_3), 13.15 (s, *C*H_2-O), 0.18 (s, *C*H_2-O); ATR-IR (cm^{-1}): $\tilde{\upsilon}$ = 2530 (s, B-H st), 1603 (m, C=C st), 1090 (br s, Si-O st); elemental analysis calcd for $C_{160}H_{376}B_{144}Fe_8N_8O_{36}Si_8$: C 36.84, H 7.26, N 2.15; found: C 37.50, H 6.90, N 1.79.

References

[1] a) P. D. Lickiss, F. Rataboul, in *Adv. Organomet. Chem., Vol. Volume 57* (Eds.: F. H. Anthony, J. F. Mark), Academic Press, **2008**, pp. 1-116; b) D. B. Cordes, P. D. Lickiss, F. Rataboul, *Chem. Rev.* **2010**, *110*, 2081-2173; c) C. Hartmann-Thompson, *Applications of Polyhedral Oligomeric Silsesquioxanes*, Springer Netherlands, **2011**.

[2] a) C. M. Brick, Y. Ouchi, Y. Chujo, R. M. Laine, *Macromolecules* **2005**, *38*, 4661-4665; b) C. McCusker, J. B. Carroll, V. M. Rotello, *Chem. Commun.* **2005**, 996-998; c) K. Pielichowski, J. Njuguna, B. Janowski, J. Pielichowski, in *Supramolecular Polymers Polymeric Betains Oligomers, Vol. 201*, Springer Berlin Heidelberg, **2006**, pp. 225-296; d) J. Miao, L. Zhu, *J. Phys. Chem. B* **2010**, *114*, 1879-1887; e) U. Díaz, T. García, A. Velty, A. Corma, *Chem. Eur. J.* **2012**, *18*, 8659-8672; f) M. Singh, H. S. Chae, J. D. Froehlich, T. Kondou, S. Li, A. Mochizuki, G. E. Jabbour, *Soft Matter* **2009**, *5*, 3002-3005; g) K. Tanaka, N. Kitamura, K. Naka, Y. Chujo, *Chem. Commun.* **2008**, 6176-6178

[3] X. Yang, J. D. Froehlich, H. S. Chae, S. Li, A. Mochizuki, G. E. Jabbour, *Adv. Funct. Mater.* **2009**, *19*, 2623-2629

[4] a) C. M. Casado, I. Cuadrado, M. Morán, B. Alonso, M. Barranco, J. Losada, *Appl. Organomet. Chem.* **1999**, *13*, 245-259; b) A. Wang, C. Ornelas, D. Astruc, P. Hapiot, *J. Am. Chem. Soc.* **2009**, *131*, 6652-6653; c) S. Bruña, D. Nieto, A. M. González-Vadillo, J. Perles, I. Cuadrado, *Organometallics* **2012**, *31*,

3248-3258; d) -Armada, C. M. Casado, *Organometallics* **2012**, *31*, 6344-6350

[5] R. N. Grimes, in *Carboranes (Second Edition)* (Ed.: R. N. Grimes), Academic Press, Oxford, **2011**, pp. 1053-1082.

[6] I. B. Sivaev, V. I. Bregadze, *Collect. Czech. Chem. Commun.* **1999**, *64*, 783-805

[7] M. Corsini, F. F. de Biani, P. Zanello, *Coord. Chem. Rev.* **2006**, *250*, 1351-1372

[8] a) A. Pepiol, F. Teixidor, R. Sillanpää, M. Lupu, C. Viñas, *Angew. Chem. Int. Ed.* **2011**, *50*, 12491-12495; b) P. González-Cardoso, A.-I. Stoica, P. Farràs, A. Pepiol, C. Viñas, F. Teixidor, *Chem. Eur. J.* **2010**, *16*, 6660-6665

[9] M. Lupu, A. Zaulet, F. Teixidor, E. Ruiz, C. Viñas, *Chem. Eur. J.* **2015**, *21*, 6888-6897

[10] a) S. S. Graham, P. A. Jelliss, *Inorg. Chim. Acta* **2014**, *410*, 195-201; b) M. Tarrès, V. S. Arderiu, A. Zaulet, C. Viñas, F. Fabrizi de Biani, F. Teixidor, *Dalton Trans.* **2015**, *44*, 11690-11695

[11] A. A. Semioshkin, I. B. Sivaev, V. I. Bregadze, *Dalton Trans.* **2008**, 977-992

[12] a) š k ü háč k l Cí ř vá Čá v ký *J. Organomet. Chem.* **2007**, *692*, 4801-4804; b) F. Teixidor, J. Pedrajas, I. Rojo, C. Viñas, R. Kivekäs, R. Sillanpää, I. Sivaev, V. Bregadze, S. Sjöberg, *Organometallics* **2003**, *22*, 3414-3423

[13] R. H. Grubbs, D. J. O'Leary, *Handbook of metathesis: Applications in organic synthesis*, John Wiley & Sons, **2015**.

[14] a) S. Sulaiman, A. Bhaskar, J. Zhang, R. Guda, T. Goodson, R. M. Laine, *Chem. Mater.* **2008**, *20*, 5563-5573; b) A. Ferrer-Ugalde, E. J. Juárez-Pérez, F. Teixidor, C. Viñas, R. Núñez, *Chem. Eur. J.* **2013**, *19*, 17021-17030

[15] R. Núñez, E. J. Juárez-Pérez, F. Teixidor, R. Santillan, N. Farfán, A. Abreu, R. Yépez, C. Viñas, *Inorg. Chem.* **2010**, *49*, 9993-10000

[16] A. M. Cioran, F. Teixidor, C. Vinas, *Dalton Trans.* **2015**, *44*, 2809-2818

[17] M. G. Voronkov, V. I. Lavrent'yev, in *Inorganic Ring Systems*, Springer Berlin Heidelberg, Berlin, Heidelberg, **1982**, pp. 199-236.

[18] E. J. Juárez-Pérez, C. Viñas, A. González-Campo, F. Teixidor, R. Sillanpää, R. Kivekäs, R. Núñez, *Chem. Eur. J.* **2008**, *14*, 4924-4938

[19] C. Kim, I. Jung, *J. Organomet. Chem.* **2000**, *599*, 208-215

[20] a) E. J. Juárez-Pérez, C. Viñas, F. Teixidor, R. Núñez, *Organometallics* **2009**, *28*, 5550-5559; b) E. J. Juárez-Pérez, C. Viñas, F. Teixidor, R. Santillan, N. Farfán, A. Abreu, R. Yépez, R. Núñez, *Macromolecules* **2010**, *43*, 150-159

[21] D. R. Abad, J. Henig, H. A. Mayer, T. Reißig, B. Speiser, *Organometallics* **2014**, *33*, 4777-4783

[22] H. Sun, W. Chen, A. E. Kaifer, *Organometallics* **2006**, *25*, 1828-1830

[23] a) E. J. Juárez-Pérez, C. Viñas, F. Teixidor, R. Núñez, *J. Organomet. Chem.* **2009**, *694*, 1764-1770; b) D. Brusselle, P. Bauduin, L. Girard, A. Zaulet, C. Viñas, F. Teixidor, I. Ly, O. Diat, *Angew. Chem. Int. Ed.* **2013**, *52*, 12114-12118

[24] C. Ornelas, J. Ruiz, C. Belin, D. Astruc, *J. Am. Chem. Soc.* **2009**, *131*, 590-601

[25] E. O. Dare, L.-K. Liu, J. Peng, *Dalton Trans.* **2006**, 3668-3671